Graduate School for Cellular and Biomedical Sciences

University of Bern

Functional and Structural Studies of Membrane Transporters

PhD Thesis submitted by

Hüseyin Ilgü

from **Turkey**

for the degree of

PhD of Science in Biochemistry and Molecular Biology

Supervisor
Prof. Dr. Dimitrios Fotiadis
Institute of Biochemistry and Molecular Medicine
Faculty of Medicine of the University of Bern

Co-advisor
Prof. Dr. Jean-Louis Reymond
Department of Chemistry and Biochemistry
Faculty of Science of the University of Bern

Accepted by the Faculty of Medicine, the Faculty of Science and the Vetsuisse Faculty of the University of Bern at the request of the Graduate School for Cellular and Biomedical Sciences

Bern, Dean of the Faculty of Medicine

Bern, Dean of the Faculty of Science

Bern, Dean of the Vetsuisse Faculty Bern

Abstract

The structural information on membrane proteins (MPs) is critical to understand the molecular mechanism of ligand recognition, selectivity and transport. For structural studies and many other purposes, MPs need to be extracted by the help of detergents from their native environment, the lipid bilayer. The literature about the amounts of detergent and endogenous phospholipid molecules bound to MPs after purification was limited. In order to have a better understanding on this concept, we carried out a systematic study with three model integral MPs of different oligomeric states purified in nine different commonly used detergents. The insights gained from this study can be summarized as follows. 1) Purified integral MPs are ternary complexes consisting of protein, lipid, and detergent. 2) The amount of detergent and endogenous phospholipids bound to purified proteins are dependent on the size of the hydrophobic lipid-accessible protein surface areas and the physicochemical properties of the detergents used. 3) The size of the detergent-lipid belt surrounding the hydrophobic lipid-accessible surface of purified MPs can be tuned by appropriate choice of detergent. 4) The detergents *n*-nonyl-*β*-D-glucopyranoside (NG) and 5-cyclohexyl-1-pentyl-*β*-D-maltoside (Cymal-5) showed exceptional delipidating effects on the model proteins during purification. 5) The types of endogenous phospholipids bound to MPs could vary depending on the detergent used for solubilization and purification. 6) Size-exclusion chromatography (SEC) was shown to be a reliable method for estimating the molecular mass of ternary complexes of integral MPs. These findings propose a strategy to control and tune the number of detergent and endogenous phospholipid molecules bound to MPs. Importantly, control of the composition of these ternary complexes is fundamental for the successful crystallization of MPs and consequently for MP structure determination by crystallographic approaches. By applying this strategy we could minimize the size of the detergent-lipid belt around the L-arginine (Arg)/agmatine (Agm) antiporter AdiC from *Escherichia coli* (*E. coli*) and make the formation of crystal contacts between proteins sterically possible. As a result, we could crystallize and solve the crystal structure of the wild-type (wt) form of AdiC at the unprecedented resolution of 2.2 Å in the substrate-free outward-open conformation, and for the first time with the substrate Agm at 2.6 Å resolution in the same conformation of the translocation cycle. The Agm-bound crystal structure indicated that Agm binds to the same binding pocket as Arg in the previously published outward-facing occluded conformation. The identified subtle differences between the Arg- and Agm-bound AdiC structures describe for the first time the different affinities of this transporter at the molecular level. In the light of our findings and the previously published AdiC structures, we could describe the conformational changes of AdiC connected with the release of Agm into the periplasmic space.

Table of Contents

1. List of Publications

This thesis is based on the following publications indexed by the Roman numerals I to II.

I. **Variation of the detergent-binding capacity and phospholipid content of membrane proteins when purified in different detergents.**

Ilgü H, Jeckelmann JM, Gachet MS, Boggavarapu R, Ucurum Z, Gertsch J, Fotiadis D. (2014) *Biophys J.* 106(8):1660-1670.

Contribution to publication: Protein expression, purification, size-exclusion chromatography analyses, detergent and lipid content determination.

II. **Molecular bases for substrate recognition of the wild-type L-arginine/agmatine antiporter AdiC -** (manuscript enclosed).

Ilgü H et al.

Contribution to publication: Protein expression, purification, crystallization, X-ray diffraction data collection and analysis, and functional characterization of AdiC.

Supporting publication with relevance to the thesis is indexed by the Roman numeral III.

III. **Detergent-induced stabilization and improved 3D map of the human heteromeric amino acid transporter 4F2hc-LAT2.**

Meury M, Costa M, Harder D, Stauffer M, Jeckelmann JM, Brühlmann B, Rosell A, **Ilgü H**, Kovar K, Palacín M, Fotiadis D. (2014) *PLoS One*. 9(10):1-6.

Contribution to publication: Detergent and lipid content analyses of the purified 4F2hc-LAT2.

2. Introduction

2.1. Significance of Membrane Proteins

Biological membranes fence and compartmentalize cells of all organisms, acting as effective insulators and selective filters between the inner and the outer environment. Membranes are composed of a lipid bilayer and apart from having highly specialized functions, they harbor particular proteins and protein complexes (Engelman 2005; Simons and Ikonen 1997). These proteins are fully or partially embedded in the lipid bilayer, and they represent complex molecular machineries responsible for the exchange and transport of various molecules essential for life; e.g., water, ions, nutrients, waste products, vitamins, cofactors, and drugs. The so-called membrane proteins (MPs), furthermore, are participating to the translocation of solutes and biopolymers, such as proteins and nucleic acids, the transmission of signals, and the propagation of electrical impulses (von Heijne 2007). Also, as being part of the cellular cytoskeleton, MPs mediate the stability and the organization of the cell and its compartments. Moreover, some of them are involved in modulation of the attachment to neighboring cells or to the extracellular matrix, regulation of intracellular vesicular transport, and the homeostasis of the lipid composition (Kell et al. 2011).

In the human genome, about 25% of the genes encode for MPs (Dobson et al. 2015; Uhlén et al. 2015). Remarkably, these proteins account for more than 60% of all proteins targeted by the most relevant class of pharmaceutical drugs approved by U.S. Food and Drug Administration (FDA) (Dobson et al. 2015; Uhlén et al. 2015; Yildirim et al. 2007). Any kind of genetic mutations or single-nucleotide polymorphisms have the potential to alter the structure and/or function of MPs (George 2004). Asthma, Alzheimer's disease, cardiac arrhythmias, epilepsy, schizophrenia, unipolar and bipolar depression, hypertension, obesity, diabetes are some examples of common human diseases caused by such kind of genetic alterations occurring in these proteins (Roses et al. 2005; Thompson et al. 2005).

2.2. Membrane Transporters and Other Large Membrane Protein Families

The biological cell membrane is a selective permeable barrier between the cell and the extracellular environment. Across the membrane, small hydrophobic and uncharged non-polar molecules, such as O_2, CO_2 and N_2 may diffuse easily; H_2O, urea and glycerol can pass by osmosis or diffusion. However, the transport through the membrane of nutrients such as sugars, amino acids, nucleotides, inorganic ions, and vitamins and some other chemicals such as drugs is controlled by specific membrane transport proteins (Lodish et al. 2003). Transporters are the gatekeepers of the cell and comprise coupled transporters, exchangers, passive transporters, mitochondrial and vesicular transporters, water channels, ion channels, adenosine triphosphate (ATP)-driven pumps, and ATP-binding cassette (ABC) transporters, Figure 1 (Hediger et al. 2013).

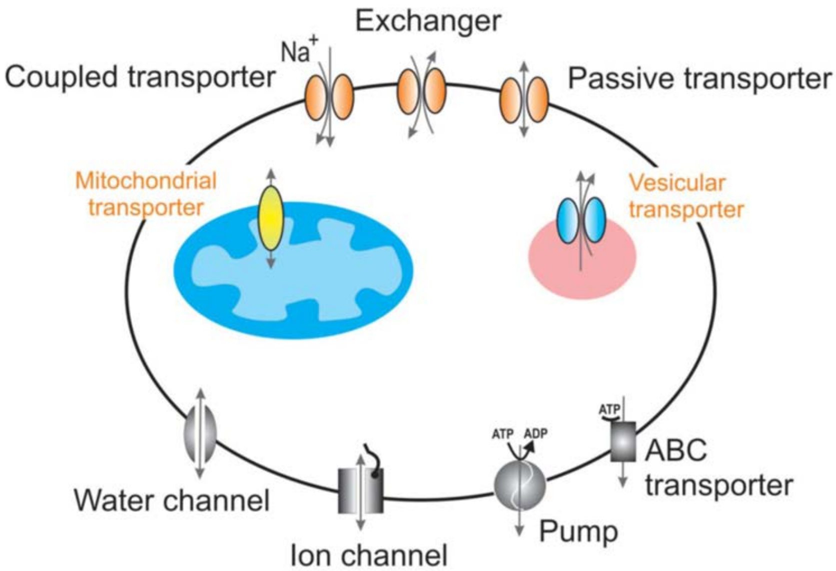

Figure 1. Types of membrane transporters. Figure adapted from Hediger et al. *Mol. Aspects Med.* 2013.

To summarize the functions of individual membrane transporters: Water channel proteins, named aquaporins are integral MPs that transport water bidirectional. In some cases, these proteins also transport small solutes, such as glycerol, urea, and ions (Finn and Cerda 2015; Takata et al. 2004). Ion channels are also channel proteins which arrange themselves in a way that they form a substrate specific passageway or pore extending from one side of the membrane to the other (Kunzelmann 2005). Pumps are another kind of transporters which generally transport ions against a concentration gradient and the energy for translocation originating from ATP hydrolysis (Piddock 2006). ABC transporters, having 48 members in the human genome, transport a large variety of substances, e.g., ions, amino acids, peptides, sugars, carbohydrates, lipids, xenobiotics and other molecules that are mostly hydrophilic (https://www.boundless.com/). In the last two decades, the critical roles of MPs in various diseases and cancer have been reported (Fletcher et al. 2010). The rest of the transporters, represented in Figure 1, are grouped in the SLC (SoLute Carriers) superfamily that involves 52 families and 395 transporter genes in the human genome including almost 50% of all human transporters (Hediger et al. 2013).

Another important family of MPs, and actually the largest one, represents the G-Protein Coupled Receptor (GPCR) family. GPCRs bind but do not transport solutes and are involved in a myriad of signal transduction pathways triggered by hormones, peptides, proteins, odorants, and other types of ligands (Katritch 2013; Lappano and Maggiolini 2011). In the human genome, there are more than 1000 GPCRs encoded (Zhang et al. 2015). These receptors not only mediate cellular response to a variety of extracellular signals (Lagerstrom and Schioth 2008) but also play a substantial role in signal transduction which is fundamental for various physiological processes (Kypreos et al. 2014; Tyndall and Sandilya 2005). Furthermore, GPCRs were reported to be related in activation of extracellular-signal-regulated kinase (ERK) signaling pathways (Eishingdrelo and Kongsamut 2013) that regulate cell growth, proliferation, and differentiation in response to growth factors, cytokines, and hormones (Robinson and Cobb 1997).

2.3. Membrane Proteins in Human Diseases

As MPs are key players for communication between cells and environment, failure in their function can pave the way for various diseases. In the UniProt database (http://www.uniprot.org/), currently, there are 3254 genes having experimental evidence for being involved in various disease conditions, including cancer, neurologic, systemic and cardiovascular diseases (http://www.proteinatlas.org/humanproteome/). Especially, MPs account for 38% of all the disease-related proteins, Figure 2 (Yildirim et al. 2007). In a recent study, Uhlén and colleagues described the tissue-based map of the human proteome and based on this study, around 60% of the FDA-approved drugs target membrane-bound or secreted proteins (Uhlén et al. 2015).

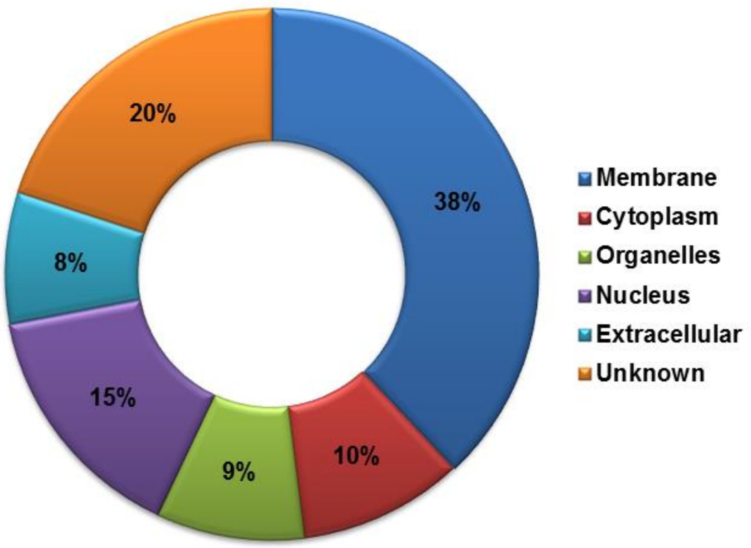

Figure 2. Disease-related proteins. Figure adapted from Yildirim et al. *Nat. Biotech.* 2007.

MPs have been connected to a variety of cancer and disease types (Kampen 2011). For example, ion channels are related with epilepsy, cardiac arrhythmias, skeletal muscle disorders and diabetes (Bronstein-Sitton 2003; Pedersen and Stock 2013). Amino acid transporters have been shown to be responsible in variety of diseases such as epilepsy, ischemia, Alzheimer's disease, Niemann-Pick disease, amyotrophic lateral sclerosis, Huntington's disease, schizophrenia (Bröer and Palacín 2011). The roles of the L-type Amino acid Transporters (LATs) are summarized in Section 2.5.1.1. On GPCRs, the structural and functional knowledge has increased exponentially in the last decade. They represent the largest therapeutic target class in drug discovery (Katritch 2013), especially, 34% of the drugs in the market target GPCRs (Rask-Andersen, Almén, and Schiöth 2011). To date, 24 distinct GPCR crystal structures have been solved, 15 of them are human GPCRs which is of great value for structure-based drug design (Lappano and Maggiolini 2011; Zhang et al. 2015). Unlike for the GPCR class, there are only a few atomic structures of human transporters known, e.g., the glucose transporter 1 from the SLC5 family (Deng et al. 2014), the Rh C glycoprotein (RhCG) from the SLC42 family (Gruswitz et al. 2010) and the ATP-binding cassette transporter (ABCB10) (Shintre et al. 2013).

2.4. Structural Biology of Membrane Proteins

In the history of MP crystallography, in 1985, one very important report on the high-resolution structure of the *Rhodopseudomonas viridis* photosynthetic reaction center structure using X-ray crystallography has shown that MPs could be crystallized (Deisenhofer et al. 1985). This was one of the events, which increased the motivation of the researchers in the structural biology field to apply X-ray crystallography to the other MPs. Of course, solution of the crystal structure of the potassium channel (Zhou et al. 2001) is another landmark in the field, which ultimately led to Roderick MacKinnon's Nobel Prize in Chemistry in 2003.

Knowing that MPs are responsible for numerous cellular processes, one can think of a large architectural diversity for these proteins comparable to water soluble. However, this is not the case because MP structures are restricted by the dielectric gradient of the membrane bilayer (Vinothkumar and Henderson 2010). Due to the high thermodynamic cost of burying polar peptide bonds in a lipid membrane, by using relatively weak van der Waals interactions and hydrogen bonding or electrostatic interactions, MPs fold in certain conformations to minimize their energies (Kennedy 1978; White and Wimley 1999). After folding in the lipid bilayer, not only these forces but also possible lipid-protein interactions that occur on the hydrophobic surface, contribute to the stability of MPs. The main structural elements, observed to date within the transmembrane domains (TMD) of MPs are α-helix bundles and β-strands assembled in β-barrels, Figure 3 (Salom and Palczewski 2011). Compared to β-strands, α-helical bundles show more structural and functional diversity; serving as receptors, channels, transporters, electron transporters, and redox facilitators (Salom and Palczewski 2011). β-Barrels are generally found in Gram-negative bacterial outer membranes as well as in mitochondrial and chloroplast outer membranes. These structures function as channels for nutrients, proteins, hydrophobic toxic substances, and other molecules (Koebnik et al. 2000; Salom and Palczewski 2011). So far, there are around 568 unique (12 from human) MP structures deposited to Protein Data Bank (PDB), and importantly, 90% of these structures are α-helical proteins.

2.4. Structural Biology of Membrane Proteins

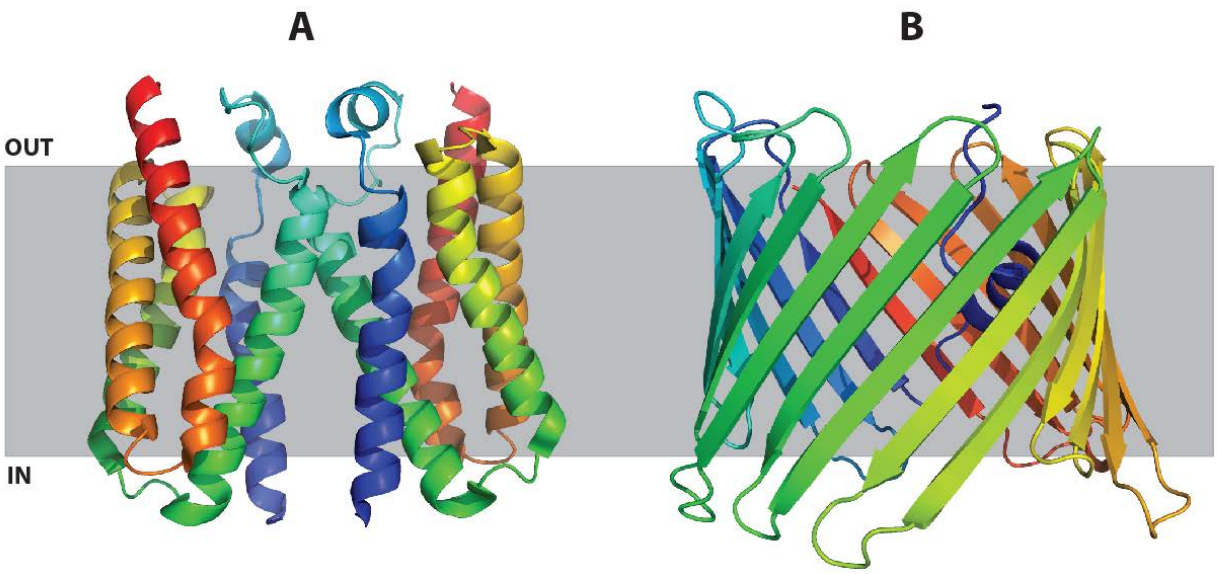

Figure 3. The two architectures observed in MP structures: α-helix bundle (A) and β-barrel (B). (A) X-ray structure of a mitochondrial translocator protein (TSPO) (Guo et al. 2015). (B) Crystal structure of a voltage-dependent anion channel-1 (Ujwal et al. 2008). Both structures are represented as cartoons (representations were done using the program PyMOL, https://www.pymol.org/). The gray rectangle represents the hypothetical position of the lipid bilayer.

The important rule, which holds for both structures, is that the inner part of the protein generally consists of polar and charged residues allowing the passage of water-soluble molecules. The surrounding, lipid neighboring part is amphipathic, consisting of hydrophobic and hydrophilic regions (Alberts et al. 2002; Lodish et al. 2000). Hydrophobic regions, composed of nonpolar and uncharged residues, pass through the membrane and interact with the hydrophobic portion of the lipid molecules (Alberts et al. 2002; Lodish et al. 2000). To fit this rule, certain amino acids have become more abundant in the interior of transmembrane regions, such as leucine, isoleucine, valine, phenylalanine, alanine, glycine, serine, and threonine (Senes et al. 2000). Taken together, these amino acids account for 75% of the amino acids in transmembrane regions. According to this rule, on the hydrophobic lipid-interacting surface, preferentially the hydrophobic residues are located (Senes et al. 2000). Notably, data analyses, using deposited MP structures, showed that α-helical proteins form certain motifs, such as the GxxxG like, polar, leucine zippers, proline and hydrogen bonding motifs (Mackenzie 2006). Unlike α-helical counterparts, in the structure of the β-barrel MPs, there are few defined motifs other than hydrogen bonds (Noinaj et al. 2013). Examples of the motifs observed in this type of MPs are more specific to single cases, e.g., the Trp-rich motif in cholesterol-dependent cytolysins (CDCs) (Galdiero et al. 2007). However, the little information gained from a limited number of β-barrel structures published is not enough to make general statements about repeating patterns.

In the PDB, there are about 110,000 soluble and about 2600 MP structures available (http://www.rcsb.org/ and http://pdbtm.enzim.hu/). Table 1 summarizes how the numbers of the structures of soluble proteins and MPs deposited to the PDB increased in the last decade. The difference between these two values clearly shows how difficult it is to solve the structure of MPs.

Table 1. The numbers of protein structures deposited to Protein Data Bank.

The number of structures in PDB	in 2005	in 2015
Membrane proteins	573	2613
Soluble proteins	33493	110876

The number of protein-coding genes in humans is 20,356, and of these about 5,600 are MPs (Human Protein Atlas, http://www.proteinatlas.org/). So far, only a few percent of the human MPs structures have been solved (http://blanco.biomol.uci.edu/mpstruc/). However, the increase in the last decade is remarkable which is due to the development of new technologies for structural studies/structure analyses and improved methodologies for MP overexpression.

In order to understand the ligand recognition and selectivity, and the detailed working mechanisms of MPs at the molecular level, structural information about these proteins is extremely important. The knowledge of human MP structures will bring new opportunities for the development of new drug candidates, especially for structure-based drug design approaches (Blundell et al. 2002).

2.4.1. Preparation, Isolation and Purification of Membrane Proteins

Biochemical and biophysical studies but especially structure elucidation of MPs require large quantities of purified, homogeneous, stable and functional protein (Robinson and Loll 2011). Therefore, the challenging task is to obtain sufficient amounts of healthy MPs to carry out these studies. The best source to get the target protein is from native tissue. In some cases, researchers could do so and also proceed to the ultimate goal solving the MP's structure. For example, in 1985, the structure of the photosynthetic reaction center from the purple bacterium *Rhodopseudomonas viridis* was solved using native tissue (Deisenhofer et al. 1985). Another example is the first high-resolution crystal structure of a GPCR, which was made possible by purifying the GPCR rhodopsin from native disk membranes isolated from bovine rod outer segment (ROS) (Palczewski et al. 2000). Such examples are scarce, since only few MPs are naturally abundant in their cell membranes. Because of this reason, heterologous expression systems have been established for the overexpression of MPs.

Because working with *Escherichia coli* (*E. coli*) is faster and cheaper than working with eukaryotic protein expression systems, it is for most structural biologists the expression system of choice, preferentially for prokaryotic target MPs (Baker 2010). Most bacterial MPs can be thoroughly produced in *E. coli*; however, as the production of functional human MPs is more complicated, eukaryotic hosts may be required (Grisshammer and Tate 1995; Tate 2001). Nevertheless, by using fusion proteins, low-copy number plasmids, weak promoters, low expression temperatures, and different bacterial strains certain human MPs could be produced in *E. coli* in a functional form (Bernaudat et al. 2011; Galluccio et al. 2012, 2013; Leviatan et al. 2010; Tucker and Grisshammer 1996). The main problem when using prokaryotic hosts arises from lacking post-translational modifications, such as glycosylation that take place during protein biosynthesis in higher organisms (Wagner et al. 2006). Also, the quality of the expressed protein can be altered due to the difference in environmental conditions between *E. coli* and eukaryotic hosts, e.g., lipid composition and absence of sterols (Opekarová and Tanner 2003; Tate 2001).

In the last decade, scientists have been searching for alternatives to *E. coli* for the expression of eukaryotic membrane transport proteins, e.g., yeast species: *Saccharomyces cerevisiae* (*S. cerevisiae*) and *Pichia pastoris* (*P. pastoris*), baculovirus-insect cells, *Lactococcus lactis* (*L. lactis*) and mammalian cell lines. Considering the expression systems used for the eukaryotic MPs of which the structures have been solved, the baculovirus expression system seems to be the most successful method (43%), followed by *P. pastoris* (19%), *S. cerevisiae* (9%), and finally mammalian cells (4%) (He et al. 2014; Parker and Newstead 2014). When we analyze the number of different types of MPs of which the structures have been published and the hosts used for the production of target MPs in these studies, it is obvious that yeast species are superior to the others. These organisms are simple eukaryotes, having similar protein-folding pathways as higher eukaryotes. Moreover, like *E. coli*, yeasts are also cost effective and can be easily handled (Clark et al. 2010; Parker and Newstead 2014). *S. cerevisiae* has itself the cotranslational machinery, post-translational modifications and the lipid environment similar to higher eukaryotes as well as dynamic cellular responses. Genomic studies and high-throughput vector systems have considerably increased the success rate of *S. cerevisiae* as an expression system (Clark et al. 2010; Hays et al. 2009). Cell toxicity and growth defects upon MP expression have been reported to be a common problem in *S. cerevisiae* (Osterberg et al. 2006). The other yeast-based system, the *P. pastoris* system*,* is used not only for the industrial production of industrially relevant proteins but also for heterologous expression of MPs. The main reason for this is that it can reach very high cell densities in normal cultivation flask (up to 130 g/l dry cell weight (Cereghino and Cregg 2000)), resulting in higher expression yields (Alkhalfioui et al. 2011; Macauley-Patrick et al. 2005).

The other alternatives to *E. coli* are *L. lactis* and mammalian cell lines. *L. lactis* is a Gram-positive homofermentative bacterium that has been used for the production of lactic acid in fermented food products (Gasson 1993; de Vos 1999). Thanks to the development of genetic engineering and the molecular characterization tools, *L. lactis* has become useful for the expression of both, prokaryotic and eukaryotic MPs. The main advantages of *L. lactis* are: well-tunable promoter systems, limited proteolytic activity, rare inclusion body formation, has only a single membrane with a high fraction of glycolipids (Frelet-Barrand et al. 2010; Marreddy et al. 2011). Mammalian cells have been used predominantly in the context of mammalian MP expression. In fact, they are often preferred in the production of biotherapeutics because of their ability to perform correct protein folding and post-translational modifications (Eifler et al. 2007; Omasa et al. 2010; Wurm 2004). The common cell lines for the protein expression are human embryonic kidney cells (HEK293), human epithelioid carcinoma (HeLa), baby hamster kidney cells (BHK-21), monkey kidney fibroblast cells (COS-7) and Chinese hamster ovary cells (CHO) (Andréll and Tate 2013). As an example, by using HEK cells, Gruswitz and colleagues could produce nearly 0.5 mg of human RhCG per liter cell culture and solve the crystal structure at 2.1 Å resolution (Gruswitz et al. 2010).

Finally, cell-free expression is an emerging approach that offers promising new perspectives for the sufficient production of MPs for functional and structural applications (Klammt et al. 2004; Savage et al. 2007). This system has certain advantages over the others, for example, several principal problems occurring during production in living host cells are eliminated by using cell-free extracts. Second, toxic or growth inhibitory effects upon MP expression can be avoided, and ^{15}N and ^{13}C isotope labeling of the target MPs can be done rapidly and selectively (Klammt et al. 2004). Furthermore, direct insertion of the MPs into detergent micelles or lipid bilayers can be done by the addition of certain detergents or lipids to the cell extracts (Ishihara et al. 2005; Kalmbach et al. 2007).

2.4.1.1. The Role of Detergent for Purification of Membrane Proteins

As the name implies, MPs are in contact with the membrane being fully or partially embedded in the lipid bilayer. Therefore, MPs need to be extracted from the biological membrane by the help of detergents for biochemical, biophysical and structural analyses.

Structure determination of MPs still remains a big challenge. The main reason for this is the amphipathic nature of these proteins. Compared to soluble proteins, expression level of MPs is very low. MPs consist of hydrophobic domains, which are embedded in the lipid bilayer, and hydrophilic domains that protrude out of the membrane into the cytosol and extracellular space. For structure determination, MPs are therefore extracted from the biological membrane. For purification and crystallization, it is imperative that the target MP is stable and monodisperse in the selected detergent (Garavito et al. 1996; Rosenbusch et al. 2001) or detergent mixtures (Columbus et al. 2009; O'Malley et al. 2011). Therefore, the choice of the optimal detergent(s) is fundamental and will have an enormous impact on the success of the experimental outcome.

In the literature, the important role played by detergent in extraction, stabilization and crystallization of ternary complexes has been recognized and addressed in the past (Arachea et al.

2012; Le Maire, Champeil, and Møller 2000; Ostermeier and Michel 1997; Privé 2007; Seddon et al. 2004). However, the presence of phospholipids in such purified complexes has been to some extent neglected in the past (Kunji et al. 2008), in spite of the important roles of lipids in function,purification and crystallization of MPs (Ilgü et al. 2014). The potential impact of the lipid amount remaining bound to the purified protein was previously shown by Lemieux et al. on the glycerol-3-phosphate transporter (GlpT) (Lemieux et al. 2003). In 2014, we have published a report on the composition of resulting ternary complexes when MPs are purified in detergents of different physicochemical properties (Ilgü et al. 2014). In that work, all three components of the ternary complex of purified MPs have been characterized in a systematic way. The findings presented in this study suggest a strategy to control and to tune the numbers of detergent and endogenous phospholipid molecules bound to MPs (Ilgü et al. 2014). These two parameters are potentially important for the successful crystallization of MPs for structure determination by crystallographic approaches.

2.4.2. Techniques Used for Crystallization, Data Collection and Structure Elucidation of Membrane Proteins

On the way to structure determination of MPs, the main challenge appears at the crystallization of the target protein after protein preparation. To overcome this barrier, in the last decade, nanoliter dispensing robotic systems have also been used as for soluble proteins which increased the rate of efficiency and success of X-ray crystallography in producing high-resolution structures of MPs as well as of soluble proteins (Bill et al. 2011). Utilization of such robotics (TTP Labtech; http://www.ttplabtech.com/) dramatically decreased the amount of protein consumption and made it easy to screen thousands of different crystallization conditions in a 96-well format. The software includes programs for both, sitting drop and hanging drop vapor diffusion methods. In many cases, MP crystallization using conventional techniques fail. Alternatives approaches to the conventional ones are, 2D crystallization (Jap et al. 1992), lipidic bicelle crystallization (Ujwal and Bowie 2011) and lipidic cubic phase crystallization (LCP) (Cherezov 2011) which provide a membrane-mimicking environment that may stabilize MPs and support their crystallization. For the latter two techniques, commercial robotic systems have also been developed which are applicable in the small-scale sample volume range (TTP Labtech; http://www.ttplabtech.com/). In addition to automation, the commercially available sparse matrix screening solutions eased the initial hit search significantly (Hampton Research screen solutions: http://www.hamptonresearch.com/; Molecular Dimensions screen solutions: http://www.moleculardimensions.com/).

Crystal size is another important factor to be considered. The recent developments at the third-generation synchrotron radiation sources allow diffraction data collection from micrometer-sized crystals using a microfocus beam with 5 to 50 µm diameter. Additionally, these microfocus beams enable to screen different regions within the same crystal. This allows data to be collected from the best diffracting area within one crystal (Bowler et al. 2010). Moreover, the installation of the rapid readout silicon pixel Pilatus detectors increased the data quality remarkably by enabling data collection with low noise. Therefore, the detection of weak signals coming from the crystal and the collection of low intensity of X-ray light at high redundancy is now possible. That feature of the Pilatus detectors minimized the radiation damage, which usually occurs during the data collection process. The data collection time decreased significantly: a couple of minutes suffice to collect a full dataset. Another development in third-generation synchrotron radiation sources is the automated sample exchange, which sped up crystal screening significantly. Before starting the data collection, parameters like beam intensity, wavelength, time of exposure, oscillation angle, and detector distance should be optimized depending on the structure determination approach, e.g., Molecular Replacement (MR), Multi wavelength Anomalous Dispersion (MAD), Single wavelength Anomalous Dispersion (SAD) and Multiwavelength Isomorphous Replacement (MIR).

After diffraction data collection, the data is processed where the aim is to extract the relative intensities of the diffracted X-ray beam. Variety of computer programs exist for this purpose, such as Mosflm (Leslie and Powell 2007), part of the CCP4 package (Winn et al. 2011), XDS (Kabsch 2010), HKL-2000 (Otwinowski and Minor 1997) and HKL-3000 (Minor et al. 2006). After processing the data, the next step is to get an initial structural model, which is then automatically and manually refined in order to improve the model. The programs used for these purposes are under the CCP4 (Winn et al. 2011) and Phenix (Adams et al. 2010) software suites.

Alternative techniques to X-ray crystallography used for structural analysis of MPs are Nuclear Magnetic Resonance (NMR) (Marassi and Opella 1998), cryo-Electron Microscopy (cryo-EM) of 2D crystals (Electron Crystallography) (Goldie et al. 2014), Single Particle Analysis (SPA)-cryo-EM (Cheng 2015; Ruprecht and Nield 2001), and Serial Femtosecond Crystallography (SFX) by using X-ray Free-Electron Lasers (XFEL) (Chapman et al. 2011). According to the PDB (http://www.rcsb.org/pdb/) records, X-ray crystallography is the most used technique for structure elucidation of MPs, as of soluble proteins. One reason might be the accessibility of tools for X-ray crystallography, for example, there are 47 synchrotron radiation sources (http://www.lightsources.org/) and many more home sources located at institutions all over the world. In the last decade, 13 free electron lasers have been established (http://www.lightsources.org/) which is recently combined with the SFX technique for structural analysis of MPs (Neutze and Moffat 2012).

SPA-cryo-EM has recently experienced a revolution with the introduction of a new electron detection system (Ruskin et al. 2013). Previously, for detection either charge-coupled device (CCD) or complementary metal oxide semiconductor (CMOS) cameras were used where the electron signals are converted to light signals, thus limiting the resolution (Cheng 2015). Currently developed direct electron detection (DED) camera systems function differently anddetect the electrons directly which results in much better signal-to-noise ratio on electron micrographs (Cheng 2015; McMullan et al. 2009). Because of these recent developments, SPA-cryo-EM is revolutionizing the field of structural biology, including the structure determination of MPs.

Last but not the least, several computational approaches have been developed to predict the model, the secondary structure, the transmembrane spans, and the topology of MPs, such as comparative modeling techniques, *de novo* methods, and molecular dynamics (MD) simulations (Leman et al. 2015).

2.5. Amino Acid Transporters

Amino acids, i.e., the 20 proteinogenic amino acids, are the building blocks of proteins in mammalian cells (Verrey et al. 2009). They have key roles in a myriad of biochemical reactions in living cells, such as in protein synthesis, energy fueling and as precursors for a variety of metabolites (Bröer and Palacín 2011; Verrey et al. 2009). As an example, the neutral amino acids leucine, isoleucine, methionine, and valine are used for the production of brain neurotransmitters, like glutamate or acetylcholine (Bröer 2006). Moreover, it has been shown that the aromatic amino acids serve as precursors for serotonin, noradrenaline and dopamine, and branched-chain amino acids provide tricarboxylic acid intermediates for the production of glutamate and γ-aminobutyric acid (GABA) (Murai et al. 1988). Regardless of being cancerous or not, cells are dependent on external supply to acquire essential amino acids as Thr, Met, Phe, Trp, His, Val, Ile, Leu and Lys. Not only these amino acids, but also the other ones need to be imported from the environment when the endogenous production does not meet the needs, e.g., at a higher proliferation rate (Bhutia et al. 2015; Bröer and Palacín 2011; Verrey et al. 2009). In order to do so, the transport of amino acids through the cell membrane is facilitated by specific amino acid transporters.

In nature, there are large varieties of amino acid transporters. In humans, around 20% of the transporters, described in the SLC series, are classified as amino acid transporters (Bröer and Palacín 2011; Höglund et al. 2011). Some of them are specific to a single amino acid, whereas some are nonspecific and can transport different types of small molecules. Amino acid transporters were grouped in SLC families according to their amino acid sequence identities and similarities (Bröer and Palacín 2011; Wong et al. 2012). Several of these transporters were reported to be expressed in different cell types in the human body and related to varieties of diseases (Table 2) (Bröer and Palacín 2011; Wang and Holst 2015).

2.5. Amino Acid Transporters

Table 2. Amino acid transporters, their properties and involvement in human diseases.

SLC	Acronym	Substrate(s)	Function/coupling ion	Disease/phenotype
SLC1A1	EAAT3	D, E, Cn	System $X^{-}AG$	Huntington's disease, Epilepsy, Ischemia, Alzheimer's disease, Niemann-Pick disease, Obsessive-compulsive disorder
SLC1A2	EAAT2	D, E	System $X^{-}AG$	Amyotrophic lateral sclerosis, Alzheimer's disease, Huntington's disease, Epilepsy, Ischemia, Schizophrenia
SLC1A3	EAAT1	D, E	System $X^{-}AG$	Alzheimer's disease, Huntington's disease, Epilepsy, Cerebellar ataxia type 7, Schizophrenia
SLC1A4	ASCT1	A, S, C	System ASC	
SLC1A5	ASCT2	A, S, C, T, Q	System ASC	Tumor growth
SLC1A6	EAAT5	D, E	System $X^{-}AG$	Spinocerebellar ataxia type 5
SLC1A7	EAAT4	D, E	System $X^{-}AG$	
SLC3A1	rBAT	Trafficking subunits	Heavy chains of heteromeric AAT	Cystinuria, hypotonia-cystinuria syndrome
SLC3A2	4F2hc	Trafficking subunits	Heavy chains of heteromeric AAT	
SLC6A5	GlyT2	G	System Gly	Hyperekplexia, schizophrenia
SLC6A7	PROT	P	Proline transporter	Asthma
SLC6A9	GlyT1	G	System Gly	Hypertension
SLC6A14	$ATB^{0,+}$	All neutral and cationic amino acids	System $B^{0,+}$	Obesity?
SLC6A15	$B^{0}AT2$	P, L, V, I, M	System B^{0}	Major depression
SLC6A17	XT1	L, M, P, C, A, Q, S, H, G	System B^{0}	
SLC6A18	XT2	G, A	System Gly	Hyperglycinuria? Hypertension?
SLC6A19	$B^{0}AT1$	All neutral amino acids	System B^{0}	Hartnup disorder, hypertension?
SLC6A20	XT3	P	System IMINO	Iminoglycinuria
SLC7A1	CAT-1	K, R, O	System y^{+}	
SLC7A2	CAT-2	K, R, O	System y^{+}	
SLC7A3	CAT-3	K, R, O	System y^{+}	
SLC7A5	LAT1/4F2hc*	H, M, L, I, V, F, Y, W	System L	Tumor growth
SLC7A6	$y^{+}LAT2$/4F2hc*	K, R, Q, H, M, L	System $y^{+}L$	
SLC7A7	$y^{+}LAT1$/4F2hc*	K, R, Q, H, M, L, A, C	System $y^{+}L$	Lysinuric protein intolerance
SLC7A8	LAT2/4F2hc*	All neutral amino acids, except P	System L	
SLC7A9	$b^{0,+}AT$/rBAT*	R, K, O, Cn	$b^{0,+}$	Cystinuria
SLC7A10	Asc-1/4F2hc*	G, A, S, C, T	System asc	
SLC7A11	xCT/4F2hc*	D, E, Cn	System $x^{-}c$	
SLC7A12	Asc-2	G, A, S, C, T	System asc	
SLC7A13	AGT1	D, E	Asp, Glu transporter	
SLC16A10	TAT1	W, Y, F	System T	Blue diaper syndrome?
SLC17A6	VGLUT2	E	Vesicular Glu transporter	
SLC17A7	VGLUT1	E	Vesicular Glu transporter	
SLC17A8	VGLUT3	E	Vesicular Glu transporter	Autosomal dominant non-syndromic deafness
SLC25A2	ORC2	K, R, H, O, Cit	Orn/Cit carrier	Autosomal dominant non-syndromic deafness
SLC25A12	AGC1	D, E	Asp/Glu carrier	Global cerebral hypomyelination, autism
SLC25A13	AGC2	D, E	Asp/Glu carrier	Type II citrullinaemia, neonatal intrahepatic cholestasis
SLC25A15	ORC1	K, R, H, O, Cit	Orn/Cit carrier	HHH syndrome
SLC25A18	GC2	E	Glu carrier	
SLC25A22	GC1	E	Glu carrier	Early epileptic encephalopathy
SLC32A1	VIAAT	G,GABA	Vesicular Gly/GABA transporter	Parkinson's disease?
SLC36A1	PAT1	G, P, A	Proton AAT	Hair color (horses), prostate cancer?

Table continued

Table continued

SLC36A2	PAT2	G, P, A	Proton AAT	Iminoglycinuria, peripheral neuropathy
SLC36A4	PAT4	P, W	Amino acid sensor	Diabetes?
SLC38A1	SNAT1	G, A, N, C, Q, H, M	System A	Colorectal cancer?
SLC38A2	SNAT2	G, P, A, S, C, Q, N, H, M	System A	Mammary carcinoma
SLC38A3	SNAT3	Q, N, H	System N	
SLC38A4	SNAT4	G, A, S, C, Q, N, M	System A	
SLC38A5	SNAT5	Q, N, H, A	System N	
SLC43A1	LAT3	L, I, M, F, V	System L	Expression in androgen-dependent cancers
SLC43A2	LAT4	L,I,M,F,V	System L	
Not assigned	Cystinosin	Cn	Lysosomal Cys transporter	Cystinosis

*4F2hc is classified as SLC3A2 and rBAT as SLC3A1. Activities of the corresponding proteins are, in some cases, reported to be dependent on 4F2hc or rBAT and thus they were listed together. Amino acid substrates are given in one-letter code. Other abbreviations: Cit, citrulline; Cn, cystine; O, ornithine; AAT, amino acid transporter and HHH, Hyperornithinemi-hyperammonemia-homocitrullinuria syndrome. The 'Function' column includes references to amino acid transport systems. Uppercase letters indicate Na^+-dependent transporters (except for system L, system T, and the proton amino acid transporters); lower case is used for Na^+-independent transporters (for example asc, y^+ and x^-_c). X^- or x^- indicates transporters for anionic amino acids (as in X^-_{AG} and x^-_c). The subscript AG indicates that the transporter accepts aspartate and glutamate, and the subscript c indicates that the transporter also accepts cysteine. Y^+ or y^+ refer to transporters for cationic amino acids (a Na^+-dependent cationic AAT has not been unambiguously defined and as a result Y^+ is not used), B or b refers to AATs of broad specificity with superscript 0 indicating a transporter accepting neutral amino acids and superscript + indicating a transporter for cationic amino acids. T stands for a transporter for aromatic amino acids, and system N indicates selectivity for amino acids with nitrogen atoms in the side chain. The substrates are indicated by the one-letter code of amino acids. For example, system L refers to a leucine-preferring transporter and system ASC to a transporter preferring alanine, serine, and cysteine. Proline and hydroxyproline are referred to as imino acids. Table adapted from Bröer and Palacín *Biochemical Journal* 2011, and updated with the information from http://slc.bioparadigms.org/.

2.5.1. Amino Acid-Polyamine-Organocation Transporter Superfamily

Amino acid transporters are classified under the Amino acid-Polyamine-organoCation (APC) transporter superfamily which is one of the largest superfamily in nature (Jack et al. 2000; http://www.tcdb.org/search/result.php?tc=2.A.3). Under this family, not only amino acid transporters but also some other transporters of amino acid derivatives and sugars are classified (Schweikhard and Ziegler 2012). The APC superfamily (Clan: APC (CL0062)), according to the protein families database classification (Pfam) (Finn et al. 2014), is comprised of 20 subfamilies with representatives in all kingdoms of life (Finn et al. 2014; Saier 2000). The members of this superfamily have been also classified based on their function as H^+-coupled symporters or substrate-product antiporters, covering a large spectrum of amino acids (Jack et al. 2000). The polypeptide length of these amino acid transport proteins varies between 300 and 900 residues. The prokaryotic proteins are generally smaller while the eukaryotic ones are larger. The transporters display between 10 and 14 TMDs, but most of them adopting a 12 TMD topology with intracellular N- and C-termini (Jack et al. 2000).

The first structural information on APC superfamily was published in 2008 by Casagrande and co-workers, the cryo-EM projection structure of AdiC (L-arginine/agmatine antiporter, a bacterial homolog of LAT1) at 6.5 Å resolution (Casagrande et al. 2008). In the following years, crystal structures of AdiC and other members were reported and a better structural insight on APC superfamily gained (Fang et al. 2009; Gao et al. 2010; Gorbunov et al. 2014; Kowalczyk et al. 2011; Krishnamurthy and Gouaux 2012; Lu et al. 2011; Ma et al. 2012; Perez et al. 2012; Schulze et al. 2010; Shaffer et al. 2009; Watanabe et al. 2010; Weyand et al. 2008; Yamashita et al. 2005). The structural data published in the last couple of years showed that the members of this family share either 5+5 TMD or 7+7 TMD inverted repeat folds (Västermark and Saier 2014). In the first case, the first five TMDs are related to the second five TMDs by a pseudo two-fold symmetry. In the second case, the same relation is observed between the first 7 and the second 7 TMDs (Forrest et al. 2011; Shi 2013). Examples for the 5+5 fold are AdiC, ApcT (Na^+-independent amino acid transporter), GadC (glutamate–GABA antiporter), LeuT (Na^+-dependent leucine transporter), Mhp1 (benzylhydantoin transporter), BetP (Na^+ glycine betaine symporter), CaiT (L-carnitine γ-butyrobetaine antiporter) and SglT (Na^+ galactose symporter), and for 7+7 fold are UraA (uracil transporter) and Prestin/SulP (homology model). From these transporters, AdiC, LeuT, and Mhp1 have two extra TMDs after the second duplicated domain, SglT has four extra C-terminal TMDs, and BetP has two extra TMDs before the first duplicated domain. Although differing in the total number of TMDs, all these transporters share a repeated structural motif of five TM helices.

Previously, Forrest and co-workers mentioned that this conserved helical architecture might be a result of a similar substrate translocation mechanism of these transporters (Forrest and Rudnick 2009). More recently, it was reported that multiple hairpin and domain duplication events occurred most likely during the evolution of the APC superfamily (Västermark and Saier 2014).

2.5.1.1. L-Type Amino Acid Transporters

The L-type Amino acid Transporter (LAT) family involves four Na^+-independent neutral amino acid transporters; LAT1, LAT2, LAT3 and LAT4 (Jack et al. 2000; Wang and Holst 2015). These members are grouped into two sub-families; SLC7 (LAT1 and LAT2) (Fotiadis et al. 2013) and SLC43 (LAT3 and LAT4) (Bodoy et al. 2005, 2013; Wang and Holst 2015). Biochemical characterization studies showed that both LAT1 (SLC7A5) and LAT2 (SLC7A8) are associated with the 4F2hc (4F2 antigen heavy chain; CD98 heavy chain; SLC3A2) glycoprotein, forming a heterodimeric obligatory exchanger with a high affinity for certain amino acids, which is required for its physiological function (Mastroberardino et al. 1998; Kanai et al. 1998; Pineda et al. 1999; Segawa et al. 1999; Meury et al. 2014; Wang and Holst 2015). Because of this reason, they are also called as Heteromeric Amino acid Transporters (HATs). LAT3 (SLC43A1) and LAT4 (SLC43A2) are facilitated diffusers of neutral amino acids with a low affinity, and do not appear to require a binding partner (Babu et al. 2003; Bodoy et al. 2005). Members of the LAT3 and LAT4 families transport a narrow range of neutral amino acids into cells, namely leucine, isoleucine, valine, phenylalanine, and methionine (Babu et al. 2003; Bodoy et al. 2005). LAT1 and LAT2 transport the same amino acids, and additionally tyrosine, histidine and tryptophan, Table 3 (Kanai et al. 1998; Pineda et al. 1999; Rossier et al. 1999; Segawa et al. 1999).

Table 3. Expression of LATs in human body.

Protein	Gene	Substrates	Expression pattern
LAT1	SLC7A5	Leu, Ile, Phe, Met, Tyr, His, Trp, Val	Brain, spleen, placenta, ovary, testis, colon, blood-brain barrier, fetal liver, activated lymphocytes †
LAT2	SLC7A8	Gly, Ala, Ser, Thr, Asn, Gln, Met, Leu, Ile, Val, Phe, Tyr, Trp, His	Jejunum, ileum, kidney, placenta, brain, liver, skeletal muscle, prostate, ovaries, fetal liver, testis and heart ††
LAT3	SLC43A1	Met, Leu, Ile, Val, Phe	Pancreas, skin, muscle, liver, kidney podocytes, prostate †††
LAT4	SLC43A2	Met, Leu, Ile, Val, Phe	Placenta, kidney, peripheral blood leukocytes ††††

Table adapted from Wang and Holst *Am. J. Cancer. Res.* 2015.
† (Mastroberardino et al. 1998; Kanai et al. 1998).
†† (Pineda et al. 1999; Rossier et al. 1999; Segawa et al. 1999).
††† (Babu et al. 2003; Pritchard et al. 2009; Sekine et al. 2009; Wang et al. 2013).
†††† (Bodoy et al. 2005).

L-type amino acid transporters are the major facilitators of selected amino acids, e.g., leucine. The amount of this particular amino acid together with arginine or glutamine is very important (Wang ad Holst 2015) for mTORC1 (mammalian target of rapamycin complex 1) activation. mTORC1 regulates cell growth by modulating many processes, including protein synthesis, ribosome biogenesis and autophagy (Sabatini 2006).

Upregulation of LATs in various cancer types has been reported, and also their critical role for control of protein translation and cell growth through the mTORC1 pathway (Wang and Holst 2015). In order to highlight what type of cancers show a significant increase in LAT expression compared to normal tissue, Wang and colleagues analyzed newly Oncomine microarray/sequencing datasets (Wang et al. 2011; Wang and Holst 2015). The result clearly showed that LAT1 is most commonly upregulated in multiple cancers. LAT2 was shown to be upregulated in 9 different cancer types, but LAT2's role in cancer cell growth is not yet clear. LAT3 and LAT4 showed a more restricted expression pattern in 4 or 5 different cancer types, respectively, and several publications referred on the critical role of LAT3 in prostate cancer (Chuaqui et al. 1997; Cole et al. 1998; Pritchard et al. 2009; Wang et al. 2011, 2013). Moreover, immunohistochemical analyses by Kaira and co-workers in several patient groups have shown that LAT1 overexpression in cancer correlates with cell proliferation and cancer progression. LAT1 is highly expressed in 52% of the large cell neuroendocrine carcinomas of the lung (Kaira et al. 2008 a,b), 50% of pleural mesothelioma (Kaira et al. 2011), 75% of thymic carcinomas (Kaira et al. 2009 a), 25% of high-grade gliomas (Kobayashi et al. 2008), 61% of tongue cancer (Toyoda et al. 2014), 53% of pancreatic cancer (Kaira et al. 2012) and 61% in hepatocellular carcinoma (Namikawa et al. 2014). Also, in these studies LAT1 expression correlates with proliferation marker Ki-67 (expression of the human Ki-67 protein is strictly associated with cell proliferation (Scholzen and Gerdes 2000)), suggesting that LAT1 is important for proliferation in cancer cells (Ichinoe et al. 2011; Imai et al. 2009; Kaira et al. 2009 a,b; Kaira et al. 2008 b,c; Kaira et al. 2012; Namikawa et al. 2014; Toyoda et al. 2014). Furthermore, different research groups have used LAT1 as biomarker for malignant cancer by applying Kaplan-Meier analysis, which measures the fraction of subjects surviving for a certain time period after treatment (Goel et al. 2010). This analysis showed that low LAT1 expression patients had significantly longer overall survival compared to the patients having high expression indicating that LAT1 could be a prognostic marker for predicting poor outcome after surgery (Kaira et al. 2012, 2013; Namikawa et al. 2014). Similarly, LAT1 expression in prostate cancer correlates with prognosis in poor survival patients (Sakata et al. 2009).

Even though there is a wealth of data from functional characterization studies of LATs, especially of LAT1, there is little information about the structure of these transporters. So far, Geier and colleagues constructed structural models of LAT1 based on structures of homologous APC family transporters from prokaryotic origin, namely AdiC and ApcT (Geier et al. 2013). The crystal structure of human 4F2hc ectodomain was solved in 2007 (Fort et al. 2007). Recently, the supramolecular architecture of LAT2, together with the heavy chains partner 4F2hc, was investigated using TEM and extensive crosslinking studies (Rosell et al. 2014). An improved version of this 3D map was recently published by Meury and co-workers (Meury et al. 2014). However, so far, a model of near atomic resolution is still missing and therefore as a future perspective, this family has a great potential for structural investigations regardless of the technique used.

2.5.1.1.1. L-Arginine/Agmatine Antiporter, a Structural Model Protein for LAT1

The Arg/Agm antiporter (AdiC) has been defined as the key component of the Arg-dependent acid-resistance system of *E. coli* and other Gram-negative bacteria (Audia et al. 2001), which enables to keep the cytoplasm above pH 5 during exposure to an extremely acidic environment. The other actor in this system is the cytoplasmic acid-activated arginine decarboxylase AdiA, which decarboxylates Arg to Agm by consuming a proton from the cytoplasm (Figure 4). The produced Agm, which carries the removed 'virtual proton' leaves then the bacterium through the antiporter AdiC, which exchanges in a 1:1 stoichiometry Agm by Arg from the outside, e.g., from the gastric juice. The free energy of Arg decarboxylation drives the continuous pumping of protons out of the cell. AdiC is a member of the APC superfamily, having 17-20% amino acid sequence identity to human LATs (Jack et al. 2000). Even though the amino acid sequence identity is low, in the absence of higher homologues, this transporter has potential to be used as a structural model for such transporters.

2.5.1.1.1. L-Arginine/Agmatine Antiporter, a Structural Model Protein for LAT1

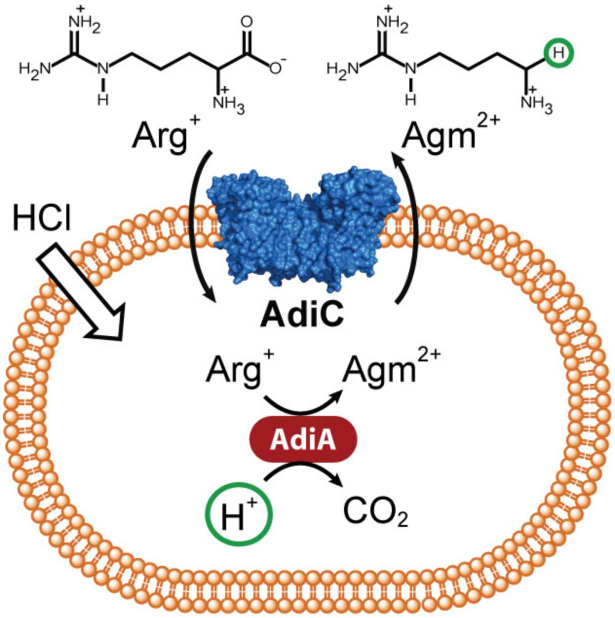

Figure 4. Schematic illustration of the arginine-dependent acid-resistance system of E. coli. Arg is decarboxylated in the cytoplasm by the acid-activated arginine-decarboxylase AdiA thereby consuming one proton (encircled in green). This 'virtual proton' ends up as C-H bond at the 1-position of the product 1-amino-4-guanidino-n-butane (Agm; 'virtual proton' indicated by a green circle) and is removed from the cell through the AdiC-mediated Arg/Agm exchange across the inner membrane.

In the last fifteen years, the working mechanism of AdiC has been characterized in terms of substrate binding and transport pathway using wt and different site-specific mutants. In early 2000, Audia and colleagues defined and worked on Arg-dependent acid-resistance in *E. coli*; not specifically with AdiC, but with the whole system (Audia et al. 2001). Then the AdiA (arginine decarboxylase) and AdiC genes were cloned, expressed, and the latter defined as an integral MP. AdiC was probed for transport of Arg and AdiA for the conversion to Agm; the decarboxylation product of Arg (Gong et al. 2003). Later on, Fang and colleagues reconstituted the detergent-solubilized AdiC into proteoliposomes and studied the kinetics with Arg and other substrate analogs (Fang et al. 2007).

In terms of structure, in 2008, Casagrande and colleagues published the projection structure of AdiC W293L mutant (defined as being the key residue for protein-ligand interaction) at 6.5 Å resolution using cryo-EM and electron crystallography (Casagrande et al. 2008). In the following year, the first crystal structure of AdiC was published at 3.6 Å resolution in the substrate-free, outward-open conformation (Gao et al. 2009), followed by a second one from *Salmonella enterica* by Fang et al. in the same conformation at a slightly better resolution of 3.2 Å (Fang et al. 2009) complexed with an Fab fragment. After having the structure solved, these two groups screened several point mutants in order to learn more about the transport mechanism. Not long after, Gao and colleagues reported another structure, this time of the AdiC-N22A-L123W double mutant (Gao et al. 2010). This time, it was the Arg-bound, outward-facing occluded state at 3.0 Å resolution. As they reported, this mutant showed six times better binding affinity to Arg compared to wt; K_m values were reported as 27 µM and 162 µM, respectively. Most likely, this empowered interaction increased the probability of having better diffracting crystals by forming more rigid bodies. The next crystal structure of a mutant AdiC protein was published in 2011, again at 3.0 Å resolution. The mutation introduced (N101A) was described to lead to a severe translocation defect (Kowalczyk et al. 2011). Interestingly, the authors of this work could co-crystallize AdiC-N101A with the substrate Arg in binding site again in the outward-open conformation.

The steady-state kinetic analyses of AdiC in a sided fashion showed that the two sides of AdiC have different pH sensitivities; AdiC has the peak activity at pH 4 as the extracellular side is acidified, while the cytoplasmic side shows an optimal pH of 5.5 (Tsai et al. 2012). More recently, a critical pH-sensing amino acid, Tyr74 in AdiC was identified (Wang et al. 2014). The replacement of Tyr74 by any other amino acid (except Phe) resulted in a loss of pH dependence (Wang et al. 2014). To briefly summarize, there are four crystal structures of AdiC, but all are at moderate resolutions and in outward-facing conformation. In addition to the information in the literature, for the first time, we could crystallize and solve the AdiC-wt structure with and without an Agm molecule bound, again in outward-open conformation at the unprecedented resolutions of 2.6 and 2.2 Å, respectively (manuscript enclosed) which is a significant improvement for the homology modeling studies.

2.6. Alternative Access Mechanism of Substrate Translocation

The alternative access mechanism was proposed nearly 50 years ago by Jardetzky using a Na^+/K^+ pump (Jardetzky 1966) which became a model to explain the working mechanism of transporter proteins. Since then, many studies/reports have been published supporting the initial idea that for substrate translocation across biological membranes, the substrate-binding site must be alternatively exposed to either side of the membrane, in other word, the ligand is not exposed to both sides of the membrane at the same time (Yan 2013). During the transport of substrate and ions, transporters undergo specific conformational changes, e.g., the outward-facing (apo), outward- or inward-facing occluded (substrate-bound) and inward-facing (apo) states (Figure 5) (Fotiadis et al. 2013; Krishnamurthy et al. 2009; Rudnick 2012). The occluded states involve a gating mechanism, where the ligand is trapped, which is generally assisted by an aromatic residue (Shi 2013).

2.6. Alternative Access Mechanism of Substrate Translocation

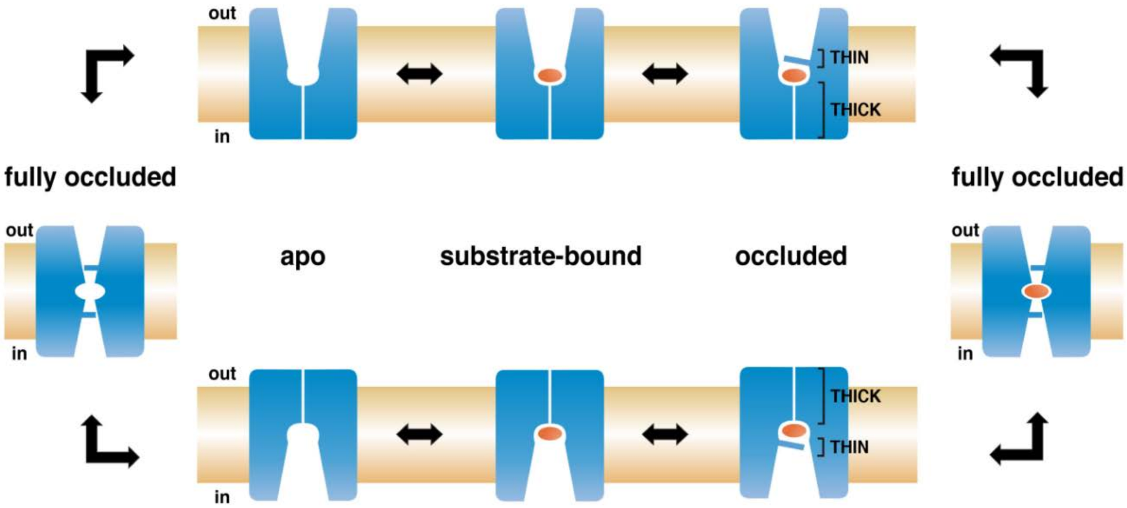

Figure 5. Alternative access mechanism model for secondary active transporters.
Substrate (red ellipse) binding to either the outward- or inward-facing apo-state of the transporter induces an occlusion of the binding site by the thin gate. The thick gate prevents diffusion of the substrate to the inside of the membrane. Translocation of the substrate to the inside of the membrane requires a transient, fully occluded transporter conformation. Figure adapted from Fotiadis et al. *Mol. Asp. of Med.* 2011.

So far, using experimental data that is the primarily structural information, researchers have applied this model to different types of transporters such as LeuT (Krishnamurthy and Gouaux 2012; Krishnamurthy et al. 2009), SglT (Na^+-coupled glucose transporter) (Forrest and Rudnick 2009), Mhp1 (sodium-hydantoin transporter) (Shimamura et al. 2010; Weyand et al. 2011), AdiC (Kowalczyk et al. 2011), LacY (lactose permease) (Kaback et al. 2011), BetP (Perez et al. 2012), MATE (multidrug and toxic compound extrusion transporter) (Lu et al. 2013), AcrB (proton/drug antiporter) (Eicher et al. 2014), ASBT (bile acid transporter) (Zhou et al. 2014). A similar mechanism has been also proposed for ABC transporters, which share probably a high degree of mechanistic similarities, e.g., inward-facing, outward-facing, inward- and outward-facing occluded states, Figure 6 (Dawson et al. 2007; Procko et al. 2009).

2.6. Alternative Access Mechanism of Substrate Translocation

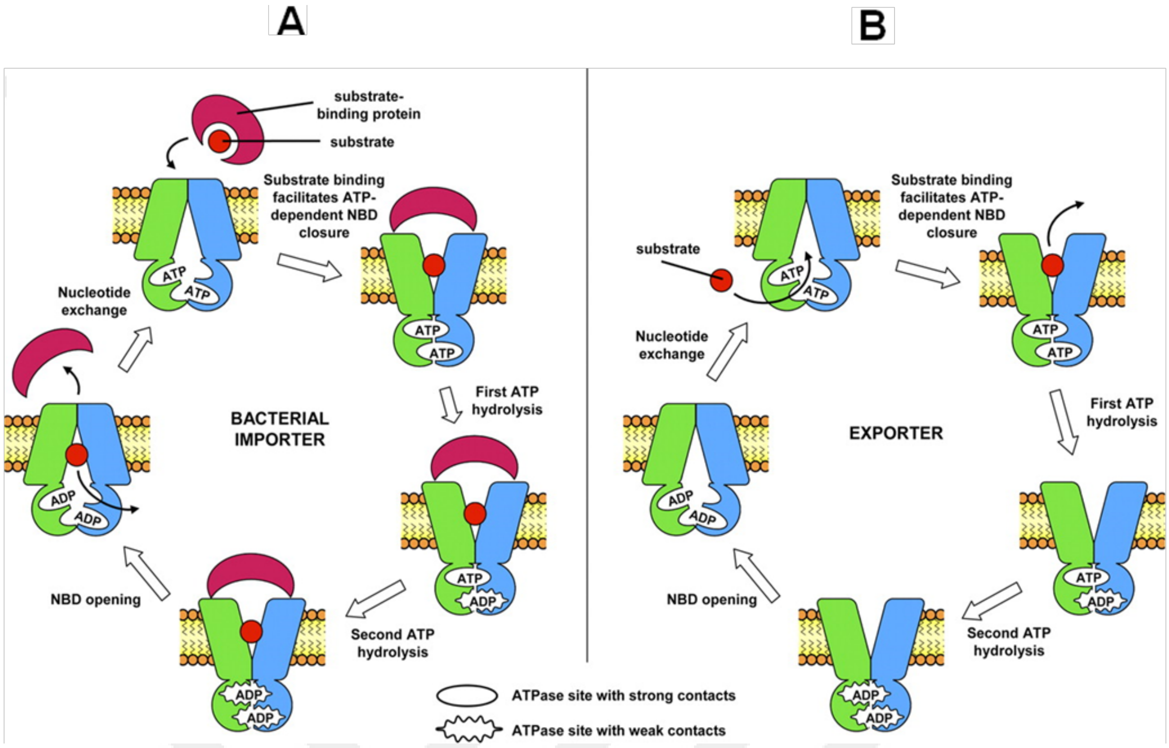

Figure 6. Proposed transport mechanism of ABC transporters.
(A) General mechanism of a bacterial importer. The Nucleotide-Binding Domains (NBD) are open in the resting state at the top left. Association with a loaded substrate-binding protein promotes ATP-dependent NBD closure, causing the TMDs to expose an extracytosolic substrate-binding cavity. The substrate-binding protein releases its substrate into the binding cavity of transporter. In order to reopen the NBDs, contacts at both ATPase sites need to be weakened, likely requiring hydrolysis of both ATP molecules for transporters with 2 consensus sites. When the NBDs return to the open conformation, the substrate-binding cavity returns to facing the cytosol as well, and substrate is released. (B) General mechanism for an exporter with 2 consensus sites. The same steps are required as for import pathway, except for that the transporter conformations that bind substrate with high or low affinity are switched. Figure adapted from Procko et al. *FASEB Journal* 2009.

Developments of new surfactants, crystallographic techniques, and technologies made the crystallization of MPs somehow easier, which is reflected in the number of structures published in the last decade (Section 2.4). Although providing different 'snapshots' of a specific transporter in different conformations is challenging, regardless of the conformation, any kind of structure of it with a reasonable resolution can help us to understand its molecular working mechanism. For this, further investigations are of great importance in order to uncover the missing parts of the substrate translocation within the transport pathways of the target MPs.

3. Conclusion

Structural information on membrane proteins plays a critical role to understand the molecular mechanism of ligand recognition, transport and selectivity. Thanks to the technological and methodological developments in the MP crystallization field (Section 2.4.2), the number of structures published in the last decade has increased significantly (Table 1). However, structural information on MP still remains scarce compared to water-soluble proteins, and thus insufficient to understand the molecular working mechanisms of MPs.

For structural studies, and biochemical and biophysical characterization, MPs need to be extracted from their native environment, the lipid bilayer, by the help of detergents. In the literature, the information about the amounts of detergent and endogenous phospholipid molecules bound to MPs after purification was largely lacking (Kunji et al. 2008; Privé 2007). Part of the work carried out in this thesis was dedicated to have a better understanding on this issue. In other words, the goal of this project was to determine the detergent and lipid content of purified transporters, and at the same time to investigate how significant the detergent selection for the purification could be. For this purpose, we carried out a systematic study with three model integral MPs of different oligomeric states purified in nine different commonly used detergents (Ilgü et al. 2014). The samples were characterized biochemically, e.g., the detergent-binding capacities and phospholipid contents of the model proteins were determined and compared. In the light of these results, we can clearly state that purified integral MPs are ternary complexes consisting of protein, lipid, and detergent (Ilgü et al. 2014). The insights gained from this study on ternary complexes can be summarized as follows. First, the amount of detergent and endogenous phospholipids bound to purified proteins are dependent on the size of the hydrophobic lipid-accessible protein surface areas and the physicochemical properties of the detergents used. Second, the size of the detergent-lipid belt surrounding the hydrophobic lipid-accessible surface of purified MPs can be tuned by appropriate choice of detergent. Third, we demonstrated that NG and Cymal-5 have exceptional delipidating properties on MPs during purification. Fourth, we demonstrated that the types of endogenous phospholipids bound to MPs can vary depending on the detergent used for solubilization and purification. Additionally and importantly, SEC is a valid and reliable method for estimating the molecular mass of ternary complexes of integral MPs. Therefore, all these findings together propose a strategy to control and tune the numbers of detergent and endogenous phospholipid molecules bound to MPs, which have great impact on the successful crystallization of MPs and consequently for structure determination by crystallographic approaches.

The second main aim of this thesis was to gain structural insights on the working mechanism of AdiC at the molecular level. In the literature, there are currently four structures at moderate resolutions of different AdiC-mutants with and without bound Arg (summarized in

Section 2.5.1.1). By applying the above-mentioned strategy (Section 2.4.1.1), we could minimize the detergent-lipid belt around AdiC, thus increasing the possibility of crystal contact formation. As a result, we could crystallize and solve the crystal structure of the AdiC-wt at the unprecedented resolution of 2.2 Å in the substrate-free, outward-open conformation, and for the first time with the substrate Agm at 2.6 Å resolution in the same conformation (Section 2.5.1.1.1). Previously, an alternative binding site for Agm compared to Arg was proposed by Gao and colleagues (Gao et al. 2010). The Agm-bound crystal structure showed that the Agm molecule binds to the same binding pocket as Arg in the outward-facing occluded conformation. In the light of our finding, for the first time, we could explain the conformational states involved in Agm release. In order to understand the transport mechanism completely, yet the missing points in the ligand recognition and transport mechanism should be enlightened. For instance, we have still no information about the inward-facing conformation. It is still unclear where the Agm molecule binds after production in the cell and where Arg binds before it is released into the cytoplasm. To this aim and to understand the whole antiport mechanism of Arg/Agm, crystal structures of the inward-facing conformations are necessary (e.g., with and without substrate, occluded, etc.).

For AdiC itself, the story of Arg-dependent acid resistance mechanism has been explained to a certain extent. AdiC has its own significance as being a part of the acid-resistance system in *E. coli*. Apart from that, AdiC structures have the potential to be used as structural bases for homology modeling of SCL7 family members, e.g., LATs, and other members of the APC superfamily. AdiC has already been used as a model for a sodium-independent exchanger of amino acids, thyroid hormones, and drugs (LAT1) (Geier et al. 2013) and for a thyroid hormone transporter (LAT2) (Hinz et al. 2015). Due to low homology of transporters from lower organisms to human-sourced counterparts, there are a limited number of examples where such transporters have been used for homology modeling. As a future perspective, it is a crucial need to have structures of transporters with higher homologies (amino acid sequence identities and similarities) to human membrane transporters or the best directly the human structures to understand the working mechanisms at the molecular level of these important MPs and for structure-based drug design.

4. Outlook

We have investigated the amounts of detergent and phospholipid molecules bound to the purified MPs and the types of phospholipids bound to the purified AdiC with two detergents; *n*-dodecyl-*β*-D-maltoside (DDM) and *n*-octyl-*β*-D-maltoside (OM) (Ilgü et al. 2014). Our investigation showed that delipidation can occur selectively during purification which is leaving some open questions behind. For example, a research on the effect(s) of the other detergent types with different hydrophobic tail or sugar in the head group on delipidation could bring more details on the selectivity of the detergent on delipidation. Also, doing the same experiments with the proteins expressed in different organisms might shed more light on this topic and possible detergent-lipid interactions.

We have reported, for the first time, the Agm-bound crystal structure of AdiC (manuscript enclosed) which paved the way to explain the Agm release to the periplasmic side. To understand the working mechanisms of AdiC completely, the structural investigation on the other conformations of AdiC is a crucial requirement for the future studies. Apart from that, even though AdiC has a limited homology to LATs, it is of a remarkable value to have the AdiC structure with a better resolution for the homology modeling studies. However, in the future, structural investigation of transporters with higher homologies to the transporters in SLC7 family that could potentially increase the quality and accuracy of the models to be used for the structure-based drug design.

5. References

Adams, Paul D. et al. 2010. “PHENIX: A Comprehensive Python-Based System for Macromolecular Structure Solution.” *Acta Crystallographica Section D: Biological Crystallography* 66(2):213–221.

Alberts, Bruce et al. 2002. *Molecular Biology of the Cell*. 4th ed. edited by D. J. Dries. Lippincott Williams & Wilkins, Inc.

Alkhalfioui, Fatima, Christel Logez, Olivier Bornert, and Renaud Wagner. 2011. “Expression Systems: Pichia Pastoris.” Pp. 75–108 in *Production of Membrane Proteins: Strategies for Expression and Isolation*, edited by A. S. Robinson. Weinheim, Germany: Wiley-VCH Verlag GmbH & Co. KGaA.

Andréll, Juni and Christopher G. Tate. 2013. “Overexpression of Membrane Proteins in Mammalian Cells for Structural Studies.” *Molecular Membrane Biology* 30(1):52–63.

Arachea, Buenafe T. et al. 2012. “Detergent Selection for Enhanced Extraction of Membrane Proteins.” *Protein Expression and Purification* 86(1):12–20.

Audia, J. P., C. C. Webb, and J. W. Foster. 2001. “Breaking through the Acid Barrier: An Orchestrated Response to Proton Stress by Enteric Bacteria.” *International Journal of Medical Microbiology* 291(2):97–106.

Babu, Ellappan et al. 2003. “Identification of a Novel System L Amino Acid Transporter Structurally Distinct from Heterodimeric Amino Acid Transporters.” *Journal of Biological Chemistry* 278(44):43838–43845.

Baker, Monya. 2010. “Making Membrane Proteins for Structures: A Trillion Tiny Tweaks.” *Nature Methods* 7(6):429–434.

Bernaudat, Florent et al. 2011. “Heterologous Expression of Membrane Proteins: Choosing the Appropriate Host.” *PLoS One* 6(12):1–17.

Bhutia, Y. D., E. Babu, S. Ramachandran, and V. Ganapathy. 2015. “Amino Acid Transporters in Cancer and Their Relevance to ‘Glutamine Addiction’: Novel Targets for the Design of a New Class of Anticancer Drugs.” *Cancer Research* 75(9):1782–1788.

Bill, Roslyn M. et al. 2011. “Overcoming Barriers to Membrane Protein Structure Determination.” *Nature Biotechnology* 29(4):335–340.

Blundell, Tom L., Harren Jhoti, and Chris Abell. 2002. “High-Throughput Crystallography for Lead Discovery in Drug Design.” *Nature Reviews. Drug Discovery* 1:45–54.

Bodoy, Susanna et al. 2005. “Identification of LAT4, a Novel Amino Acid Transporter with System L Activity.” *Journal of Biological Chemistry* 280(12):12002–12011.

Bodoy, Susanna, Dimitrios Fotiadis, Claudia Stoeger, Yoshikatsu Kanai, and Manuel Palacín. 2013. “The Small SLC43 Family: Facilitator System L Amino Acid Transporters and the Orphan EEG1.” *Molecular Aspects of Medicine* 34(2-3):638–645.

Bowler, Matthew W. et al. 2010. “Diffraction Cartography: Applying Microbeams to Macromolecular Crystallography Sample Evaluation and Data Collection.” *Acta Crystallographica Section D: Biological Crystallography* 66(8):855–864.

Bröer, Stefan. 2006. “The SLC6 Orphans Are Forming a Family of Amino Acid Transporters.” *Neurochemistry International* 48(6-7):559–567.

Bröer, Stefan and Manuel Palacín. 2011. “The Role of Amino Acid Transporters in Inherited and Acquired Diseases.” *Biochemical Journal* 436:193–211.

Bronstein-Sitton, Noemí. 2003. “Ion Channels in Cancer.” *Modulator* (17):1–7.

5. References

Casagrande, Fabio et al. 2008. "Projection Structure of a Member of the Amino Acid/polyamine/organocation Transporter Superfamily." *Journal of Biological Chemistry* 283(48):33240–33248.

Cereghino, J. L. and J. M. Cregg. 2000. "Heterologous Protein Expression in the Methylotrophic Yeast Pichia Pastoris." *FEMS Microbiology Reviews* 24(1):45–66.

Chapman, Henry N. et al. 2011. "Femtosecond X-Ray Protein Nanocrystallography." *Nature* 470(7332):73–77.

Cheng, Yifan. 2015. "Single-Particle Cryo-EM at Crystallographic Resolution." *Cell* 161(3):450–457.

Cherezov, Vadim. 2011. "Lipidic Cubic Phase Technologies for Membrane Protein Structural Studies." *Current Opinion in Structural Biology* 21(4):559–566.

Chuaqui, Rodrigo F. et al. 1997. "Identification of a Novel Transcript up-Regulated in a Clinically Aggressive Prostate Carcinoma." *Urology* 50(2):302–307.

Clark, Kathleen M. et al. 2010. "Purification of Transmembrane Proteins from Saccharomyces Cerevisiae for X-Ray Crystallography." *Protein Expression and Purification* 71(2):207–223.

Cole, K. A. et al. 1998. "cDNA Sequencing and Analysis of POV1 (PB39): A Novel Gene up-Regulated in Prostate Cancer." *Genomics* 51(2):282–287.

Columbus, Linda et al. 2009. "Mixing and Matching Detergents for Membrane Protein NMR Structure Determination." *Journal of the American Chemical Society* 131(21):7320–7326.

Dawson, Roger J. P., Kaspar Hollenstein, and Kaspar P. Locher. 2007. "Uptake or Extrusion: Crystal Structures of Full ABC Transporters Suggest a Common Mechanism." *Molecular Microbiology* 65(2):250–257.

Deisenhofer, J., O. Epp, K. Miki, R. Huber, and H. Michel. 1985. "Structure of the Protein Subunits in the Photosynthetic Reaction Centre of Rhodopseudomonas Viridis at 3A Resolution." *Nature* 318(6047):618–624.

Deng, Dong et al. 2014. "Crystal Structure of the Human Glucose Transporter GLUT1." *Nature* 510(7503):121–125.

Dobson, László, István Reményi, and Gábor E. Tusnády. 2015. "The Human Transmembrane Proteome." *Biology Direct* 10(1):1–18.

Eicher, Thomas et al. 2014. "Coupling of Remote Alternating-Access Transport Mechanisms for Protons and Substrates in the Multidrug Efflux Pump AcrB." *eLife* 3:1–26.

Eifler, Nora et al. 2007. "Functional Expression of Mammalian Receptors and Membrane Channels in Different Cells." *Journal of Structural Biology* 159:179–193.

Eishingdrelo, Haifeng and Sathapana Kongsamut. 2013. "Minireview: Targeting GPCR Activated ERK Pathways for Drug Discovery." *Current Chemical Genomics and Translational Medicine* 7:9–15.

Engelman, Donald M. 2005. "Membranes Are More Mosaic than Fluid." *Nature* 438(7068):578–580.

Fang, Yiling et al. 2009. "Structure of a Prokaryotic Virtual Proton Pump at 3.2 A Resolution." *Nature* 460(7258):1040–1043.

Fang, Yiling, Ludmila Kolmakova-Partensky, and Christopher Miller. 2007. "A Bacterial Arginine-Agmatine Exchange Transporter Involved in Extreme Acid Resistance." *Journal of Biological Chemistry* 282(1):176–182.

Finn, Robert D. et al. 2014. "Pfam: The Protein Families Database." *Nucleic Acids Research* 42(D1):222–30.

Finn, Roderick Nigel and Joan Cerda. 2015. "Evolution and Functional Diversity of Aquaporins." *The Biological Bulletin* 229:6–23.

Fletcher, Jamie I., Michelle Haber, Michelle J. Henderson, and Murray D. Norris. 2010. "ABC Transporters in Cancer: More than Just Drug Efflux Pumps." *Nature Reviews. Cancer* 10(2):147–156.

Forrest, Lucy R., Reinhard Krämer, and Christine Ziegler. 2011. "The Structural Basis of Secondary Active

Transport Mechanisms.” *Biochimica et Biophysica Acta* 1807(2):167–188.

Forrest, Lucy R. and Gary Rudnick. 2009. “The Rocking Bundle: A Mechanism for Ion-Coupled Solute Flux by Symmetrical Transporters.” *Physiology* 24:377–386.

Fort, Joana et al. 2007. “The Structure of Human 4F2hc Ectodomain Provides a Model for Homodimerization and Electrostatic Interaction with Plasma Membrane.” *Journal of Biological Chemistry* 282(43):31444–31452.

Fotiadis, Dimitrios, Yoshikatsu Kanai, and Manuel Palacín. 2013. “The SLC3 and SLC7 Families of Amino Acid Transporters.” *Molecular Aspects of Medicine* 34(2-3):139–158.

Frelet-Barrand, Annie, Sylvain Boutigny, Edmund R. S. Kunji, and Rolland Norbert. 2010. “Membrane Protein Expression in Lactococcus Lactis.” Pp. 67–86 in *Heterologous Expression of Membrane Proteins - Methods and Protocols*, edited by I. Mus-Veteau. London: Humana Press.

Galdiero, Stefania, Massimiliano Galdiero, and Carlo Pedone. 2007. “Beta-Barrel Membrane Bacterial Proteins: Structure, Function, Assembly and Interaction with Lipids.” *Current Protein and Peptide Science* 8(1):63–82.

Galluccio, Michele et al. 2012. “Over-Expression in E. Coli and Purification of the Human OCTN2 Transport Protein.” *Molecular Biotechnology* 50(1):1–7.

Galluccio, Michele, Piero Pingitore, Mariafrancesca Scalise, and Cesare Indiveri. 2013. “Cloning, Large Scale over-Expression in E. Coli and Purification of the Components of the Human LAT 1 (SLC7A5) Amino Acid Transporter.” *Protein Journal* 32(6):442–448.

Gao, Xiang et al. 2009. “Structure and Mechanism of an Amino Acid Antiporter.” *Science (New York, N.Y.)* 324(5934):1565–1568.

Gao, Xiang et al. 2010. “Mechanism of Substrate Recognition and Transport by an Amino Acid Antiporter.” *Nature* 463(7282):828–832.

Garavito, R. M., D. Picot, and P. J. Loll. 1996. “Strategies for Crystallizing Membrane Proteins.” *Journal of Bioenergetics and Biomembranes* 28(1):13–27.

Gasson, MJ. 1993. “Progress and Potential in the Biotechnology of Lactic Acid Bacteria.” *FEMS Microbiology Reviews* 12(1-3):3–19.

Geier, Ethan G. et al. 2013. “Structure-Based Ligand Discovery for the Large-Neutral Amino Acid Transporter 1, LAT-1.” *Proceedings of the National Academy of Sciences of the United States of America* 110(14):5480–5485.

George, Alfred L. 2004. “Inherited Channelopathies Associated with Epilepsy.” *Epilepsy Currents* 4(2):65–70.

Goel, Manish Kumar, Pardeep Khanna, and Jugal Kishore. 2010. “Understanding Survival Analysis: Kaplan-Meier Estimate.” *International Journal of Ayurveda Research* 1(4):274–278.

Goldie, K. N. et al. 2014. “Cryo-Electron Microscopy of Membrane Proteins.” *Methods in Molecular Biology* 1117:325–341.

Gong, Shimei, Hope Richard, and John W. Foster. 2003. “YjdE (AdiC) Is the Arginine : Agmatine Antiporter Essential for Arginine-Dependent Acid Resistance in Escherichia Coli.” 185(15):4402–4409.

Gorbunov, Dmitry et al. 2014. “Molecular Architecture and the Structural Basis for Anion Interaction in Prestin and SLC26 Transporters.” *Nature communications* 5(3622):1–13.

Grisshammer, R. and C. G. Tate. 1995. “Overexpression of Integral Membrane Proteins for Structural Studies.” *Quarterly Reviews of Biophysics* 28(3):315–422.

Gruswitz, Franz et al. 2010. “Function of Human Rh Based on Structure of RhCG at 2.1 A.” *Proceedings of the National Academy of Sciences of the United States of America* 107(21):9638–9643.

Guo, Youzhong et al. 2015. “Structure and Activity of Tryptophan-Rich TSPO Proteins.” *Science* 347(6221):551–555.

5. References

Hays, Franklin A. et al. 2009. “Ratiocinative Screen of Eukaryotic Integral Membrane Protein Expression and Solubilization for Structure Determination.” *Journal of Structural and Functional Genomics* 10(1):9–16.

He, Yuan, Kan Wang, and Nieng Yan. 2014. “The Recombinant Expression Systems for Structure Determination of Eukaryotic Membrane Proteins.” *Protein & Cell* 5(9):658–672.

Hediger, Matthias a, Benjamin Clémençon, Robert E. Burrier, and Elspeth a Bruford. 2013. “Molecular Aspects of Medicine The ABCs of Membrane Transporters in Health and Disease.” *Molecular Aspects of Medicine* 34(2-3):95–107.

von Heijne, G. 2007. “The Membrane Protein Universe: What’s out There and Why Bother?” *Journal of Internal Medicine* 261(6):543–557.

Hinz, Katja Meyer, Anita Kinne, Ralf Schülein, Josef Köhrle, and Gerd Krause. 2015. “Structural Insights Into Thyroid Hormone Transport Mechanisms of the L-Type Amino Acid Transporter 2.” *Molecular Endocrinology* 29(6):933–942.

Höglund, Pär J., Karl J. V Nordström, Helgi B. Schiöth, and Robert Fredriksson. 2011. “The Solute Carrier Families Have a Remarkably Long Evolutionary History with the Majority of the Human Families Present before Divergence of Bilaterian Species.” *Molecular Biology and Evolution* 28(4):1531–1541.

Ichinoe, Masaaki et al. 2011. “High Expression of L-Type Amino-Acid Transporter 1 (LAT1) in Gastric Carcinomas: Comparison with Non-Cancerous Lesions.” *Pathology International* 61(5):281–289.

Ilgü, Hüseyin et al. 2014. “Variation of the Detergent-Binding Capacity and Phospholipid Content of Membrane Proteins When Purified in Different Detergents.” *Biophysical Journal* 106(8):1660–1670.

Imai, Hisao et al. 2009. “L-Type Amino Acid Transporter 1 Expression Is a Prognostic Marker in Patients with Surgically Resected Stage I Non-Small Cell Lung Cancer.” *Histopathology* 54(7):804–813.

Ishihara, Goshi et al. 2005. “Expression of G Protein Coupled Receptors in a Cell-Free Translational System Using Detergents and Thioredoxin-Fusion Vectors.” *Protein Expression and Purification* 41(1):27–37.

Jack, D. L., I. T. Paulsen, and Jr Saier. 2000. “The Amino Acid/polyamine/organocation (APC) Superfamily of Transporters Specific for Amino Acids, Polyamines and Organocations.” *Microbiology* 146(8):1797–1814.

Jap, B. K. et al. 1992. “2D Crystallization: From Art to Science.” *Ultramicroscopy* 46(1-4):45–84.

Jardetzky, O. 1966. “Simple Allosteric Model for Membrane Pumps.” *Nature* 211(5052):969–970.

Junge, F. et al. 2008. “Large-Scale Production of Functional Membrane Proteins.” *Cellular and Molecular Life Sciences* 65(11):1729–1755.

Kaback, H. Ronald, Irina Smirnova, Vladimir Kasho, Yiling Nie, and Yonggang Zhou. 2011. “The Alternating Access Transport Mechanism in LacY.” *Journal of Membrane Biology* 239(1-2):85–93.

Kabsch, Wolfgang. 2010. “XDS.” *Acta Crystallographica Section D: Biological Crystallography* 66(2):125–132.

Kaira, K. et al. 2012. “Prognostic Significance of L-Type Amino-Acid Transporter 1 Expression in Surgically Resected Pancreatic Cancer.” *British Journal of Cancer* 107(4):632–638.

Kaira, K. (a) et al. 2008. “Prognostic Significance of L-Type Amino Acid Transporter 1 Expression in Resectable Stage I-III Nonsmall Cell Lung Cancer.” *British Journal of Cancer* 98(4):742–748.

Kaira, K. (a) et al. 2009. “L-Type Amino Acid Transporter 1 (LAT1) Is Frequently Expressed in Thymic Carcinomas but Is Absent in Thymomas.” *Journal of Surgical Oncology* 99(7):433–438.

Kaira, K. (b) et al. 2008. “Expression of L-Type Amino Acid Transporter 1 (LAT1) in Neuroendocrine Tumors of the Lung.” *Pathology Research and Practice* 204(8):553–561.

Kaira, K. (b) et al. 2009. “Prognostic Significance of L-Type Amino Acid Transporter 1 (LAT1) and 4F2 Heavy Chain (CD98) Expression in Surgically Resectable Stage III Non-Small Cell Lung Cancer.” *Experimental and*

Therapeutic Medicine 1(5):799–808.

Kaira, K. (c) et al. 2008. “L-Type Amino Acid Transporter 1 and CD98 Expression in Primary and Metastatic Sites of Human Neoplasms.” *Cancer Science* 99(12):2380–2386.

Kaira, Kyoichi et al. 2011. “L-Type Amino Acid Transporter 1 (LAT1) Expression in Malignant Pleural Mesothelioma.” *Anticancer Research* 31(12):4075–4082.

Kaira, Kyoichi et al. 2013. “Clinicopathological Significance of L-Type Amino Acid Transporter 1 (LAT1) Expression in Patients with Adenoid Cystic Carcinoma.” *Pathology Oncology Research : POR* 19(4):649–656.

Kalmbach, Rolf et al. 2007. “Functional Cell-Free Synthesis of a Seven Helix Membrane Protein: In Situ Insertion of Bacteriorhodopsin into Liposomes.” *Journal of Molecular Biology* 371(3):639–648.

Kampen, Kim R. 2011. “Membrane Proteins: The Key Players of a Cancer Cell.” *The Journal of Membrane Biology* 242(2):69–74.

Katritch, V. 2013. “Structure-Function of the G Protein-Coupled Receptor Superfamily.” *Annual review of …* (7):531–556.

Kell, Douglas B., Paul D. Dobson, and Stephen G. Oliver. 2011. “Pharmaceutical Drug Transport: The Issues and the Implications That It Is Essentially Carrier-Mediated Only.” *Drug Discovery Today* 16(15-16):704–714.

Kell, Douglas B. and Stephen G. Oliver. 2014. “How Drugs Get into Cells: Tested and Testable Predictions to Help Discriminate between Transporter-Mediated Uptake and Lipoidal Bilayer Diffusion.” *Frontiers in Pharmacology* 5(October):1–32.

Kennedy, S. J. 1978. “Structures of Membrane Proteins.” *The Journal of Membrane Biology* 42(3):265–279.

Klammt, Christian et al. 2004. “High Level Cell-Free Expression and Specific Labeling of Integral Membrane Proteins.” *European Journal of Biochemistry* 271(3):568–580.

Kobayashi, Keiichi et al. 2008. “Enhanced Tumor Growth Elicited by L-Type Amino Acid Transporter 1 in Human Malignant Glioma Cells.” *Neurosurgery* 62(2):493–503.

Koebnik, R., K. P. Locher, and P. Van Gelder. 2000. “Structure and Function of Bacterial Outer Membrane Proteins: Barrels in a Nutshell.” *Molecular Microbiology* 37(2):239–253.

Kowalczyk, Lukasz et al. 2011. “Molecular Basis of Substrate-Induced Permeation by an Amino Acid Antiporter.” *Proceedings of the National Academy of Sciences of the United States of America* 108(10):3935–3940.

Krishnamurthy, Harini and Eric Gouaux. 2012. “X-Ray Structures of LeuT in Substrate-Free Outward-Open and Apo Inward-Open States.” *Nature* 481(7382):469–474.

Krishnamurthy, Harini, Chayne L. Piscitelli, and Eric Gouaux. 2009. “Unlocking the Molecular Secrets of Sodium-Coupled Transporters.” *Nature* 459(7245):347–355.

Kunji, Edmund R. S., Marilyn Harding, P. Jonathan G. Butler, and Pearl Akamine. 2008. “Determination of the Molecular Mass and Dimensions of Membrane Proteins by Size Exclusion Chromatography.” *Methods* 46(2):62–72.

Kunzelmann, Karl. 2005. “Ion Channels and Cancer.” *Journal of Membrane Biology* 205(3):159–173.

Kypreos, M., T. Banerjee, and D. Mukherjee. 2014. “G Protein-Coupled Receptors--Potential Roles in Clinical Pharmacology.” *Cardiovasc. Hematol. Agents Med. Chem.* 12(1):29–33.

Lagerstrom, M. C. and H. B. Schioth. 2008. “Structural Diversity of G Protein-Coupled Receptors and Significance for Drug Discovery.” *Nature Reviews. Drug Discovery* 7(4):339–357.

Lappano, Rosamaria and Marcello Maggiolini. 2011. “G Protein-Coupled Receptors: Novel Targets for Drug Discovery in Cancer.” *Nature reviews. Drug discovery* 10(1):47–60.

5. References

Leman, Koehler J., Martin B. Ulmschneider, and Jeffrey J. Gray. 2015. “Computational Modeling of Membrane Proteins.” *Proteins: Structure, Function, and Bioinformatics* 83(1):1–24.

Lemieux, Joanne et al. 2003. “Three-Dimensional Crystallization of the Escherichia Coli Glycerol-3-Phosphate Transporter: A Member of the Major Facilitator Superfamily.” *Protein Science* 12:2748–2756.

Leslie, Andrew G. W. and Harold R. Powell. 2007. “Processing Diffraction Data with MOSFLM.” *Evolving Methods for Macromolecular Crystallography* (245):41–51.

Leviatan, Shani, Keisuke Sawada, Yoshinori Moriyama, and Nathan Nelson. 2010. “Combinatorial Method for Overexpression of Membrane Proteins in Escherichia Coli.” *Journal of Biological Chemistry* 285(31):23548–23556.

Lodish, H. et al. 2003. *Molecular Cell Biology*. 5. ed. Portland, Oregon: W. H. Freeman & Company.

Lu, Feiran et al. 2011. “Structure and Mechanism of the Uracil Transporter UraA.” *Nature* 472(7342):243–246.

Lu, Min, Martha Radchenko, Jindrich Symersky, Rongxin Nie, and Yi Guo. 2013. “Structural Insights into H+-Coupled Multidrug Extrusion by a MATE Transporter.” *Nature Structural & Molecular Biology* 20(11):1310–1317.

Ma, Dan et al. 2012. “Structure and Mechanism of a glutamate–GABA Antiporter.” *Nature* 483(7391):632–636.

Macauley-Patrick, Sue, Mariana L. Fazenda, Brian McNeil, and Linda M. Harvey. 2005. “Heterologous Protein Production Using the Pichia Pastoris Expression System.” *Yeast (Chichester, England)* 22(4):249–270.

Mackenzie, Kevin R. 2006. “Folding and Stability of Alpha-Helical Integral Membrane Proteins.” *Chemical Reviews* 106(5):1931–1977.

Le Maire, Marc, Philippe Champeil, and Jesper V. Møller. 2000. “Interaction of Membrane Proteins and Lipids with Solubilizing Detergents.” *Biochimica et Biophysica Acta - Biomembranes* 1508(1-2):86–111.

Marassi, F. M. and S. J. Opella. 1998. “NMR Structural Studies of Membrane Proteins.” *Current Opinion in Structural Biology* 8(5):640–648.

Marreddy, Ravi K. R. et al. 2011. “The Response of Lactococcus Lactis to Membrane Protein Production.” *PLoS One* 6(8):1–15.

Mastroberardino, L. et al. 1998. “Amino-Acid Transport by Heterodimers of 4F2hc/CD98 and Members of a Permease Family.” *Nature* 395(6699):288–291.

McMullan, G., a. T. Clark, R. Turchetta, and a. R. Faruqi. 2009. “Enhanced Imaging in Low Dose Electron Microscopy Using Electron Counting.” *Ultramicroscopy* 109(12):1411–1416.

Meury, Marcel et al. 2014. “Detergent-Induced Stabilization and Improved 3D Map of the Human Heteromeric Amino Acid Transporter 4F2hc-LAT2.” *PLoS One* 9(10):1–6.

Minor, Wladek, Marcin Cymborowski, Zbyszek Otwinowski, and Maksymilian Chruszcz. 2006. “HKL-3000: The Integration of Data Reduction and Structure Solution - From Diffraction Images to an Initial Model in Minutes.” *Acta Crystallographica Section D: Biological Crystallography* 62(8):859–866.

Murai, S., H. Saito, Y. Masuda, and T. Itoh. 1988. “Rapid Determination of Norepinephrine, Dopamine, Serotonin, Their Precursor Amino Acids, and Related Metabolites in Discrete Brain Areas of Mice within Ten Minutes by HPLC with Electrochemical Detection.” *Journal of Neurochemistry* 50(2):473–479.

Namikawa, Masashi et al. 2014. “Expression of Amino Acid Transporters (LAT1, ASCT2 and xCT) as Clinical Significance in Hepatocellular Carcinoma.” *Hepatology Research* 44(1):1–9.

Neutze, Richard and Keith Moffat. 2012. “Time-Resolved Structural Studies at Synchrotrons and X-Ray Free Electron Lasers: Opportunities and Challenges.” *Current Opinion in Structural Biology* 22(5):651–659.

Noinaj, Nicholas et al. 2013. “Structural Insight into the Biogenesis of β-Barrel Membrane Proteins.” *Nature*

501(7467):385–390.

Omasa, Takeshi, Masayoshi Onitsuka, and Wook-Dong Kim. 2010. “Cell Engineering and Cultivation of Chinese Hamster Ovary (CHO) Cells.” *Current Pharmaceutical Biotechnology* 11(3):233–240.

Opekarová, M. and W. Tanner. 2003. “Specific Lipid Requirements of Membrane Proteins - A Putative Bottleneck in Heterologous Expression.” *Biochimica et Biophysica Acta - Biomembranes* 1610(1):11–22.

Osterberg, Marie et al. 2006. “Phenotypic Effects of Membrane Protein Overexpression in Saccharomyces Cerevisiae.” *Proceedings of the National Academy of Sciences of the United States of America* 103(30):11148–11153.

Ostermeier, Christian and Hartmut Michel. 1997. “Crystallization of Membrane Proteins.” *Current Opinion in Structural Biology* 7:697–701.

Otwinowski, Zbyszek and Wladek Minor. 1997. “Processing of X-Ray Diffraction Data Collected in Oscillation Mode.” *Methods in Enzymology* 276:307–326.

Palczewski, K. et al. 2000. “Crystal Structure of Rhodopsin: A G Protein-Coupled Receptor.” *Science* 289(5480):739–745.

Parker, Joanne L. and Simon Newstead. 2014. “Method to Increase the Yield of Eukaryotic Membrane Protein Expression in Saccharomyces Cerevisiae for Structural and Functional Studies.” *Protein Science* 23:1309–1314.

Pedersen, S. F. and C. Stock. 2013. “Ion Channels and Transporters in Cancer: Pathophysiology, Regulation, and Clinical Potential.” *Cancer Research* 73(6):1658–1661.

Perez, Camilo, Caroline Koshy, Özkan Yildiz, and Christine Ziegler. 2012. “Alternating-Access Mechanism in Conformationally Asymmetric Trimers of the Betaine Transporter BetP.” *Nature* 490(7418):126–130.

Piddock, Laura J. V. 2006. “Multidrug-Resistance Efflux Pumps - Not Just for Resistance.” *Nature Reviews. Microbiology* 4(8):629–636.

Pineda, Marta et al. 1999. “Identification of a Membrane Protein, LAT-2, That Co-Expresses with 4F2 Heavy Chain, an L-Type Amino Acid Transport Activity with Broad Specificity for Small and Large Zwitterionic Amino Acids.” *Journal of Biological Chemistry* 274(28):19738–19744.

Pritchard, Colin et al. 2009. “Conserved Gene Expression Programs Integrate Mammalian Prostate Development and Tumorigenesis.” *Cancer Research* 69(5):1739–1747.

Privé, Gilbert G. 2007. “Detergents for the Stabilization and Crystallization of Membrane Proteins.” *Methods* 41(4):388–397.

Procko, Erik, M. L. O’Mara, W. F. D. Bennett, D. P. Tieleman, and R. Gaudet. 2009. “The Mechanism of ABC Transporters: General Lessons from Structural and Functional Studies of an Antigenic Peptide Transporter.” *The Federation of American Societies for Experimental Biology Journal* 23(5):1287–1302.

Rask-Andersen, Mathias, Markus Sällman Almén, and Helgi B. Schiöth. 2011. “Trends in the Exploitation of Novel Drug Targets.” *Nature Reviews Drug Discovery* 10(8):579–590.

Robinson, Anne Skaja and Patrick J. Loll. 2011. “Introduction.” Pp. 1–9 in *Production of Membrane Proteins: Strategies for Expression and Isolation*, edited by A. S. Robinson. Weinheim, Germany: Wiley-VCH Verlag GmbH & Co. KGaA.

Robinson, M. J. and M. H. Cobb. 1997. “Mitogen-Activated Protein Kinase Pathways.” *Current Opinion in Cell Biology* 9(2):180–186.

Rosell, Albert et al. 2014. “Structural Bases for the Interaction and Stabilization of the Human Amino Acid Transporter LAT2 with Its Ancillary Protein 4F2hc.” *Proceedings of the National Academy of Sciences of the United States of America* 111(8):2966–2671.

Rosenbusch, J. P., A. Lustig, M. Grabo, M. Zulauf, and M. Regenass. 2001. “Approaches to Determining

Membrane Protein Structures to High Resolution: Do Selections of Subpopulations Occur?” *Micron* 32(1):75–90.

Roses, Allen D., Daniel K. Burns, Stephanie Chissoe, Lefkos Middleton, and Pamela St Jean. 2005. “Disease-Specific Target Selection: A Critical First Step down the Right Road.” *Drug Discovery Today* 10(3):177–189.

Rossier, Grégoire et al. 1999. “LAT2, a New Basolateral 4F2hc/CD98-Associated Amino Acid Transporter of Kidney and Intestine.” *Journal of Biological Chemistry* 274(49):34948–34954.

Rudnick, Gary. 2012. “The Cytoplasmic Permeation Pathway of Neurotransmitter Transporters.” *Biochemistry* 50(35):7462–7475.

Ruprecht, Jonathan and Jon Nield. 2001. “Determining the Structure of Biological Macromolecules by Transmission Electron Microscopy, Single Particle Analysis and 3D Reconstruction.” *Progress in Biophysics and Molecular Biology* 75(3):121–164.

Ruskin, R. S., Z. Yu, and N. Grigorieff. 2013. “Quantitative Characterization of Electron Detectors for Transmission Electron Microscopy.” *Journal of Structural Biology* 184(3):385–393.

Sabatini, David M. 2006. “mTOR and Cancer: Insights into a Complex Relationship.” *Nature Reviews. Cancer* 6(9):729–734.

Saier, Jr. 2000. “Families of Transmembrane Transporters Selective for Amino Acids and Their Derivatives.” *Microbiology* 146(8):1775–1795.

Sakata, Takeshi et al. 2009. “L-Type Amino-Acid Transporter 1 as a Novel Biomarker for High-Grade Malignancy in Prostate Cancer.” *Pathology International* 59(1):7–18.

Savage, David F., Corey L. Anderson, Yaneth Robles-Colmenares, Zachary E. Newby, and Robert M. Stroud. 2007. “Cell-Free Complements in Vivo Expression of the E. Coli Membrane Proteome.” *Protein science : a publication of the Protein Society* 16(5):966–976.

Scholzen, Thomas and Johannes Gerdes. 2000. “The Ki-67 Protein: From the Known and the Unknown.” *Journal of Cellular Physiology* 182(1999):311–322.

Schulze, Sabrina, Stefan Köster, Ulrike Geldmacher, Anke C. Terwisscha van Scheltinga, and Werner Kühlbrandt. 2010. “Structural Basis of Na(+)-Independent and Cooperative Substrate/product Antiport in CaiT.” *Nature* 467(7312):233–236.

Schweikhard, Eva S. and Christine M. Ziegler. 2012. “Amino Acid Secondary Transporters: Toward a Common Transport Mechanism.” *Current Topics in Membranes* 70:1–28.

Seddon, Annela M., Paul Curnow, and Paula J. Booth. 2004. “Membrane Proteins, Lipids and Detergents: Not Just a Soap Opera.” *Biochimica et Biophysica Acta - Biomembranes* 1666(1-2):105–117.

Segawa, H. et al. 1999. “Identification and Functional Characterization of a Na+-Independent Neutral Amino Acid Transporter with Broad Substrate Selectivity.” *Journal of Biological Chemistry* 274(28):19745–19751.

Sekine, Yuji et al. 2009. “Amino Acid Transporter LAT3 Is Required for Podocyte Development and Function.” *Journal of the American Society of Nephrology* 20(7):1586–1596.

Senes, a, M. Gerstein, and D. M. Engelman. 2000. “Statistical Analysis of Amino Acid Patterns in Transmembrane Helices: The GxxxG Motif Occurs Frequently and in Association with Beta-Branched Residues at Neighboring Positions.” *Journal of Molecular Biology* 296(3):921–936.

Shaffer, P. L., A. Goehring, A. Shankaranarayanan, and E. Gouaux. 2009. “Structure and Mechanism of a Na+-Independent Amino Acid Transporter.” *Science* 325(5943):1010–1014.

Shi, Yigong. 2013. “Common Folds and Transport Mechanisms of Secondary Active Transporters.” *Annual Review of Biophysics* 42:51–72.

Shimamura, Tatsuro et al. 2010. “Molecular Basis of Alternating Access Membrane Transport by the Sodium-

Hydantoin Transporter Mhp1.” *Science* 328(April):470–473.

Shintre, Chitra a et al. 2013. “Structures of ABCB10, a Human ATP-Binding Cassette Transporter in Apo- and Nucleotide-Bound States.” *Proceedings of the National Academy of Sciences of the United States of America* 110(24):9710–9715.

Simons, K. and E. Ikonen. 1997. “Functional Rafts in Cell Membranes.” *Nature* 387(6633):569–572.

Takata, Kuniaki, Toshiyuki Matsuzaki, and Yuki Tajika. 2004. “Aquaporins: Water Channel Proteins of the Cell Membrane.” *Progress in Histochemistry and Cytochemistry* 39(1):1–83.

Tate, G. C. 2001. “Overexpression of Integral Membrane Proteins for Structural Studies.” *FEBS Letters* 504:94–98.

Thompson, Miles D., W. McIntyre Burnham, and David E. C. Cole. 2005. “The G Protein-Coupled Receptors: Pharmacogenetics and Disease.” *Critical Reviews in Clinical Laboratory Sciences* 42(4):311–392.

Toyoda, M. et al. 2014. “Prognostic Significance of Amino-Acid Transporter Expression (LAT1, ASCT2, and xCT) in Surgically Resected Tongue Cancer.” *British Journal of Cancer* 110(10):2506–2513.

Tsai, M. Y., F. Fang, and C. Miller. 2012. “Sided Functions of an Arginine-Agmatine Antiporter Oriented in Liposomes.” *Biochemistry* 29(6):997–1003.

Tucker, J. and R. Grisshammer. 1996. “Purification of a Rat Neurotensin Receptor Expressed in Escherichia Coli.” *The Biochemical journal* 317 (Pt 3:891–899.

Tyndall, Joel D. A. and Radhika Sandilya. 2005. “GPCR Agonists and Antagonists in the Clinic.” *Medicinal Chemistry* 1(4):405–421.

Uhlén, Mathias et al. 2015. “Tissue-Based Map of the Human Proteome.” *Proteomics* 347(6220):394–402.

Ujwal, Rachna et al. 2008. “The Crystal Structure of Mouse VDAC1 at 2.3 A Resolution Reveals Mechanistic Insights into Metabolite Gating.” *Proceedings of the National Academy of Sciences of the United States of America* 105(46):17742–17747.

Ujwal, Rachna and James U. Bowie. 2011. “Crystallizing Membrane Proteins Using Lipidic Bicelles.” *Methods* 55(4):337–341.

Västermark, Åke and Milton H. Saier. 2014. “Evolutionary Relationship between 5+5 and 7+7 Inverted Repeat Folds within the Amino Acid-Polyamine-Organocation Superfamily.” *Proteins: Structure, Function and Bioinformatics* 82(2):336–346.

Verrey, François et al. 2009. “Kidney Amino Acid Transport.” *Pflügers Archiv - European Journal of Physiology* 458(1):53–60.

Vinothkumar, Kutti R. and Richard Henderson. 2010. “Structures of Membrane Proteins.” *The Journal of membrane biology* 41(1):65–158.

de Vos, W. M. 1999. “Gene Expression Systems for Lactic Acid Bacteria.” *Current opinion in microbiology* 2(3):289–295.

Wagner, Samuel, Mirjam Lerch Bader, David Drew, and Jan-Willem de Gier. 2006. “Rationalizing Membrane Protein Overexpression.” *Trends in biotechnology* 24(8):364–371.

Wang, Qian et al. 2011. “Androgen Receptor and Nutrient Signaling Pathways Coordinate the Demand for Increased Amino Acid Transport during Prostate Cancer Progression.” *Cancer Research* 71(24):7525–7536.

Wang, Qian et al. 2013. “Targeting Amino Acid Transport in Metastatic Castration-Resistant Prostate Cancer: Effects on Cell Cycle, Cell Growth, and Tumor Development.” *Journal of the National Cancer Institute* 105(19):1463–1473.

Wang, Qian and Jeff Holst. 2015. “L-Type Amino Acid Transport and Cancer.” *American Journal of Cancer*

Research 5(4):1281–1294.

Wang, S., R. Yan, X. Zhang, Q. Chu, and Y. Shi. 2014. “Molecular Mechanism of pH-Dependent Substrate Transport by an Arginine-Agmatine Antiporter.” *Proceedings of the National Academy of Sciences* 111(35):12734–12739.

Watanabe, Akira et al. 2010. “The Mechanism of Sodium and Substrate Release from the Binding Pocket of vSGLT.” *Nature* 468(7326):988–991.

Weyand, Simone et al. 2008. “Structure and Molecular Mechanism of a Nucleobase-Cation-Symport-1 Family Transporter.” *Science* 322(5902):709–713.

Weyand, Simone et al. 2011. “The Alternating Access Mechanism of Transport as Observed in the Sodium-Hydantoin Transporter Mhp1.” *Journal of Synchrotron Radiation* 18(1):20–23.

White, Stephen H. and William C. Wimley. 1999. “Membrane Protein Folding and Stability: Physical Principles.” *Annual Review of Biophysics and Biomolecular Structure* 28(1):319–365.

Winn, Martyn D. et al. 2011. “Overview of the CCP4 Suite and Current Developments.” *Acta Crystallographica Section D: Biological Crystallography* 67(4):235–242.

Wong, Foon H. et al. 2012. “The Amino Acid-Polyamine-Organocation Superfamily.” *Journal of Molecular Microbiology and Biotechnology* 22(2):105–113.

Wurm, Florian M. 2004. “Production of Recombinant Protein Therapeutics in Cultivated Mammalian Cells.” *Nature biotechnology* 22(11):1393–1398.

Y Kanai, H Segawa, Miyamoto K, Uchino H, Takeda E, Endou H. 1998. “Expression Cloning and Characterization Acids Activated by the Heavy Chain of 4F2 Expression Cloning and Characterization of a Transporter for Large Neutral Amino Acids Activated by the Heavy Chain of 4F2 Antigen.” 2–6.

Yamashita, Atsuko, Satinder K. Singh, Toshimitsu Kawate, Yan Jin, and Eric Gouaux. 2005. “Crystal Structure of a Bacterial Homologue of Na+/Cl--Dependent Neurotransmitter Transporters.” *Nature* 437(7056):215–223.

Yan, Nieng. 2013. “Structural Advances for the Major Facilitator Superfamily (MFS) Transporters.” *Trends in Biochemical Sciences* 38(3):151–159.

Yildirim, Muhammed a, Kwang-Il Goh, Michael E. Cusick, Albert-László Barabási, and Marc Vidal. 2007. “Drug-Target Network.” *Nature Biotechnology* 25(10):1119–1126.

Zhang, Jian, Jianyi Yang, Richard Jang, and Yang Zhang. 2015. “GPCR-I-TASSER : A Hybrid Approach to G Protein- Coupled Receptor Structure Modeling and the Application to the Human Genome Resource GPCR-I-TASSER : A Hybrid Approach to G Protein-Coupled Receptor Structure Modeling and the Application to the Human Genome.” *Structure* 23:1538–1549.

Zhou, Xiaoming et al. 2014. “Structural Basis of the Alternating-Access Mechanism in a Bile Acid Transporter.” *Nature* 505(7484):569–573.

Zhou, Y., J. H. Morais-Cabral, A. Kaufman, and R. MacKinnon. 2001. “Chemistry of Ion Coordination and Hydration Revealed by a K+ Channel-Fab Complex at 2.0 A Resolution.” *Nature* 414(6859):43–48.

6. Acknowledgements

First of all, I would like to express my gratitude to my supervisor Prof. Dimitrios Fotiadis for accepting me and giving me the chance to learn and to study membrane protein biochemistry in his lab. From the first day on, he has been a wonderful mental and scientific guide to me. Without his invaluable support, this work wouldn't have been possible.

I have special thanks to Dr. Jean-Marc Jeckelmann as being a great fellow and guide to me after my supervisor, also, for his efforts and comments during my studies to make this work much more valuable.

For being a very nice teacher in many aspects, I would like to thank to Dr. Daniel Harder. He was always so patient in teaching me the functional assays and he is one of the guys made me like and learn German language.

Thanks to Dr. Marcel Meury, in the beginning, I could get used to the lab environment and the techniques applied in the lab. The same thing applies for our lab technician, Zöhre Ucurum-Fotiadis and I am thankful for her efforts in preparing several constructs and being my Turkish speaking fellow in the lab. I would like to thank to Dr. Rajendra Boggavarapu V.R.N. for valuable scientific and social discussions. Special thanks to nice and cheerful 'colegita' Dr. Meritxell Costa, she has been a very helpful. Also, I have to thank to David Kalbermatter, Stephan Hirschi, Mirko Stauffer and Dr. Patrick Bosshart, apart from scientific discussions, for teaching me new things in German and speaking with me in 'high' German which helped me to improve my ability a lot. I am also thankful to our other lab colleagues Satish Kantipudi and Sara Bonetti.

I would also thank to my co-advisor Prof. Jean-Louis Reymond and to my mentor Prof. Beat Trueb for their valuable comments and support during my thesis studies.

For technical support, I would like to thank to Thomas Schneeberger, Thomas Leuenberger, Laurent Götschmann and Daniel Schüpbach for helping me in finding tools and solutions, and to secretariat workers for their guide in managing paper works.

I would like to thank to the members of IBMM as being a part of this nice environment.

I have to mention few other important people for me; my supervisor during the master studies, Prof. Gülşah Şanli-Mohamed, my brother, Dr. Müslüm Ilgü, and my former fellows Ali Kemal Havare and Serdal Okur who have been a great guide and mental support.

Last but not the least, I have very special thanks to my parents and my well beloved wife Ekin Öztürk-Ilgü, without their great support, this work wouldn't have been possible.

7. Curriculum Vitae

Contact Information

Hüseyin Ilgü

Weidmattweg 16	Sehit Mehmet Cavus Street, 2/9
CH-3018 Bern, Switzerland	Eryaman, Ankara, Turkey

Date of birth: August 16, 1985

Place of birth: Ankara, Turkey

E-mail: hilgu1985@gmail.com

Education

Ph.D. Student 2011 - 2016

Institute of Biochemistry and Molecular Medicine

Univerisity of Bern, Switzerland

M.Sc. in Biochemistry 2008 - 2011

Department of Chemistry

İzmir Institute of Technology, Turkey

B.Sc. in Chemistry 2003 - 2008

Department of Chemistry

İzmir Institute of Technology, Turkey

Work Experience

Teaching Assistant 2008 – 2011

Department of Chemistry

İzmir Institute of Technology, Turkey

Visiting Scientist July – October 2010

Nelson Lab., Iowa State University, US

Industrial training June – July 2008

Küçükbay Oil Inc. Company, İzmir

8. Declaration of Originality

Last name, first name: Ilgü, Hüseyin

Matriculation number: 11-118-833

I hereby declare that this thesis represents my original work and that I have used no other sources except as noted by citations. All data, tables, figures and text citations which have been reproduced from any other source, including the internet, have been explicitly acknowledged as such.
I am aware that in case of non-compliance, the Senate is entitled to withdraw the doctorate degree awarded to me on the basis of the present thesis, in accordance with the “Statut der Universität Bern (Universitätsstatut; UniSt)”, Art. 69, of 7 June 2011.

Place, date: Bern, 07.12.2015

Signature:

9. Abbreviations

MP	Membrane Protein
FDA	U.S. Food and Drug Administration
ATP	Adenosine triphosphate
ABC	ATP-binding cassette
SLC	Solute carrier
GPCR	G-protein coupled receptor
ERK	Extracellular-signal-regulated kinase
LAT	L-type amino acid transporter
TMD	Transmembrane domain
PDB	Protein data bank
TSPO	Mitochondrial translocator protein
CDC	Cholesterol-dependent cytolysin
ROS	Rod outer segment
E. coli	*Escherichia coli*
S. cerevisiae	*Saccharomyces cerevisiae*
P. pastoris	*Pichia pastoris*
L. lactis	*Lactococcus lactis*
HEK293	Human embryonic kidney cells
HeLa	Human epithelioid carcinoma
BHK-21	Baby hamster kidney cells
COS-7	Monkey kidney fibroblast cells
CHO	Chinese hamster ovary
GlpT	Glycerol-3-phosphate transporter
LCP	Lipidic cubic phase crystallization
MR	Molecular replacement
MAD	Multi wavelength anomalous dispersion
SAD	Single wavelength anomalous dispersion
MIR	Multiwavelength isomorphous replacement
NMR	Nuclear magnetic resonance
Cryo-EM	Cryo-electron microscopy
SPA	Single particle analysis
SFX	Serial femtosecond crystallography
XFEL	X-ray free-electron lasers
CCD	Charge-coupled device
CMOS	Complementary metal oxide semiconductor

9. Abbreviations

DED	Direct electron detection
MD	Molecular dynamics
NG	*n*-nonyl-β-D-glucopyranoside
Cymal-5	5-cyclohexyl-1-pentyl-β-D-maltoside
GABA	γ-Aminobutyric acid
AAT	Amino acid transporter
HHH	Hyperornithinemia-hyperammonemia-homocitrullinuria
APC	Amino acid-polyamine-organocation
Pfam	Protein families database classification
AdiC	L-arginine/agmatine antiporter
ApcT	Na^+-independent amino acid transporter
GadC	Glutamate–GABA antiporter
LeuT	Na^+-dependent leucine transporter
Mhp1	Benzylhydantoin transporter
BetP	Na^+ glycine betaine symporter
CaiT	L-carnitine γ-butyrobetaine antiporter
SglT	Na^+ galactose symporter
UraA	Uracil transporter
4F2hc	4F2 antigen heavy chain
HAT	Heteromeric amino acid transporter
mTORC1	Mammalian target of rapamycin complex 1
Arg	L-Arginine
Agm	Agmatine
wt	Wild-type
LacY	Lactose permease
MATE	Multidrug and toxic compound extrusion transporter
AcrB	Proton/drug antiporter
ASBT	Bile acid transporter
NBD	Nucleotide-binding domain
SEC	Size-exclusion chromatography
DDM	*n*-dodecyl-β-D-maltoside
OM	*n*-octyl-β-D-maltoside

I

Variation of the Detergent-Binding Capacity and Phospholipid Content of Membrane Proteins When Purified in Different Detergents

Hüseyin Ilgü, Jean-Marc Jeckelmann, María Salomé Gachet, Rajendra Boggavarapu, Zöhre Ucurum, Jürg Gertsch, and Dimitrios Fotiadis*
Institute of Biochemistry and Molecular Medicine, and Swiss National Centre of Competence in Research (NCCR) TransCure, University of Bern, Bern, Switzerland

ABSTRACT Purified membrane proteins are ternary complexes consisting of protein, lipid, and detergent. Information about the amounts of detergent and endogenous phospholipid molecules bound to purified membrane proteins is largely lacking. In this systematic study, three model membrane proteins of different oligomeric states were purified in nine different detergents at commonly used concentrations and characterized biochemically and biophysically. Detergent-binding capacities and phospholipid contents of the model proteins were determined and compared. The insights on ternary complexes obtained from the experimental results, when put into a general context, are summarized as follows. 1), The amount of detergent and 2) the amount of endogenous phospholipids bound to purified membrane proteins are dependent on the size of the hydrophobic lipid-accessible protein surface areas and the physicochemical properties of the detergents used. 3), The size of the detergent and lipid belt surrounding the hydrophobic lipid-accessible surface of purified membrane proteins can be tuned by the appropriate choice of detergent. 4), The detergents *n*-nonyl-β-D-glucopyranoside and Cymal-5 have exceptional delipidating effects on ternary complexes. 5), The types of endogenous phospholipids bound to membrane proteins can vary depending on the detergent used for solubilization and purification. 6), Furthermore, we demonstrate that size-exclusion chromatography can be a suitable method for estimating the molecular mass of ternary complexes. The findings presented suggest a strategy to control and tune the numbers of detergent and endogenous phospholipid molecules bound to membrane proteins. These two parameters are potentially important for the successul crystallization of membrane proteins for structure determination by crystallographic approaches.

INTRODUCTION

Studying the function, and in particular the structure, of membrane proteins still remains a challenge. The main reason for this is the amphipathic nature of membrane proteins. They consist of hydrophobic domains, which are embedded in the lipid bilayer membrane, and hydrophilic domains that protrude out of the membrane into the cytosol and extracellular space. For structure determination, membrane proteins are extracted from the biological membrane, purified, and then crystallized. For purification and crystallization, it is imperative that the target membrane protein is stable and monodisperse in the selected detergent (1,2) or detergent mixtures (3,4). Therefore, the choice of the optimal detergent(s) is fundamental and will have an enormous impact on the success of the experimental outcome.

Purified membrane proteins are essentially ternary complexes composed of protein, lipid, and detergent. Here, we address the composition of ternary complexes when purified in detergents of different physicochemical properties. The important role played by detergent in the stabilization and crystallization of ternary complexes has been recognized and addressed in the past (5–8). However, the presence of phospholipids in such complexes has been to some extent neglected. In this work, we characterized all three components of the ternary complex of purified membrane proteins in a systematic way. Nine nonionic detergents commonly used in membrane protein biochemistry and crystallography were selected to isolate ternary complexes of three model proteins. The model proteins were the urea transporter (UT), from *Desulfovibrio vulgaris*, and the L-arginine/agmatine antiporter (AdiC) and lactose permease (LacY), from *Escherichia coli*. These membrane proteins were selected based on their different oligomeric states, i.e., trimer (UT), dimer (AdiC), and monomer (LacY), and the availability of their atomic structures (9–11). The UT consists of 10 transmembrane helices and two reentrant helices (9), whereas AdiC and LacY are comprised of 12 transmembrane helices (10,11).

The aim of this study was to characterize the ternary complexes obtained after purification of membrane proteins in different detergents. Knowledge about the amounts of detergent and lipid associated with purified membrane proteins is important for their successful crystallization and subsequent structure determination (12,13). We demonstrate that the size of the detergent and lipid belt surrounding the hydrophobic lipid-accessible surface of purified membrane proteins can be tuned by proper selection of the detergent used for purification. From a sterical point of view, minimization of the detergent/lipid belt volume by the appropriate detergent might allow the formation of crystal contacts and

Submitted June 10, 2013, and accepted for publication February 26, 2014.
*Correspondence: dimitrios.fotiadis@ibmm.unibe.ch
Editor: Robert Nakamoto.

0006-3495/14/04/1660/11 $2.00

http://dx.doi.org/10.1016/j.bpj.2014.02.024

consequently the growth of membrane protein crystals for x-ray crystallography (12,13).

MATERIALS AND METHODS

Materials

All detergents, i.e., *n*-dodecyl-β-D-maltopyranoside (DDM), *n*-undecyl-β-D-maltopyranoside (UDM), *n*-decyl-β-D-maltopyranoside (DM), *n*-nonyl-β-D-maltopyranoside (NM), *n*-octyl-β-D-maltopyranoside (OM), 7-cyclohexyl-1-heptyl-β-D-maltopyranoside (Cymal-7), 6-cyclohexyl-1-hexyl-β-D-maltopyranoside (Cymal-6), 5-cyclohexyl-1-pentyl-β-D-maltopyranoside (Cymal-5), and *n*-nonyl-β-D-glucopyranoside (NG) were from Affymetrix. UDM and NM were Anagrade, whereas the others were Sol-Grade.

E. coli polar lipid extract (cat. no. 100600C) and *E. coli* total lipid extract (cat. no. 100500C) were from Avanti Polar Lipids (Alabaster, AL). High-performance-liquid-chromatography-grade methanol (CH_3OH) and chloroform ($CHCl_3$) were from Fisher Scientific (Leicestershire, United Kingdom) and Biosolve (Valkenswaard, The Netherlands), respectively. Acetic acid (glacial) was from Merck KGaA (Darmstadt, Germany). Phosphate-buffered saline (PBS) was purchased from Sigma-Aldrich and prepared according to the manufacturer's protocol by dissolving it in ultrapure water (18.2 MΩ $\times$ cm) obtained from an ELGA Purelab Ultra water system (VWS, Marlow, United Kingdom).

Cloning of UT, AdiC, and LacY

The gene of the urea transporter UT was cloned from genomic DNA of the bacterium *Desulfovibrio vulgaris* strain Hildenborough by polymerase chain reaction (PCR) using the forward primer 5′ AAA CAT ATG TTT GGA GAA CAG TTG CTT AAG 3′ and the reverse primer 5′ AAA GGA TCC TCA GCG AGA CCC GAT CGC GAG 3′. PCR products were digested with the restriction enzymes NdeI and BamHI, and ligated into the pET-15b vector (Novagen, Madison, WI). The pET-15b-UT construct expresses a recombinant UT protein with hexa-His tag at the N-terminus.

The amino acid transporter AdiC from *E. coli* was cloned as described previously (14) into the vector pTrcHisA (Invitrogen, Carlsbad, CA). The pTrcHisA-AdiC construct results in a recombinant AdiC protein with a hexa-His tag at the N-terminus.

The lactose transporter LacY from *E. coli* was cloned into a modified version of the previously described vector pET-21b-rbs-T7-His (15). To generate the vector for the overexpression of LacY, a point mutation was first introduced into the pET-21b-rbs-T7-YdgR-His construct (15) after the STOP codon to generate a SacI restriction site using the forward primer 5′ CAC CAC CAC CAC TGA GCT CCG GCT GCT AAC 3′ and the reverse primer 5′ GTT AGC AGC CGG AGC TCA GTG GTG GTG GTG 3′, and the QuikChange site-directed mutagenesis kit (Stratagene, La Jolla, CA). Next, the construct was digested with *Hin*dIII and SacI to remove the *ydgR* gene and its C-terminal extension. The two prehybridized complementary oligonucleotide fragments, which have *Hin*dIII and SacI compatible ends, were then inserted into the vector: upper, 5′ (*Hin*dIII) AGC TTG CGG CCG CAC TCG AGC TGG AAG TTC TGT TCC AGG GCC CCG TCG ACC ATC ACC ACC ATC ATC ACC ATC ACC ACC ACT GAG CT (SacI) 3′ and lower, 3′ (*Hin*dIII) CAG TGG TGG TGA TGG TGA TGA TGG TGG TGA TGG TCG ACG GGC CCC TGG AAC AGA ACT TCC AGC TCG AGT GCG GCC GCA (SacI) 5′. These oligonucleotides introduce a multiple cloning site for the restriction enzymes *Hin*dIII, NotI, and XhoI. The *lacY* gene was cloned from genomic *E. coli* strain K12 DNA by PCR using the forward primer 5′ AAA AAA GCT TAT GTA CTA TTT AAA AAA CAC 3′ and the reverse primer 5′ AAA ACT CGA GAG CGA CTT CAT TCA CC 3′. PCR products were digested with the restriction enzymes *Hin*dIII and XhoI and ligated into the new vector (pZUDF21-rbs-3C-10His). In this construct, the target protein has the C-terminal amino acid extension LELEVLFQGPVDHHHHHHHHHH, which contains a Prescission (human rhinovirus 3C) protease cleavage site and a deca-His tag. All DNA constructs were verified by sequencing. The calculated molecular masses of the three monomeric recombinant model membrane proteins are ~41.1 kDa (UT), ~50.9 kDa (AdiC), and ~49.2 kDa (LacY).

Overexpression and purification of membrane proteins

For overexpression, pET-15b-UT was transformed into Rosetta 2 (DE3), and pTrcHisA-AdiC and pZUDF21-rbs-LacY-3C-10His into BL21(DE3) pLysS *E. coli* cells. Cultures were grown in Luria Bertani medium supplemented with 0.1 mg/mL ampicillin at 37°C in an orbital shaker. Induction of the protein overexpression was initiated at OD_{600} of 0.5–0.6 with 0.3 mM (UT), 0.3 mM (AdiC), and 0.5 mM (LacY) isopropyl-β-D-thiogalactopyranoside and incubated at 37°C for 3 h. Cells were then harvested by centrifugation (7200 $\times$ *g* for 25 min at 4°C), resuspended in Lysis buffer (20 mM Tris-HCl, pH 8.0, and 150 mM NaCl) and stored at −20°C. For membrane preparation, frozen cells were thawed and incubated for 5 min with DNase I from bovine pancreas (Sigma-Aldrich, St. Louis, MO; 400 μg for cells from 12 L of culture) before lysis through a Microfluidizer M-110P (Microfluidics, Newton, MA) at 16,000 psi (four passages). Cell debris were removed by centrifugation (12,000 $\times$ *g* for 20 min at 4°C) and from the supernatant, membranes were collected by ultracentrifugation (150,000 $\times$ *g* for 1 h at 4°C). The pellet was homogenized in 20 mM Tris-HCl, pH 8.0, 500 mM NaCl, and 5 mM EDTA. An additional ultracentrifugation was performed, the pellet was homogenized in a small volume of Lysis buffer, i.e., 12 mL final total volume, and aliquoted into 2 mL fractions (corresponding to membranes from 2 L of cell culture). Membrane aliquots were stored at −20°C until further use.

For purification, one aliquot of membrane suspension was solubilized for 90 min at 4°C on a rotational shaker in Buffer S (20 mM Tris-HCl, pH 8.0, 300 mM NaCl, 250 mM betaine, 10% glycerol, and 0.01% (w/v) NaN_3) plus the corresponding concentration of detergent (see Table S1 in the Supporting Material, *Solubilization*; $V_{tot} = 7$ mL). After ultracentrifugation (100,000 $\times$ *g* for 1 h at 4°C), the supernatant was diluted twofold with 5 mM L-histidine in Buffer S and incubated with 0.5 mL preequilibrated Ni-NTA Superflow beads (Qiagen, Valencia, CA) for 2 h at 4°C on a rotational shaker (metal affinity chromatography). The beads were then transferred into a column and washed three times with 5 mL of 5 mM L-histidine in Buffer S plus the corresponding detergent (see Table S1, *Washing/Elution/SEC*). Finally, the protein was eluted from the beads in the same buffer containing 400 mM imidazole instead of 5 mM L-histidine.

Size-exclusion chromatography of purified membrane proteins

Size-exclusion chromatography (SEC) experiments were performed at 8°C using a Superdex 200 10/300 GL column (GE Healthcare, Wauwatosa, WI) on an Äkta Purifier system (GE Healthcare). The column was calibrated using a commercial high-molecular-weight gel filtration calibration kit (GE Healthcare). Marker proteins were thyroglobulin (669 kDa), ferritin (440 kDa), aldolase (158 kDa), conalbumin (75 kDa), and ovalbumin (43 kDa). The column was equilibrated with 1.5 column volumes of 20 mM Tris-HCl, pH 8.0, and 150 mM NaCl containing the corresponding detergent (SEC buffer; see Table S1 for detergent concentrations). Before injection, purified protein samples were centrifuged at 100,000 $\times$ *g* for 30 min at 4°C. The sample was injected into the fast-protein liquid chromatography system using a 200 μL loading loop. The flow rate was 0.5 mL/min during SEC. Peak fractions were collected and stored at 4°C for subsequent protein, detergent, and phospholipid determinations. Protein concentrations ranged from 0.1 to 0.4 mg/mL. It is important to point out that to avoid co-concentration of detergent, SEC peak fractions were never concentrated.

Determination of the membrane protein content in SEC peak fractions

The bicinchoninic acid assay (Pierce, Thermo Scientific, Waltham, MA) was used for protein determination because of its compatibility with detergents, low variability, and high sensitivity (16).

Determination of the detergent content in SEC peak fractions

The detergent content in SEC peak fractions of purified membrane proteins was determined by measuring the diameters of detergent-containing drops on a hydrophobic surface similar to Engel et al. (17) and Kaufmann et al. (18). This method is based on the drop diameter as a function of the surface tension (detergent content). Briefly, standard solutions at concentrations below the critical micelle concentration (CMC) of the corresponding detergent were prepared for, e.g., UDM: 0.1, 0.2, 0.3, 0.5, and 0.6 × CMC_{UDM}. From these solutions, 20 μL drops were deposited on a flattened-parafilm surface together with the samples from SEC. Before deposition, test samples were diluted in SEC buffer (without detergent) below the CMC of the corresponding detergent (10–100 times, depending on the CMC) and incubated overnight at 18°C. Dilution below the CMC dissolves the micelles into detergent monomers, thus avoiding possible disturbing effects (18). Images of the drops were recorded from above with a digital camera, and the diameters of the drops were measured in pixels using the image processing software Adobe Photoshop. To determine the amount of detergent in SEC peak fractions, standard curves were generated by plotting drop diameters versus $\log_{10}$ of the concentrations of the standard solutions. The amount of detergent bound to membrane proteins was calculated by subtracting the amount of detergent in the corresponding SEC buffer from the total amount of detergent in the SEC peak fraction (which also contains membrane proteins). Detergent concentrations in SEC peak fractions of the studied membrane proteins ranged from 1 (DDM) to 34 mM (OM).

Determination of the phospholipid content in SEC peak fractions

The total amount of phosphorus, and thus of phospholipids, in samples of purified membrane proteins was determined spectrophotometrically as described on the Avanti Polar Lipids web site (www.avantilipids.com; see Determination of Total Phosphorus). This protocol is based on Chen et al. (19), and Fiske and Subbarow (20). From SEC peak fractions of membrane proteins purified in different detergents, 100–200 μL samples were pipetted into 16 × 125 mm disposable glass tubes with screw cap closures. In a similar way, different amounts of phosphorus standard solution (cat no. P3869, Sigma-Aldrich; [P] = 0.65 mM) were placed into six separate tubes, i.e., 0 μL (0 μmol), 50 μL (0.0325 μmol), 100 μL (0.065 μmol), 125 μL (0.08125 μmol), 250 μL (0.1625 μmol), and 350 μL (0.2275 μmol) to generate a calibration curve. To each standard tube, 100–200 μL (depending on the detergent) of the corresponding SEC buffer was also added. To decompose the organic sample and produce inorganic phosphate, 450 μL of 8.9 N H_2SO_4 solution was added to each tube and heated in a heating block in a hood at 200–225°C for 30 min. Tubes were then removed from the block and allowed to cool before addition to each tube of 150 μL of 30% (w/w) H_2O_2 (cat no. 216763, Sigma-Aldrich) and continued heating for an additional 30 min. After this step, if any brown color persisted, 50 μL of 30% (w/w) H_2O_2 was added to all cooled tubes, and the samples were heated for another 15 min. Then, the tubes were removed from the heating block and cooled to room temperature. To each tube were added 3.9 mL of deionized water and 0.5 mL of ammonium molybdate (IV) tetrahydrate (2.5% (w/v); cat. no. A1343, Sigma-Aldrich). Samples were mixed with a vortex mixer five to seven times. Then, 0.5 mL of freshly prepared ascorbic acid solution (10% (w/v); cat. no. A5960, Sigma-Aldrich) was added and the samples were mixed again. The tubes were closed with the screw cap to prevent evaporation and heated at 100°C for 7 min in a water bath. After cooling to ambient temperature, samples were analyzed spectrophotometrically. The wavelength of the spectrophotometer was set to 820 nm, and the instrument was blanked against air before the samples were measured. From the phosphorus standards, a calibration curve was generated, and the amounts of the phosphorus in the test samples were determined. Multiplication of the obtained amount of phosphorus by 0.950 yielded the correct amount of phospholipids. This factor considers the presence of cardiolipin (CL), which contains two phosphate moieties per lipid molecule, in contrast to phosphatidylethanolamine (PE) and phosphatidylglycerol (PG). See Table S2 for more information.

Estimation of the average molecular mass of an *E. coli* phospholipid

For the calculation of the average molecular mass of an *E. coli* phospholipid (766.39 Da), the relative ratio of the three main phospholipids, i.e., PE/PG/CL = 71.39:23.36:5.25 mol/mol %, as well as the average molecular masses of PE (719.302 Da), PG (761.073 Da), and CL (1429.954 Da) (Avanti Polar Lipids), were considered. See Table S2 for more information.

Calculation of the lipid-accessible surface of membrane proteins

The PDB file of the corresponding membrane protein, i.e., UT (3K3F (9)), AdiC (3LRB (10)), and LacY (2V8N (11)), oriented in the lipid bilayer was downloaded from the OPM (Orientations of Proteins in Membranes) database (http://opm.phar.umich.edu/) (21). The lipid-accessible surface ($Å^2$) was calculated by the Gerstein method (22,23) using a probe radius of 1.88 Å (approximate radius of a methylene group) (24) and considering atoms from amino acids within the membrane boundaries.

Lipid extraction from SEC peak fractions of purified AdiC in DDM and OM for mass spectrometry

Lipid extraction was performed according to a slightly modified version of the method described by Bligh and Dyer (25). Briefly, 150 μL PBS, 500 μL CH_3OH, and 250 μL $CHCl_3$ were added to 50 μL of SEC peak fraction (~0.4 mg/mL protein concentration) to yield a 1:2:0.8 ratio (PBS/CH_3OH/$CHCl_3$). The mixture was vortexed for 1 min and centrifuged at 9500 × *g* for 5 min at 4°C (single-phase extraction). The supernatant was recovered and 250 μL PBS and 250 μL $CHCl_3$ were added immediately to yield a 1.8:2:2 ratio (PBS/CH_3OH/$CHCl_3$). The mixture was vortexed again for 1 min and centrifuged (9500 × *g* for 5 min at 4°C) (two-phase extraction). The lipids recovered from the lower organic phase were dried under nitrogen and stored at −20°C. The lipid extraction was done one day before electrospray ionization-mass spectrometry (ESI-MS) analysis.

For the direct infusion, samples were dissolved in 1 mL methanol containing 0.2% acetic acid, vortexed for 1 min, and centrifuged (9500 × *g* for 5 min at 4°C). The supernatant was transferred to a high-performance liquid chromatography glass vial and analyzed by direct infusion into the ESI-MS.

Mass spectrometry

Equipment

ESI-MS analyses were conducted on an API 4000 QTrap mass spectrometer equipped with a TurboIonSpray probe (AB Sciex, Concord, Ontario, Canada). Data acquisition and analysis were performed using the Analyst software version 1.5.1 (AB Sciex).

MS Detection

The TurboIonSpray probe was operated in negative and positive ionization modes (MS− and MS+). The source parameters, run at room temperature using nitrogen as a curtain gas and nebulizer, were capillary voltage in positive and negative modes, −4.2 kV and +4.5 kV; curtain gas, 20 psi; GS1, 20 psi; GS2, 0 psi; declustering potential, 70 V; entrance potentials, 10 V; and interface heater ON. Q1/Q3 resolutions were set to −0.7/−0.5 Da and 1/1 Da for both PS and NL in negative and positive modes. The collision energy was set at 40 eV and 50 eV in negative and positive modes, respectively. Collision exit potential was set to 10 V in all experiments. The parameters for tandem MS (MS/MS) experiments on PE and PG in negative and positive modes were precursor ion scan (PS) of −196 (PS−196), neutral loss (NL) of +141 (NL+141), PS of −153 (PS−153), and NL of +171 (NL+171). When charged phospholipids (PLs) lose a diagnostic fragment (neutral or charged) of a defined mass, these fragments can be detected in NL and PS, e.g., neutral fragments of 141 Da for PE and 171 Da for PG in NL. The samples were directly infused using a syringe pump at a speed rate of 10 μL/min. Each sample was first infused for 3 min to stabilize the signal and the experiments were run consecutively in the order MS−, PS−169, PS−153, MS+, NL+141, and NL+196. The duty cycle was 2 s and the scans were gained during 3 min in multiple-channel acquisition mode. All experiments were acquired in the range 600–900 Da.

MS/MS experiments were performed only in negative mode, using a similar setup as described above except that the mass range recorded was from 100 Da to 10 Da above the molecular mass of the corresponding phospholipid. Experiments were recorded for 2 min.

Model generation of AdiC ternary complexes

The AdiC structure (PDB 3LRB) was placed into a 1-palmitoyl-2-oleoyl-*sn*-glycero-3-phosphoethanolamine (POPE) bilayer by applying the Membrane Builder Tool of the CHARMM-GUI (http://www.charmm-gui.org/?doc=input/membrane/) (26,27). Next, phospholipids were removed manually and only molecules that were in close contact to AdiC were kept. To position detergent molecules appropriately, the former model was used as input file for a PACKMOL run (28). The numbers of phospholipid and detergent molecules arranged around AdiC were according to the experimentally determined values of AdiC purified in DDM and OM.

RESULTS AND DISCUSSION

Determination of the apparent molecular masses of ternary complexes by SEC

The model membrane proteins UT, AdiC, and LacY were purified by metal affinity chromatography in the detergents DDM, UDM, DM, NM, OM, Cymal-7, Cymal-6, Cymal-5, and NG (see Fig. S1 for SDS-PAGE gels). Purified proteins were then submitted to SEC on Superdex 200. Fig. 1 displays representative elution profiles of UT, AdiC, and LacY in the nine different detergents. In contrast to UT and AdiC, which were stable in all detergents, LacY started to aggregate in NM and OM during purification (Fig. 1 *C*) and could not be purified in NG (no protein yield after affinity chromatography). NM, OM, and NG have relatively short alkyl chains and can be considered as harsh detergents (5). Table 1 summarizes the apparent molecular masses ($M_{app,SEC}$) of UT, AdiC, and LacY in different detergents, as determined by SEC. In all model proteins, the $M_{app,SEC}$ of the ternary complexes decreased with decreasing alkyl chain length in alkylmaltosides (DDM, UDM, DM, NM, and OM) and with decreasing length of the alkyl chain connecting the cyclohexane and maltoside moieties in Cymals (Cymal-7, Cymal-6, and Cymal-5). It should be noted that a decrease in alkyl chain length implies an increase of the CMC and a decrease of the aggregation number (see Table S3 for detergent properties). Similar trends were observed in SEC experiments with monomeric ADP/ATP carriers from *Saccharomyces cerevisiae* (29,30), corroborating our results.

Determination of the detergent-binding capacities and phospholipid contents of purified UT, AdiC, and LacY proteins

SEC peak fractions were collected for UT, AdiC, and LacY purified in alkylmaltoside and Cymal detergents, and the protein, detergent, and phospholipid contents were determined (see Materials and Methods). Because LacY tended to aggregate in NM and OM, those samples were not considered for detergent and phospholipid determinations. For the glucoside NG, phospholipid contents of UT and AdiC were determined, but not detergent-binding capacities. In contrast to the maltosides, SEC protein peaks overlapped with the empty NG micelles (Fig. S2), making determinations of the detergent content in peak fractions unreliable. LacY in NG was not considered because of aggregation and no protein yields after affinity chromatography. Figs. 2–4, *A* and *B*, summarize the determined numbers of bound phospholipids, n_{PL}, and detergent molecules, n_D, respectively, per UT trimer, AdiC dimer, and LacY monomer. Considering Figs. 2 *A*, 3 *A*, and 4 *A*, high CMC detergents had significantly stronger delipidating effects on purified UT, AdiC, and LacY than did low CMC detergents as a direct consequence of the higher detergent concentrations needed when working with high CMC detergents (Table S1). Delipidation was particularly dramatic for monomeric LacY; e.g., with DM, there was only one phospholipid per LacY protein (Fig. 4 *A*), which of the three model proteins has the smallest hydrophobic membrane-embedded surface (see also Calculation of the hydrophobic lipid-accessible surfaces of UT, AdiC, and LacY, and the correlation with the experimental data). NG and Cymal-5 had exceptional delipidating effects on the model proteins compared to the other detergents tested (Figs. 2 *A*, 3 *A*, and 4 *A*). In summary, the amount of endogenous phospholipid bound to a membrane protein after purification varies strongly with the detergent type and concentration. Delipidation as a function of decreasing detergent chain lengths is more efficient for proteins with smaller hydrophobic membrane-embedded surface. This is nicely illustrated by the abrupt decrease of phospholipids from DDM to UDM in LacY compared to UT and AdiC (Figs. 2 *A*, 3 *A*, and 4 *A*). It should also be considered that an increase of the concentration of the same detergent, e.g., from 0.01% DDM to 0.1% DDM, to

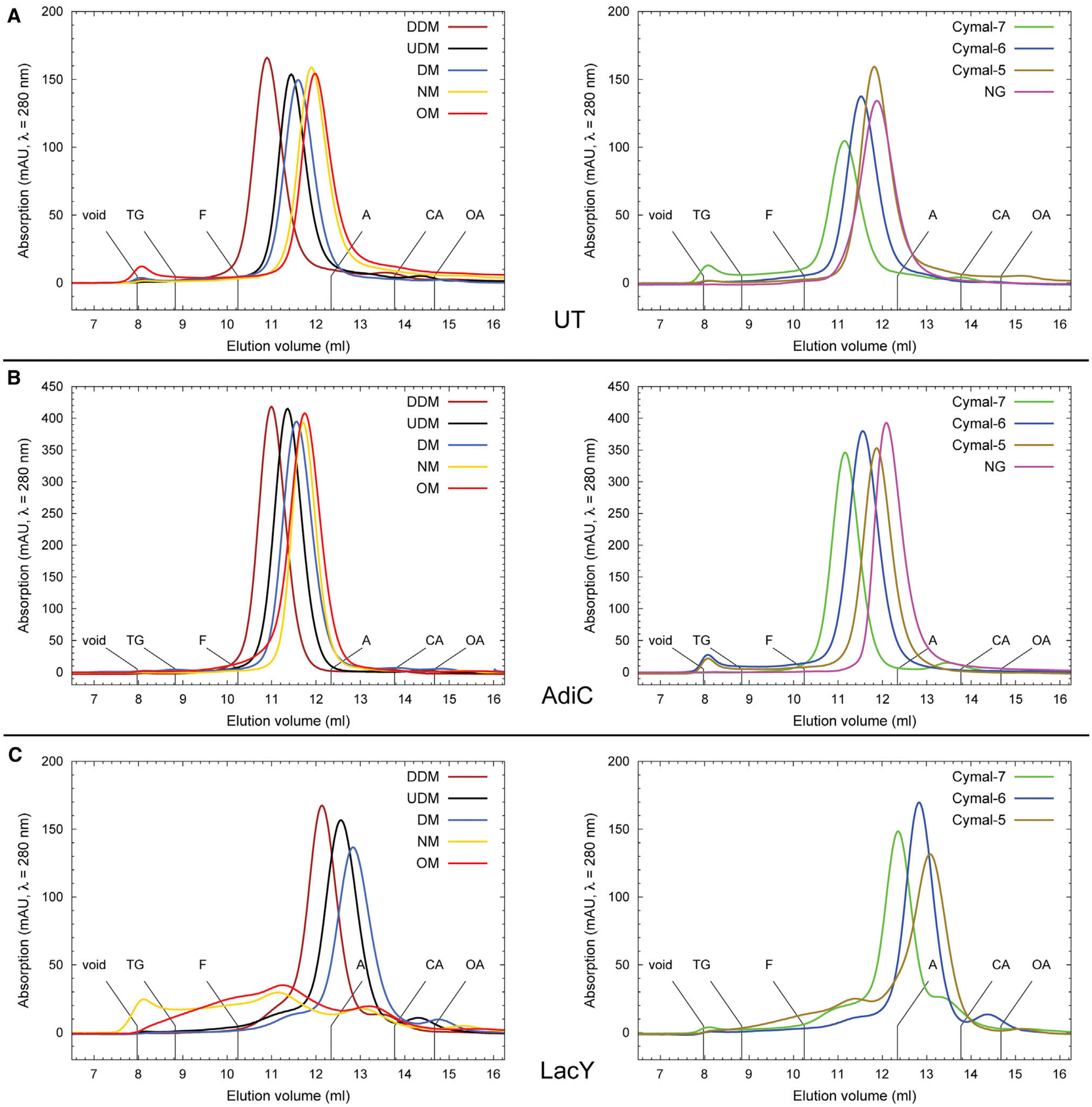

FIGURE 1 SEC analysis of the model membrane proteins UT, AdiC, and LacY purified in nine different detergents. Representative elution profiles of purified UT (*A*), AdiC (*B*), and LacY (*C*) are shown. Alkylmaltosides (DDM, UDM, DM, NM, and OM), Cymals (Cymal-7, Cymal-6, and Cymal-5), and the glucoside NG were used as detergents. UT and AdiC were stable in all detergents. SEC of LacY purified in NM and OM indicated aggregation. LacY was unstable in NG and could not be purified and submitted to SEC. Void volume and retention volumes are indicated for standard proteins thyroglobulin (*TG*, 669 kDa), ferritin (*F*, 440 kDa), aldolase (*A*, 158 kDa), conalbumin (*CA*, 75 kDa), and ovalbumin (*OA*, 43 kDa). To see this figure in color, go online.

keep the protein in solution during purification, has substantial delipidating effects on membrane proteins (31). To support this finding, we also purified AdiC using 0.12% instead of 0.04% DDM (i.e., at a threefold higher detergent concentration). This led to a reduction of the copurified phospholipids bound to one AdiC dimer from 52 (0.04% DDM) to 27 (0.12% DDM) (Fig. 3 *A*), corroborating the findings of Sigal et al. (31).

The number of detergent molecules bound to a specific, purified membrane protein strongly depended on the detergent used. For maltosides, the number of bound detergent molecules decreased with shorter alkyl chain length. The

TABLE 1 Determination of $M_{app,SEC}$ of ternary complexes by SEC

	Apparent molecular mass of ternary complex (kDa)		
Detergents	UT	AdiC	LacY
DDM	277 ± 4.6	257 ± 4.4	156 ± 10.6
UDM	222 ± 1.5	220 ± 4.9	122 ± 1.7
DM	192 ± 2.2	198 ± 1.9	106 ± 1.3
NM	183 ± 1.8	183 ± 3.0	96 ± 0.3[a]
OM	174 ± 2.4	179 ± 1.4	87 ± 2.1[a]
Cymal-7	232 ± 1.6	236 ± 1.3	135 ± 4.1
Cymal-6	203 ± 1.4	205 ± 1.5	110 ± 3.1
Cymal-5	183 ± 0.6	170 ± 3.9	97 ± 1.6
NG	171 ± 0.2	152 ± 2.6	ND

Values represent the mean ± SD from at least two SEC runs with protein from two to five independent purifications. The apparent molecular mass of the ternary complex was determined by SEC. ND (not determined) indicates that the protein aggregated during purification, and SEC could not be performed.
[a]These values are to be considered with caution, since LacY started to aggregate during purification and SEC in these two detergents.

relationship between hydrophobic membrane-embedded surface and detergent binding capacity on the one hand, and the phospholipid content on the other are further discussed below (see Calculation of the hydrophobic lipid-accessible surfaces of UT, AdiC, and LacY, and the correlation with experimental data).

Determination of the phospholipid types bound to purified AdiC in DDM and OM

Of the five alkylmaltosides tested, AdiC purified in DDM and OM had the highest and lowest amounts of bound endogenous phospholipids (Fig. 3 *A*). To determine and compare the types of phospholipids bound in these two boundary conditions, we performed ESI-MS/MS analysis of SEC peak fractions of purified AdiC in DDM and OM (Fig. 5).

Phospholipids are charged molecules that show characteristic MS/MS fragmentation patterns. Based on these fragments, different phospholipid classes can be detected in neutral loss scan (NL) and precursor ion scan (PS) experiments; e.g., NL+141 and PS−196 are used for analysis of PEs, and NL+171 and PS−153 for the analysis of PGs (see Materials and Methods) (32,33). In a first step, and as reference, we analyzed *E. coli* polar lipid extract, which only contains PE, PG, and CL, using the method described by Oursel et al. (34). Six PEs and five PGs (Table S4) were identified that corresponded to the main PEs and PGs reported in *E. coli* lipids (34). Their structure was confirmed by MS/MS analysis of the *m/z* corresponding to $[M\text{-}H]^-$ (data not shown). Because CL is a minor constituent of *E. coli* lipids, and because resolution is limited by the use of direct infusion, we were unable to identify CL with our experimental setup. Next, we analyzed *E. coli* total lipid extract and found the six PEs again in all four different

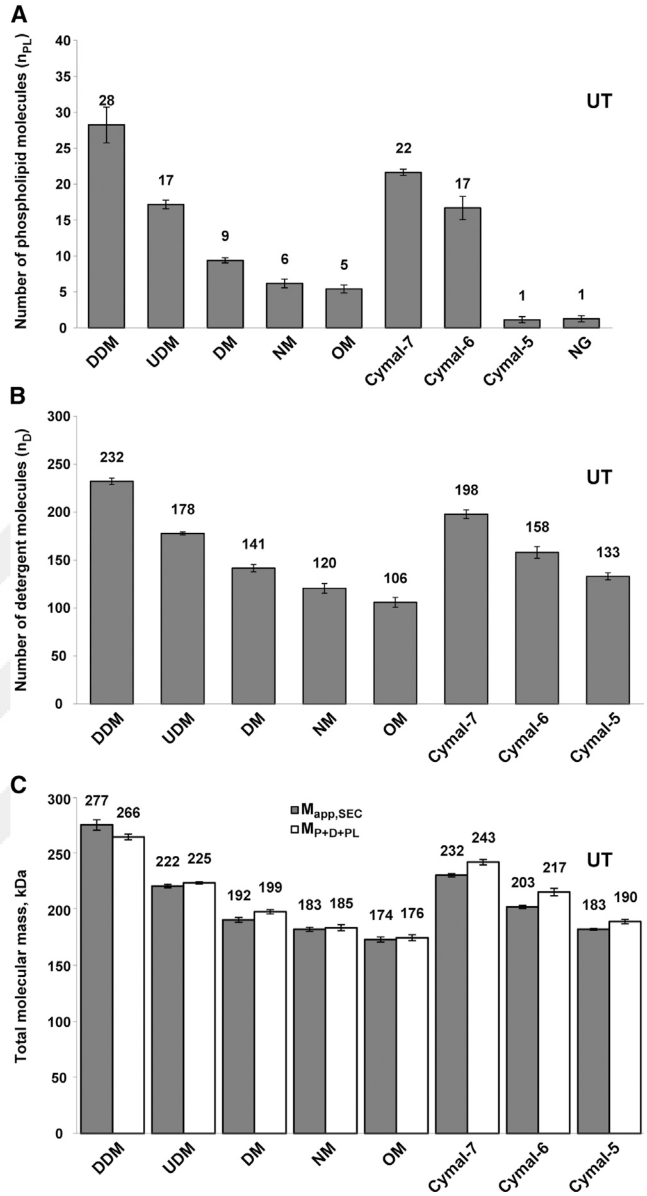

FIGURE 2 (*A* and *B*) Determination of phospholipid (*A*) and detergent molecules (*B*) bound to purified UT from SEC peak fractions. Alkylmaltosides (DDM, UDM, DM, NM, and OM), Cymals (Cymal-7, Cymal-6, and Cymal-5), and the glucoside NG were used for purification and SEC. The determined numbers of phospholipid (n_{PL}) and detergent molecules (n_D) bound to UT are indicated. Values represent the mean ± SD from at least triplicates of two to three independent purifications. (*C*) Comparison of molecular masses of UT ternary complexes in different detergents determined by SEC ($M_{app,SEC}$; Table 1), and protein, phospholipid and detergent determination (M_{P+D+PL}).

experiments (i.e., MS+, MS−, PS−196, and NL+141), whereas the positive mode NL+141 was the most sensitive (Fig. S3, *upper*). On the other hand, PG detection was in general less sensitive, and we were only able to identify the five PGs using the negative-mode PS−153 (Fig. S4, *upper*). Therefore, the NL+141 and PS−153 modes were used to determine the types of endogenous phospholipids

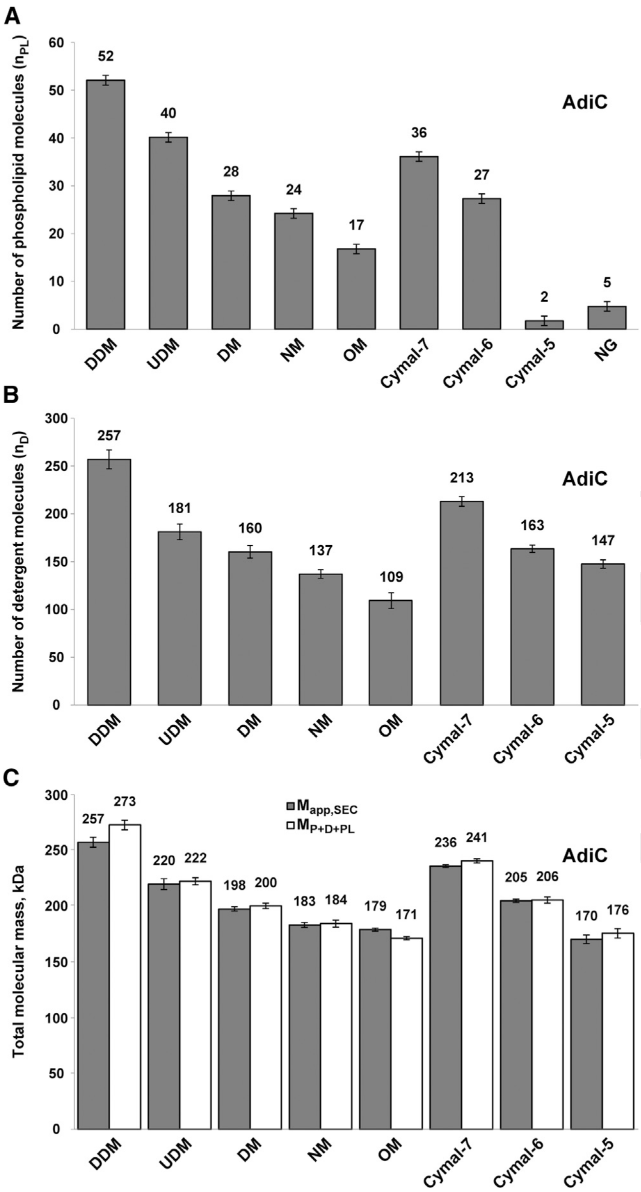

FIGURE 3 (*A* and *B*) Determination of phospholipid (*A*) and detergent molecules (*B*) bound to purified AdiC from SEC peak fractions. Alkylmaltosides (DDM, UDM, DM, NM, and OM), Cymals (Cymal-7, Cymal-6, and Cymal-5), and the glucoside NG were used for purification and SEC. The determined numbers of phospholipid (n_{PL}) and detergent molecules (n_D) bound to AdiC are indicated. Values represent the mean ± SD from at least triplicates of two to three independent purifications. (*C*) Comparison of molecular masses of AdiC ternary complexes in different detergents determined by SEC ($M_{app,SEC}$; Table 1), and protein, phospholipid and detergent determination (M_{P+D+PL}).

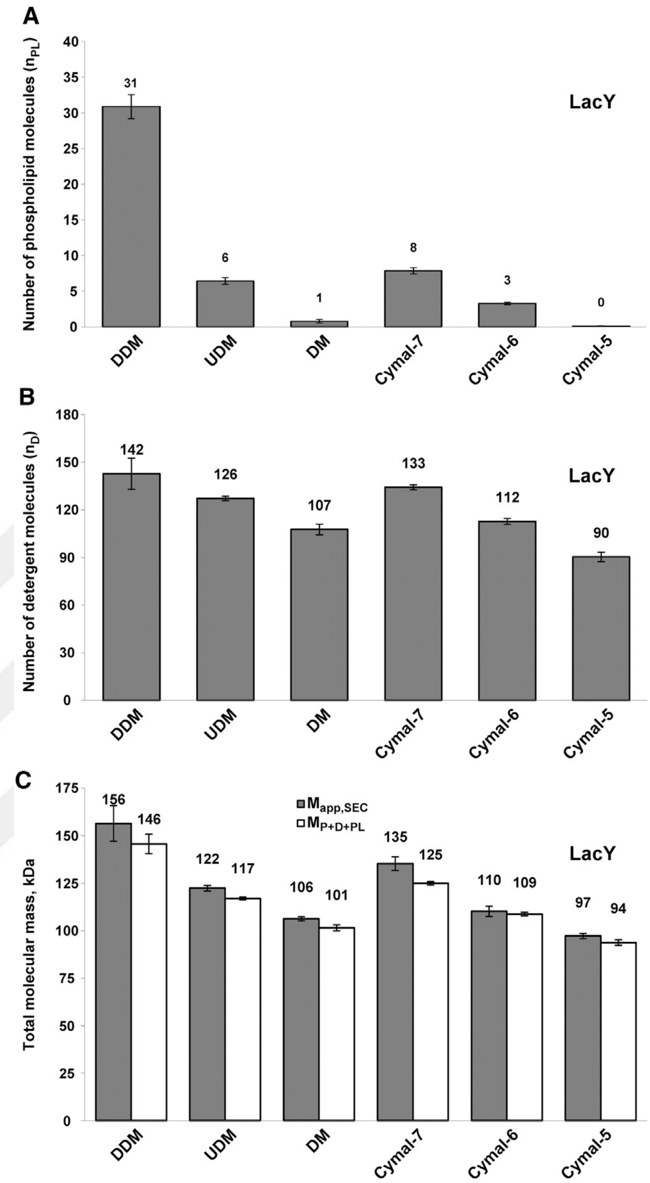

FIGURE 4 (*A* and *B*) Determination of phospholipid (*A*) and detergent molecules (*B*) bound to purified LacY from SEC peak fractions. Alkylmaltosides (DDM, UDM, and DM) and Cymals (Cymal-7, Cymal-6, and Cymal-5) were used for purification and SEC. The determined numbers of phospholipid (n_{PL}) and detergent molecules (n_D) bound to LacY are indicated. Values represent the mean ± SD from at least triplicates of two to three independent purifications. (*C*) Comparison of molecular masses of LacY ternary complexes in different detergents determined by SEC ($M_{app,SEC}$; Table 1), and protein, phospholipid, and detergent determination (M_{P+D+PL}).

bound to AdiC when purified with DDM and OM (Figs. S3 and S4, *middle* and *lower*).

Fig. 5 summarizes the results from ESI-MS/MS analysis of AdiC purified in DDM and OM, showing the identified PEs (Fig. 5 *A*) and PGs (Fig. 5 *B*). The relative amounts of bound PE and PG (Fig. 5 *C*) in AdiC purified in OM were strongly decreased compared to those purified in DDM, with the exception of PG-747 in OM (see Table S4 for phospholipid nomenclature). This interesting finding indicated that the negatively charged phospholipid PG-747 is strongly enriched in AdiC samples purified in OM. This enrichment most probably happens during membrane solubilization, where all *E. coli* lipids are still present. In general, the amount of PE in AdiC purified in OM is

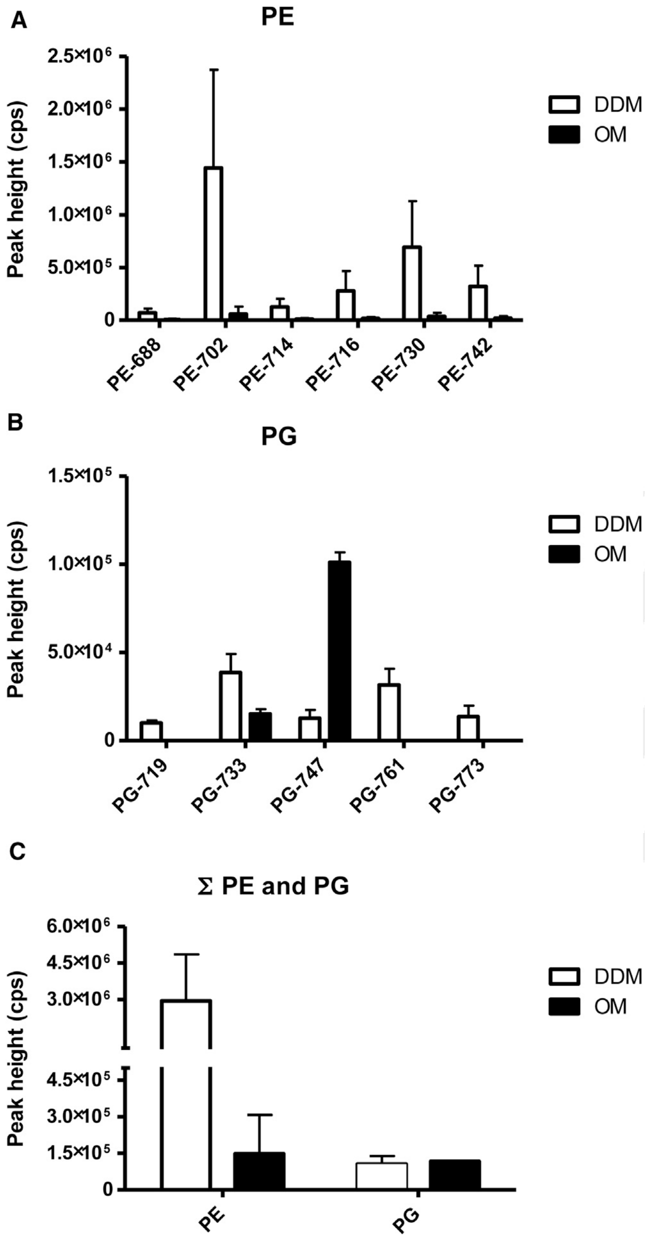

FIGURE 5 Semiquantitative analyses of PEs and PGs present in AdiC purified with DDM and OM. (*A* and *B*) Analyses of PEs and PGs using NL+141 (*A*) and PS−153 (*B*) modes. (*C*) Comparison of the relative amounts of PEs and PGs from NL+141 and PS−153 experiments. The sums of all PEs and PGs are displayed. Values represent the mean ± SD from at least duplicates of two independent purifications. cps, counts/s.

strongly reduced compared to that purified in DDM, whereas the relative amounts of PG stay similar (Fig. 5 *C*).

Comparison of molecular masses of ternary complexes determined by different methods

Knowledge of the molecular mass, oligomeric state, and amount of bound phospholipid and detergent per model membrane protein allowed calculation of the total molecular mass of the ternary complexes (M_{P+D+PL}). Calculations were done for UT, AdiC, and LacY and compared with the $M_{app,SEC}$ (Figs. 2 *C*, 3 *C*, and 4, *C*). These comparisons demonstrated that the molecular masses of the UT, AdiC, and LacY ternary complexes determined by SEC ($M_{app,SEC}$s) are in general similar to the M_{P+D+PL} values, and thus quite precise and reliable. However, considering that the $M_{app,SEC}$ values for UT and AdiC (Table 1) are comparable, particular care has to be taken when trying to deduce unknown oligomeric states of membrane proteins based on $M_{app,SEC}$ values alone (35).

Calculation of the hydrophobic lipid-accessible surfaces of UT, AdiC, and LacY, and correlation with the experimental data

The atomic structures of UT, AdiC, and LacY were solved (9–11), and the coordinate files are available. Furthermore, the OPM database provides PDB files of these proteins oriented in the lipid bilayer, indicating the membrane boundaries. Using these coordinate files, we calculated the hydrophobic lipid-accessible surfaces of our model membrane proteins as 12,397 Å^2 for UT, 12,694 Å^2 for AdiC, and 7,607 Å^2 for LacY (see Materials and Methods).

Our experimental data allowed the comparison of the phospholipid contents in trimeric (UT), dimeric (AdiC), and monomeric (LacY) membrane proteins. Comparison of UT (Fig. 2 *A*) with AdiC (Fig. 3 *A*) indicated that the phospholipid content in these two membrane proteins of different oligomeric states but having similar hydrophobic lipid-accessible surfaces varied significantly, with, for example, 28 and 52 phospholipids in DDM. This significant difference in bound endogenous phospholipids might be attributed to different physicochemical properties of the membrane-embedded surfaces of the two proteins. With the exception of DDM, the numbers of phospholipid molecules bound to LacY were significantly lower than in UT and AdiC. This makes sense, considering that LacY has only ~60% of the hydrophobic membrane-embedded surface of UT and AdiC to accommodate phospholipid molecules. Interestingly, the number of endogenous phospholipid molecules in LacY purified with DDM was high compared to purifications with the other detergents, indicating the mildness of DDM.

As mentioned above, UT and AdiC have similar hydrophobic lipid-accessible surfaces, but retain different amounts of endogenous phospholipids during purification. This makes it possible to estimate whether increased amounts of endogenous phospholipids bound to membrane proteins also significantly increase the size of the detergent micelles. For example, comparable numbers of UDM and OM molecules, i.e., 178 and 181 (UDM), and 106 and 109 (OM), were found in purified UT and AdiC, despite the significant difference in endogenous phospholipids, i.e., 17 and 40 (UDM), and 5 and 17 (OM) (Figs. 2, *A* and *B*, and 3, *A* and *B*). Based on these results, important differences in micelle size are not expected within the here determined range of bound endogenous phospholipids.

Specific amounts of detergent bound to membrane proteins are needed to keep them in solution. These detergent molecules are sequestered during the solubilization step, where isolated membranes are exposed to high detergent concentrations. Table S5 displays the amount of detergent bound to purified UT, AdiC, and LacY in terms of empty detergent micelles (see Table S3 for aggregation numbers of detergents, which define empty micelles). It is clear that the larger the hydrophobic lipid-accessible surface of the protein, the higher is the empty detergent micelle/protein (complex) ratio; e.g., 1.6, 2.0, and 2.3 empty DM micelles are needed to keep LacY, UT, and AdiC solubilized. It should be noted that dimeric AdiC has a larger hydrophobic lipid-accessible surface than trimeric UT (Table S5) despite its lower oligomeric state. Therefore, the hydrophobic lipid-accessible surface area is critical for the amount of detergent bound and is not necessarily an indicator of the oligomeric state of the membrane protein.

Finally, we evaluated whether the determined detergent binding capacities and phospholipid contents make sense and can be accommodated around the hydrophobic membrane-embedded surface of a membrane protein. To this aim, we modeled the structure of AdiC in terms of the numbers of phospholipid and detergent molecules determined at the two extremes in the alkylmaltoside series (Fig. 6). From this model, it is evident that the determined numbers of detergent and phospholipid molecules make sense and can be accommodated around the hydrophobic membrane-embedded surface. Furthermore, the models support the experimental results (Figs. 2, *A* and *B*, 3, *A* and *B*, and 4, *A* and *B*) showing that the size of the detergent and lipid belt surrounding the hydrophobic lipid-accessible surface of purified membrane proteins can be tuned by the appropriate choice of detergent.

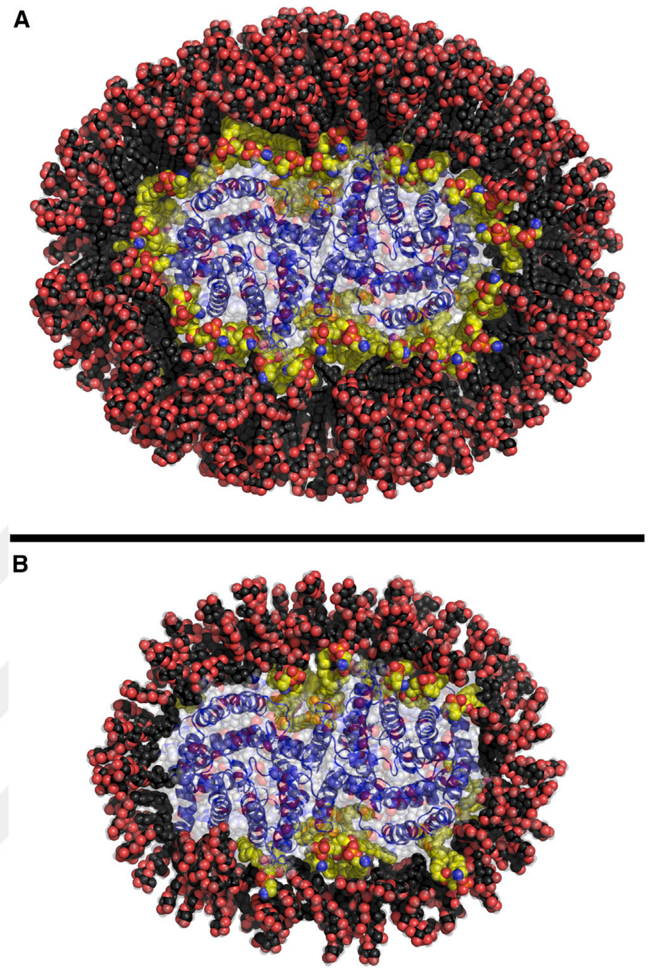

FIGURE 6 (*A* and *B*) Ternary complex models of AdiC purified in DDM (*A*) and OM (*B*). The ternary complexes shown contain the AdiC-dimer protein (*blue cartoon* and *transparent spheres*), phospholipid (*yellow spheres*), and detergent molecules (*black spheres*). Oxygen and nitrogen atoms are colored red and blue, respectively. The ternary complexes in *A* and *B* are composed of 257 DDM and 52 POPE, and 109 OM and 17 POPE molecules, respectively. These numbers for phospholipid and detergent molecules used for model building are based on the experimentally determined values (Fig. 3). Images were prepared with PyMOL software (www.pymol.org). To see this figure in color, go online.

CONCLUSION

Analyses of the amounts of detergent and endogenous phospholipid molecules bound to purified membrane proteins have been neglected in the past. Consequently, information on the composition of such ternary complexes is very sparse. We have conducted a systematic study and characterized ternary complexes of three model membrane proteins purified in nine different detergents and determined their molecular masses, detergent binding capacities, and phospholipid contents. From the experimental results, the insights gained were tentatively put into a general context as follows. 1), The number of detergent molecules bound to purified membrane proteins is dependent on the physicochemical properties of the detergents used and the hydrophobic lipid-accessible protein surfaces, i.e., the size of the surface area to which the hydrophobic detergent tail can bind. 2), The number of endogenous phospholipid molecules bound to purified membrane proteins is dependent on the hydrophobic lipid-accessible protein surfaces, as well as the detergent types and concentrations used for purification. 3), As reflected by our experimental data (Figs. 2–4 and 6), the size of the detergent and lipid belt surrounding the hydrophobic lipid-accessible surface of purified membrane proteins can be tuned by the appropriate choice of detergent. 4), Exceptional delipidating effects on membrane proteins were found for the detergents NG and Cymal-5 (see recent structure reports using NG and Cymal-5 (36–40)). In agreement, controlled delipidation together with a minimally sized detergent/lipid belt have been shown to be important in allowing crystal contact formation and growth of highly ordered membrane protein 3D crystals for structure determination (12,13). 5), As illustrated by AdiC purified with two detergents with very different physicochemical properties (i.e., DDM and OM), the types of endogenous phospholipids bound to purified membrane proteins can significantly vary depending on the detergent used. 6), Furthermore, we show that SEC is a suitable method to determine the molecular masses of ternary complexes, which might be successfully applied to other membrane proteins with structures similar to those of UT, AdiC, and LacY.

SUPPORTING MATERIAL

Four figures, five tables, and reference (41) are available at http://www.biophysj.org/biophysj/supplemental/S0006-3495(14)00261-6.

Financial support from the University of Bern, the Swiss National Science Foundation (grant 31003A_144168 to D.F.), and the National Centre of Competence in Research (NCCR) TransCure (to D.F. and J.G.) is gratefully acknowledged.

REFERENCES

1. Garavito, R. M., D. Picot, and P. J. Loll. 1996. Strategies for crystallizing membrane proteins. *J. Bioenerg. Biomembr.* 28:13–27.
2. Rosenbusch, J. P., A. Lustig, …, M. Regenass. 2001. Approaches to determining membrane protein structures to high resolution: do selections of subpopulations occur? *Micron.* 32:75–90.
3. Columbus, L., J. Lipfert, …, S. A. Lesley. 2009. Mixing and matching detergents for membrane protein NMR structure determination. *J. Am. Chem. Soc.* 131:7320–7326.
4. O'Malley, M. A., M. E. Helgeson, …, A. S. Robinson. 2011. The morphology and composition of cholesterol-rich micellar nanostructures determine transmembrane protein (GPCR) activity. *Biophys. J.* 100:L11–L13.
5. Privé, G. G. 2007. Detergents for the stabilization and crystallization of membrane proteins. *Methods.* 41:388–397.
6. Seddon, A. M., P. Curnow, and P. J. Booth. 2004. Membrane proteins, lipids and detergents: not just a soap opera. *Biochim. Biophys. Acta.* 1666:105–117.
7. le Maire, M., P. Champeil, and J. V. Moller. 2000. Interaction of membrane proteins and lipids with solubilizing detergents. *Biochim. Biophys. Acta.* 1508:86–111.
8. Ostermeier, C., and H. Michel. 1997. Crystallization of membrane proteins. *Curr. Opin. Struct. Biol.* 7:697–701.
9. Levin, E. J., M. Quick, and M. Zhou. 2009. Crystal structure of a bacterial homologue of the kidney urea transporter. *Nature.* 462:757–761.
10. Gao, X., F. Lu, …, Y. Shi. 2009. Structure and mechanism of an amino acid antiporter. *Science.* 324:1565–1568.
11. Guan, L., O. Mirza, …, H. R. Kaback. 2007. Structural determination of wild-type lactose permease. *Proc. Natl. Acad. Sci. USA.* 104:15294–15298.
12. Lemieux, M. J., R. A. Reithmeier, and D. N. Wang. 2002. Importance of detergent and phospholipid in the crystallization of the human erythrocyte anion-exchanger membrane domain. *J. Struct. Biol.* 137:322–332.
13. Lemieux, M. J., J. Song, …, D. N. Wang. 2003. Three-dimensional crystallization of the *Escherichia coli* glycerol-3-phosphate transporter: a member of the major facilitator superfamily. *Protein Sci.* 12:2748–2756.
14. Bosshart, P. D., F. Casagrande, …, D. Fotiadis. 2008. High-throughput single-molecule force spectroscopy for membrane proteins. *Nanotechnology.* 19:384014.
15. Weitz, D., D. Harder, …, H. Daniel. 2007. Functional and structural characterization of a prokaryotic peptide transporter with features similar to mammalian PEPT1. *J. Biol. Chem.* 282:2832–2839.
16. Smith, P. K., R. I. Krohn, …, D. C. Klenk. 1985. Measurement of protein using bicinchoninic acid. *Anal. Biochem.* 150:76–85.
17. Engel, A., A. Hoenger, …, M. Zulauf. 1992. Assembly of 2-D membrane protein crystals: dynamics, crystal order, and fidelity of structure analysis by electron microscopy. *J. Struct. Biol.* 109:219–234.
18. Kaufmann, T. C., A. Engel, and H. W. Rémigy. 2006. A novel method for detergent concentration determination. *Biophys. J.* 90:310–317.
19. Chen, P. S., T. Y. Toribara, and H. Warner. 1956. Microdetermination of phosphorus. *Anal. Chem.* 28:1756–1758.
20. Fiske, C. H., and Y. Subbarow. 1925. The colorimetric determination of phosphorus. *J. Biol. Chem.* 66:375–400.
21. Lomize, M. A., A. L. Lomize, …, H. I. Mosberg. 2006. OPM: orientations of proteins in membranes database. *Bioinformatics.* 22:623–625.
22. Tsai, J., R. Taylor, …, M. Gerstein. 1999. The packing density in proteins: standard radii and volumes. *J. Mol. Biol.* 290:253–266.
23. Gerstein, M., and F. M. Richards. 2001. Protein geometry: volumes, areas and distances. *In* International Tables for Crystallography. M. Rossmann and E. Arnold, editors. Kluwer, Dordrecht, pp. 531–539.
24. Tulumello, D. V., and C. M. Deber. 2012. Efficiency of detergents at maintaining membrane protein structures in their biologically relevant forms. *Biochim. Biophys. Acta.* 1818:1351–1358.
25. Bligh, E. G., and W. J. Dyer. 1959. A rapid method of total lipid extraction and purification. *Can. J. Biochem. Physiol.* 37:911–917.
26. Jo, S., T. Kim, and W. Im. 2007. Automated builder and database of protein/membrane complexes for molecular dynamics simulations. *PLoS ONE.* 2:e880.
27. Jo, S., J. B. Lim, …, W. Im. 2009. CHARMM-GUI Membrane Builder for mixed bilayers and its application to yeast membranes. *Biophys. J.* 97:50–58.
28. Martínez, L., R. Andrade, …, J. M. Martínez. 2009. PACKMOL: a package for building initial configurations for molecular dynamics simulations. *J. Comput. Chem.* 30:2157–2164.
29. Bamber, L., M. Harding, …, E. R. Kunji. 2007. The yeast mitochondrial ADP/ATP carrier functions as a monomer in mitochondrial membranes. *Proc. Natl. Acad. Sci. USA.* 104:10830–10834.
30. Kunji, E. R., M. Harding, …, P. Akamine. 2008. Determination of the molecular mass and dimensions of membrane proteins by size exclusion chromatography. *Methods.* 46:62–72.
31. Sigal, N., O. Lewinson, …, E. Bibi. 2007. *E. coli* multidrug transporter MdfA is a monomer. *Biochemistry.* 46:5200–5208.
32. Pulfer, M., and R. C. Murphy. 2003. Electrospray mass spectrometry of phospholipids. *Mass Spectrom. Rev.* 22:332–364.
33. Thomas, A., J. Deglon, …, C. Staub. 2010. High-throughput phospholipidic fingerprinting by online desorption of dried spots and quadrupole-linear ion trap mass spectrometry: evaluation of atherosclerosis biomarkers in mouse plasma. *Anal. Chem.* 82:6687–6694.
34. Oursel, D., C. Loutelier-Bourhis, …, C. M. Lange. 2007. Lipid composition of membranes of *Escherichia coli* by liquid chromatography/tandem mass spectrometry using negative electrospray ionization. *Rapid Commun. Mass Spectrom.* 21:1721–1728.
35. Slotboom, D. J., R. H. Duurkens, …, G. B. Erkens. 2008. Static light scattering to characterize membrane proteins in detergent solution. *Methods.* 46:73–82.

36. Ressl, S., A. C. Terwisscha van Scheltinga, …, C. Ziegler. 2009. Molecular basis of transport and regulation in the Na^+/betaine symporter BetP. *Nature.* 458:47–52.
37. Dang, S., L. Sun, …, N. Yan. 2010. Structure of a fucose transporter in an outward-open conformation. *Nature.* 467:734–738.
38. Schulze, S., S. Köster, …, W. Kühlbrandt. 2010. Structural basis of Na^+-independent and cooperative substrate/product antiport in CaiT. *Nature.* 467:233–236.
39. Lu, F., S. Li, …, N. Yan. 2011. Structure and mechanism of the uracil transporter UraA. *Nature.* 472:243–246.
40. Pedersen, B. P., H. Kumar, …, R. M. Stroud. 2013. Crystal structure of a eukaryotic phosphate transporter. *Nature.* 496: 533–536.
41. Oliver, R. C., J. Lipfert, …, L. Columbus. 2013. Dependence of micelle size and shape on detergent alkyl chain length and head group. *PLoS ONE.* 8:e62488.

SUPPORTING MATERIAL for:

Variation of the detergent binding capacity and phospholipid content of membrane proteins when purified in different detergents

Hüseyin Ilgü, Jean-Marc Jeckelmann, María Salomé Gachet, Rajendra Boggavarapu, Zöhre Ucurum, Jürg Gertsch and Dimitrios Fotiadis

Institute of Biochemistry and Molecular Medicine, and Swiss National Centre of Competence in Research (NCCR) TransCure, University of Bern, CH-3012 Bern, Switzerland

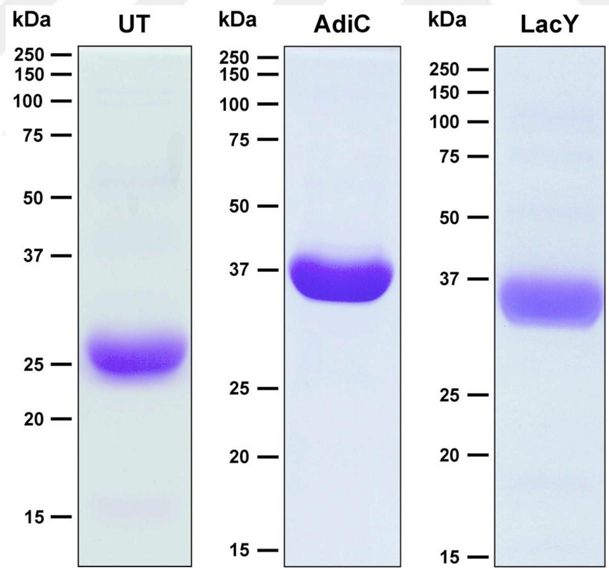

FIGURE S1 SDS-PAGE of purified UT, AdiC and LacY. As seen in the representative 13.5% SDS/polyacrylamide gels, the three proteins were highly pure after metal affinity chromatography. AdiC was purified in DDM, and UT and LacY in DM. All three SDS-PAGE gels were stained with Coomassie Brilliant Blue.

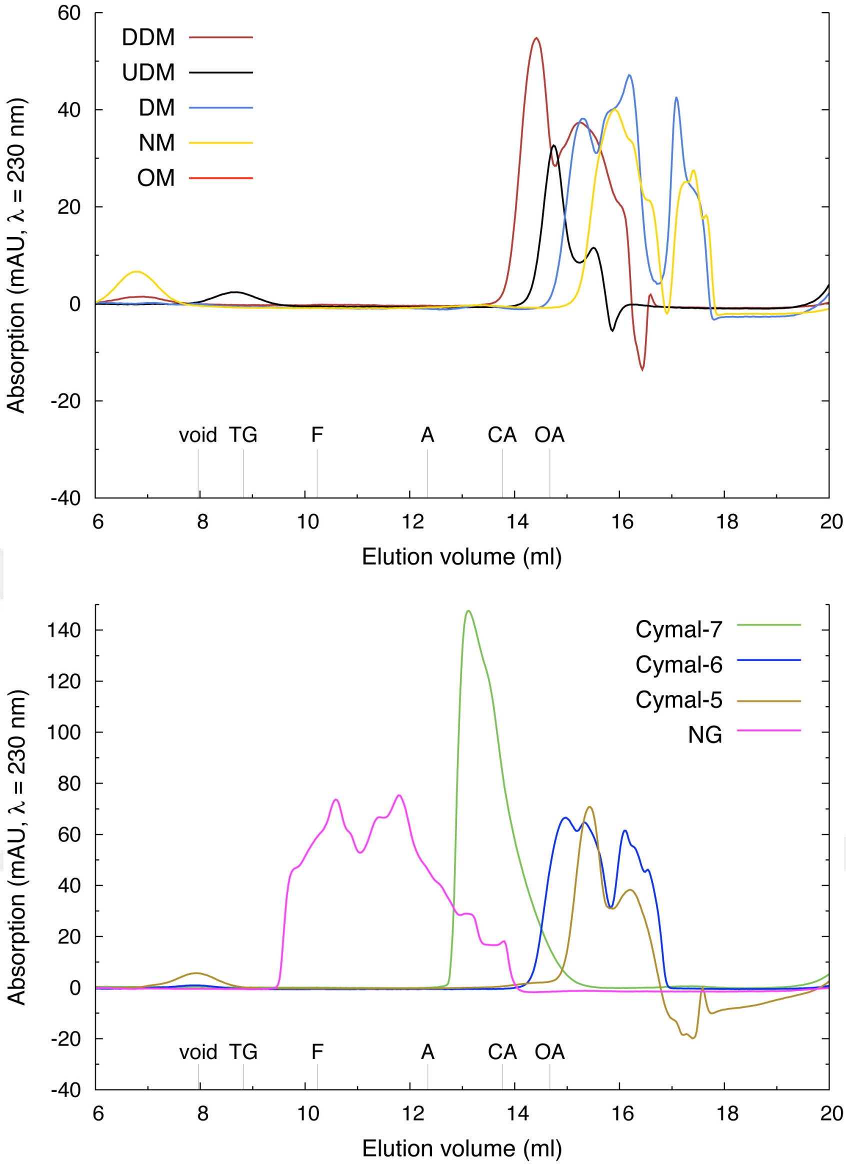

FIGURE S2 SEC analysis of detergents. Representative elution profiles of the alkyl-maltosides (DDM, UDM, DM, NM and OM), the Cymals (Cymal-7, Cymal-6 and Cymal-5) and the glucoside NG. SEC runs were performed as described in Materials and Methods for purified membrane proteins. Instead of purified proteins, 200 μL of the corresponding detergents (10% stock solution in SEC Buffer) were injected. Absorption was measured at 230 nm (maximal absorption of our detergents) instead of 280 nm. The void volume and the retention volumes of standard proteins are indicated: TG, thyroglobulin (669 kDa); F, ferritin (440 kDa); A, aldolase (158 kDa); CA, conalbumin (75 kDa) and OA, ovalbumin (43 kDa).

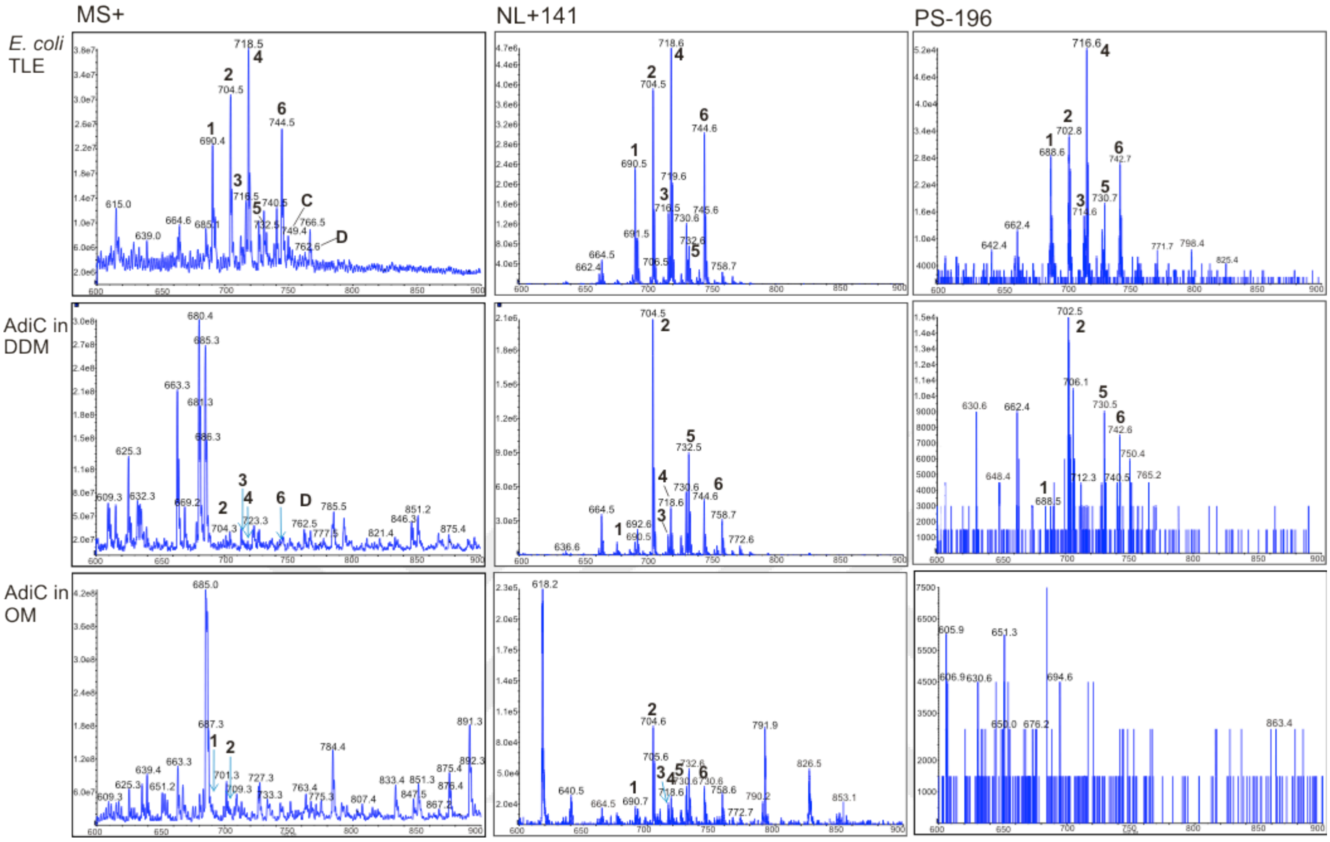

FIGURE S3: ESI-MS/MS analyses of PEs in *E. coli* TLE (top), and AdiC purified in DDM (middle) and OM (bottom) using MS+, NL+141 and PS-196 modes. The peaks marked with numbers and letters correspond to PEs and PGs, and are described in Table S4 (peak numbers and letters are in parentheses in the second column).

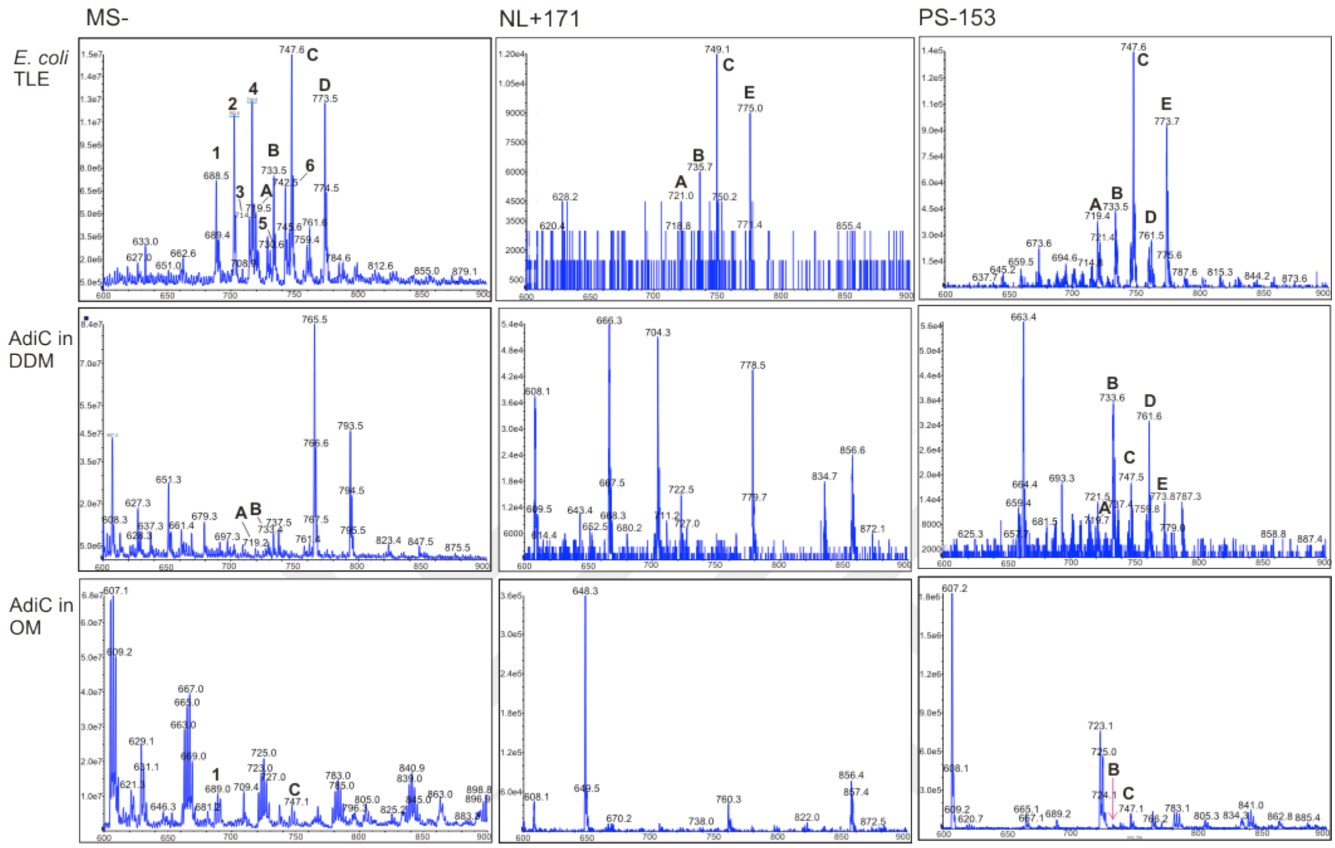

FIGURE S4: ESI-MS/MS analyses of PGs in *E. coli* TLE (top), and AdiC purified in DDM (middle) and OM (bottom) using MS-, NL+171 and PS-153 modes. The peaks marked with numbers and letters correspond to PEs and PGs, and are described in Table S4 (peak numbers and letters are in parentheses in the second column).

TABLE S1 Detergent concentrations for membrane solubilization and metal affinity chromatography

Detergents	Solubilization	Washing / Elution / SEC	
	% (w/v)	% (w/v)	mM
DDM	1.5	0.04	0.78
UDM	2	0.1	2.01
DM	2	0.3	6.22
NM	4	0.6	12.81
OM	5	1.5	33.01
Cymal-7	1.5	0.05	0.96
Cymal-6	2	0.1	1.97
Cymal-5	2.5	0.4	8.09
NG	4	0.4	13.05

TABLE S2 Calculation of the average molecular mass (M_{ave}) of an *E. coli* phospholipid

		Relative composition		mmols contained in 100 g of *E. coli* polar lipids	
Phospholipid	M_{ave}*	% w/w	% mol/mol	phospholipid	phosphorus
PE	719.302	67.00	71.39	93.15	93.15
PG	761.073	23.20	23.36	30.48	30.48
CL	1,429.954	9.80	5.25	6.85	13.71
				Average molecular weight of a phospholipid†	766.39
				Correction factor‡	0.950

* M_{ave} refers to the average molecular mass of individual phospholipids, i.e., PE, PG and CL, of *E. coli* as given by Avanti Polar Lipids, Inc.; http://www.avantilipids.com. Values are given in Da.

† The average molecular weight of an *E. coli* phospholipid is calculated by dividing 100 g by the sum of mol phospholipid. The value is given in Da.

‡ The correction factor, by which a measured amount of phosphorus has to be multiplied to determine the amount of phospholipid molecules, is calculated by dividing the sum of mmol phospholipid by the sum of mmol phosphorus in 100 g of *E. coli* lipids.

TABLE S3 Detergent properties

Detergents*	Molecular mass g/mol	CMC† mM	CMC† %	Aggregation number
DDM	510.6	0.17	0.0087	78-149
UDM	496.6	0.59	0.029	71
DM	482.6	1.8	0.087	69
NM	468.5	6	0.28	25
OM	454.4	19.5	0.89	6
Cymal-7	522.5	0.19	0.0099	150
Cymal-6	508.5	0.56	0.028	91
Cymal-5	494.5	2.4	0.12	47
NG	306.4	6.5	0.2	133

* All values are from Affymetrix: http://www.affymetrix.com and Oliver *et al.* (2013) (1).

† Critical micelle concentration.

TABLE S4 PEs and PGs identified by ESI-MS^2 in *E. coli* PLE

$[M-H]^-$	Phospholipid	Identity
688	PE (1)	C16:0/C16:1* or C14:0/C18:1
702	PE (2)	C16:0/cyC17:0
714	PE (3)	C16:1/C18:1
716	PE (4)	C16:0/C18:1
719	PG (A)	C16:1/C16:0 or PG C14:0/C18:1*
730	PE (5)	C16:0/cyC19:0 or cyC17:0/C18:1*
733	PG (B)	C16:0/C17:0
742	PE (6)	C18:1/C18:1
747	PG (C)	C16:1/C18:1
761	PG (D)	C16:0/C19:0
773	PG (F)	C18:1/C18:0* or C17:0/C19:0

The PEs and PGs presented in the table were reported as phospholipids in *E. coli* (2).

* Major PEs and PGs in *E. coli* according to Oursel *et al.* (2007) (2).

TABLE S5 Empty detergent micelle per protein (complex) ratios

	UT Trimer 12,397 Å^2	AdiC Dimer 12,694 Å^2	LacY Monomer 7,607 Å^2
DDM	1.6-3.0	1.7-3.3	1.0-1.8
UDM	2.5	2.5	1.8
DM	2.0	2.3	1.6
NM	4.8	5.5	*
OM	17.7	18.2	*
Cymal-7	1.3	1.4	0.9
Cymal-6	1.7	1.8	1.2
Cymal-5	2.8	3.1	1.9

* Protein tended to aggregate in this detergent and was therefore not considered.

The empty detergent micelle per protein (complex) ratios indicate how many empty micelles of the corresponding detergent are found in UT, AdiC and LacY based on our experimental results (panels *B* in Figs. 2, 3 and 4). Aggregation numbers defining the empty detergent micelles are listed in Table S3. Below the names of the proteins, their oligomeric state and hydrophobic, lipid-accessible surface area are indicated.

SUPPORTING REFERENCES

1. Oliver, R. C., J. Lipfert, D. A. Fox, R. H. Lo, S. Doniach, and L. Columbus. 2013. Dependence of micelle size and shape on detergent alkyl chain length and head group. *PLoS ONE* 8:e62488.
2. Oursel, D., C. Loutelier-Bourhis, N. Orange, S. Chevalier, V. Norris, and C. M. Lange. 2007. Lipid composition of membranes of Escherichia coli by liquid chromatography/tandem mass spectrometry using negative electrospray ionization. *Rapid Commun. Mass Spectrom.* 21:1721-1728.

II

Manuscript

Molecular bases for substrate recognition of the wild-type L-arginine/agmatine antiporter AdiC

Ilgü *et al.*

Institute of Biochemistry and Molecular Medicine, and Swiss National Centre of Competence in Research (NCCR) TransCure, University of Bern, CH-3012 Bern, Switzerland

INTRODUCTION

Enterobacteria from the genera *Escherichia*, *Klebsiella*, *Salmonella*, *Shigella* and *Yersinia* include members that are human intestinal pathogens. In order to reach the gut, enteric bacteria have to survive the strongly acidic gastric environment (e.g., pH 1.5-4). Enteric bacteria do so by activating extreme acid-resistance responses [1]. The arginine-dependent acid-resistance system of *Escherichia coli* has been extensively studied and is able to keep the cytoplasm above pH 5 during exposure of *E. coli* to an extremely acidic environment. The main actors in this system are the cytoplasmic acid-activated arginine decarboxylase AdiA and the inner membrane L-arginine (Arg)/agmatine (Agm) antiporter AdiC [1], a member of the amino acid/polyamine/organocation (APC) transporter superfamily [2]. AdiA decarboxylates Arg to Agm by consuming a proton from the cytoplasm (**Fig. 1a**). The produced Agm carries this 'virtual proton' in the form of a C-H bond, which then leaves the bacterium through the antiporter AdiC by exchanging in a 1:1 stoichiometry Agm by Arg from the outside, e.g., from the gastric juice. The free energy of Arg decarboxylation drives the continuous pumping of protons out of the cell [3]. Studies on the molecular genetics [4,5], protein biochemistry [2,3], transport function [2,3,6,7] and structure [2,8-11] of AdiC have been published in the past. The four reported three-dimensional AdiC structures consist of twelve transmembrane α-helices (TMs) and are in the outward-open, substrate-free [8,9], outward-open, Arg-bound [11] and outward-facing occluded, Arg-bound states [10]. The two outward-open, substrate-free structures are at the moderate resolutions of 3.2 Å [8] and 3.6 Å [9], and the only ones available of wild-type AdiC (AdiC-wt). The two other structures are with bound Arg and at 3 Å resolution, and could only be obtained thanks to the introduction of specific point mutations, i.e., AdiC-N22A [10] and AdiC-N101A [11]. The N101A mutation results in a defective AdiC protein unable to bind Arg and with a dramatically decreased turnover rate compared to wild-type [11]. It is unclear how these two functional features comply with the obtained crystal structure of AdiC-N101A in complex with Arg. The specific mutation N22A in AdiC is particularly interesting, since this amino acid residue is located near the substrate-binding pocket and increases the affinity of AdiC for Arg approximately sixfold [10]. In addition to their great value for the understanding of the molecular working mechanism of AdiC and other APC family transporters, high-resolution structures of AdiC are essential for homology modeling of certain human amino acid transporters. Because structure determination of human transporters, and eukaryotic membrane proteins in general, still represents a major challenge, homology models are of great interest and help towards understanding of transporter functions and roles in human health and disease. Recently, a homology model of the human large-neutral amino acid transporter 1 (LAT1) based on one of the available AdiC crystal structures at 3 Å resolution [10] was built and used for virtual ligand screening and the successful identification of new inhibitors [12]. Such inhibitors are of great interest since LAT1 represents a cancer drug target [13]. Importantly, high-resolution structures of AdiC would help in improving the present human LAT1 homology model [12], thus promoting its application for virtual ligand screening.

Here we present the first crystal structure of AdiC with bound Agm at 2.6 Å resolution. In addition, the structure of substrate-free AdiC was solved at the unprecedented resolution of 2.2 Å. Both structures were captured in an outward-open state. Importantly, water molecules in the substrate-binding pocket of AdiC could be determined at such high resolutions.

RESULTS

The Agm-bound and substrate-free AdiC structures

To deepen our knowledge on the transport mechanism of AdiC, we determined the structure of AdiC in complex with Agm at 2.6 Å resolution (see **Table 1** for data collection and refinement statistics). In contrast, innumerable attempts to co-crystallize AdiC-wt with Arg failed. This observation might be attributed to the approximately threefold higher affinity of AdiC-wt for Agm compared to Arg as determined by scintillation proximity assay (SPA) (**Table 2** and **Supplementary Fig. 1**). Furthermore, we solved the structure of substrate-free AdiC-wt (^{apo}AdiC-wt) at the unprecedented resolution of 2.2 Å (see **Table 1** for data collection and refinement statistics). Importantly, these high-resolution structures made possible the identification of crucial water molecules in the substrate-binding pocket of AdiC in the presence and absence of Agm. Both structures were captured in the outward-open conformation and display subtle structural differences (RMSD 0.28 Å for 437 residues, **Fig. 2**). The Agm molecule is bound at the center of the AdiC transport path (**Fig. 2**) being recognized by several amino acids from TM1, TM3, TM6, TM8 and TM10, mainly by hydrogen bonds (H-bonds) and one cation-π interaction (**Fig. 3a,**

b). Agm consists of chemically different portions: two hydrophilic, i.e., the primary amino group and the guanidinium (Gdm) group, and one hydrophobic, i.e., the aliphatic region connecting the previous two. In the AdiC-wt structure with bound Agm (^{Agm}AdiC-wt) (see **Fig. 2d** for the omit electron density map of Agm), the primary amino group donates three H-bonds to the backbone carbonyl oxygen atoms of I23 (TM1), S203 (TM6) and I205 (TM6) (**Fig. 3a, b**). The three nitrogen atoms of the Gdm group of Agm (hereafter referred to as N1, N2 and N3) **Fig. 3a, b**) interact as follows: N1 with the carbonyl oxygen atom of C97 (TM3) and the amide group oxygen atom of N101 (TM3), N2 with the carbonyl oxygen atom of A96 (TM3), and N3 with the sulfur atom of M104 (TM3). Importantly, a water molecule (H_2O1; **Fig. 3a, b**) was found interacting via H-bonds with N2, the carbonyl oxygen atom of A96 (TM3) and the hydroxyl group of S357 (TM10). The Gdm group of Agm also interacts via a cation-π interaction with W293 (TM8). This interaction was shown to be crucial for substrate binding to AdiC, because the AdiC-W293L mutant is unable to bind and transport substrates [2]. Van der Waals interactions with the aliphatic portion of Agm are present with W293 (TM8) and the side chain of I205 (TM6) (**Supplementary Fig. 3a**).

Comparison of the substrate binding sites in the Agm-bound and substrate-free AdiC structures

Fig. 3 compares the substrate binding sites of the ^{Agm}AdiC-wt and ^{apo}AdiC-wt structures. Whereas the crystallographic water molecule H_2O1 is present in both structures, three additional ones, i.e., H_2O2, H_2O3 and H_2O4, were found in the ^{apo}AdiC-wt structure (**Fig. 3c, d**). Importantly, these additional water molecules mimic most of the hydrophilic portions of Agm. Specifically, H_2O2 in the ^{apo}AdiC-wt structure is located near the position of N1 in the ^{Agm}AdiC-wt structure, thus replacing the H-bonds of N1 with the protein (**Fig. 3**). In contrast, the previously observed H-bonds of N2 with the protein and H_2O1 are not replaced by H_2O3 in the ^{apo}AdiC-wt structure, H_2O3 only being within H-bond distance with H_2O2 (see distances in **Fig. 3c, d**). Similar to H_2O2, H_2O4 also replaces a nitrogen atom of the Agm molecule, i.e, the nitrogen atom of the primary amino group, and its H-bonds to the protein (**Fig. 3**).

As mentioned above, subtle differences were found between the ^{Agm}AdiC-wt and ^{apo}AdiC-wt structures (**Fig. 2**). A significant difference in the substrate-binding pocket is the rotamer conformation of M104 (TM3). Whereas in the $^{\text{apo}}$AdiC-wt structure, the methylmercapto group of M104 (TM3) is protruding into the substrate-binding pocket, this methionine residue adopts another conformation in the $^{\text{Agm}}$AdiC-wt structure exposing its sulfur atom as hydrogen acceptor for N3 (**Fig. 3**).

Comparison of the protein-substrate interactions in the AdiC-N22A and $^{\text{Agm}}$AdiC-wt structures

In the Arg-bound AdiC-N22A structure, the positively charged α-amino group of Arg donates three H-bonds to the carbonyl oxygen atoms of I23 (TM1), and W202 and I205 in TM6 [10] (**Fig. 4a**). The two protein-substrate interactions with I23 (TM1) and I205 (TM6) persist with the primary amino group of Agm in the $^{\text{Agm}}$AdiC-wt structure (**Fig. 4b**). Due to the different conformational states of AdiC-N22A and $^{\text{Agm}}$AdiC-wt, i.e., outward-facing occluded and outward-open, the H-bonds between the primary amino groups of Arg and Agm, and W202 (TM6) differ significantly, i.e., 2.9 Å (AdiC-N22A) and 3.9 Å ($^{\text{Agm}}$AdiC-wt). As a consequence this H-bond is basically abolished in the $^{\text{Agm}}$AdiC-wt structure. An additional, in the AdiC-N22A structure previously not described amino acid, i.e., S203 (TM6), is in H-bond distance to the primary amino group of Arg. The H-bond distance between the carbonyl oxygen atom of S203 (TM6) is increased from 3.1 Å to 3.4 Å in the $^{\text{Agm}}$AdiC-wt structure compared to the AdiC-N22A structure. Globally, the distances between the interacting amino acids in the two structures are more favorable for H-bonding in the AdiC-N22A structure, thus resulting potentially in stronger binding of the primary amino group of the substrate to the protein. In both structures, the Gdm groups of Arg and Agm stack against W293 (TM8) through cation–π interactions (**Fig. 4**). All nitrogen atoms of the Arg and Agm Gdm groups in AdiC-N22A and $^{\text{Agm}}$AdiC-wt are located within H-bond distance to the three oxygen atoms of the side chain N101 (TM3), and the carbonyl oxygen atoms of A96 and C97 in TM3 (see **Fig. 4**). These H-bond distances are shorter in the $^{\text{Agm}}$AdiC-wt structure compared to the AdiC-N22A structure leading potentially to stronger binding of the substrate Gdm group (**Fig. 4**). An additional, previously described H-bond between Arg and AdiC-N22A is established between the Gdm group and the side chain hydroxyl group of S357 (TM10) [10] (**Fig. 4a**). This interaction is not present in this form in the $^{\text{Agm}}$AdiC-wt structure. Instead, the interaction of S357 with the Gdm group of Agm is bridged by a water molecule ($H_2$01) involving an additional H-bond contributed by the carbonyl oxygen atom of A96 (**Fig. 4b**). This H-bond network contributes to the binding, positioning and stabilization of the Gdm group and thus of the Agm molecule in the binding pocket. The aliphatic portion of Arg in the AdiC-N22A structure interacts with the side chains of the three hydrophobic amino acids W202 and I205 in TM6, and W293 (TM8) (**Supplementary Fig. 3b**). Interactions are similar in the ^{Agm}AdiC-wt structure with the exception of W202 (TM6), which is responsible for occlusion of Arg from the periplasm after binding. Thus, this interaction of Agm with W202 (TM6) is missing because the ^{Agm}AdiC-wt conformation is in the outward-open state and not in the outward-facing, occluded state as in the AdiC-N22A structure. In general, the described differences between substrate binding in the ^{Agm}AdiC-wt and AdiC-N22A structures result mainly because of a slightly different position of the substrate in the binding pocket (compare substrates in **Fig. 4**), a different conformational state of the transporter and the difference in substrates.

Ligand binding affinity and thermostability of AdiC-wt and selected mutants

The binding affinities of AdiC-wt for the substrates Arg and Agm were determined by SPA. AdiC-wt has with 148 µM (Arg) and 56 µM (Agm) (**Table 2** and **Supplementary Fig. 1**) an about threefold higher affinity for Agm compared to Arg. In addition, we determined the affinities of the previously reported mutants AdiC-N22A [10] and AdiC-S26A [6] for Arg and Agm (**Table 2** and **Supplementary Fig. 1**). AdiC-N22A showed an about sixfold higher affinity for Arg and an about fourfold lower affinity for Agm compared to AdiC-wt (**Table 2**). Thus, the mutation N22A in AdiC results in an inversion of the specificity for the substrates compared to AdiC-wt (**Table 2**). The affinity of AdiC-S26A for Arg was comparable to that of AdiC-wt, while that for Agm was about 1.5 times lower, but still higher than for Arg (**Table 2**). Consequently, the mutation S26A has not a significant effect and only a weak effect on the affinities of AdiC-S26A for Arg and Agm compared to AdiC-wt. The affinities of AdiC-wt, AdiC-N22A and AdiC-S26A for the Arg analogs: L-arginine methyl ester (Arg-OMe) and L-arginine amide (Arg-NH_2) were also determined by SPA (**Table 2** and **Supplementary Fig. 1**). AdiC-N22A had with 77 µM the highest affinity for Arg-OMe, followed by AdiC-wt with 293 µM and AdiC-S26A with a dramatically low affinity of 1693 µM relative to the others. All three AdiC forms had low affinities for Arg-NH_2 (**Table 2**). In addition to ligand binding affinity, we determined the effects of Arg, Agm, Arg-OMe and Arg-NH2 on the thermostability of AdiC. The general observation was an increase of the thermostability of AdiC-wt, AdiC-N22A and AdiC-S26A with increasing ligand binding affinities (**Table 2**).

DISCUSSION

Towards understanding of the molecular working mechanisms of the Arg/Agm antiporter AdiC and APC superfamily members, we have provided the first structure of the wild-type form of AdiC with bound Agm at 2.6 Å resolution. The ^{Agm}AdiC-wt structure also represents the first structure of AdiC-wt with a bound substrate in general. Furthermore, the structure of substrate-free AdiC was determined at the unprecedented resolution of 2.2 Å. The ^{Agm}AdiC-wt structure allowed the detailed description of Agm binding to AdiC at the molecular level (**Fig. 3a, b**). Both high-resolution structures made possible the identification of crucial water molecules, and protein-water and Agm-water H-bond networks in their substrate-binding pockets. Positions of specific nitrogen atoms of Agm in the ^{Agm}AdiC-wt structure were found to be replaced by water molecules in the ^{apo}AdiC-wt structure, thus specifically shaping the substrate-binding site in the absence of substrate. The water molecule $H_2$01 in the substrate-binding pockets of ^{Agm}AdiC-wt and ^{apo}AdiC-wt was found to be involved in the structuring of the substrate-binding site by stabilizing interactions between TM3 and TM10, and specific amino acids in these two TMs. The ^{Agm}AdiC-wt structure allowed a comparison with the AdiC-N22A structure, and thus of the molecular interactions involved in Arg and Agm binding (**Fig. 4**). Importantly, comparison of these two substrate bound structures that are in different conformational states, i.e., outward-open, Agm bound and outward-facing occluded, Arg bound, identified differences critical for substrate recognition (**Fig. 4**). The AdiC mutant N22A was shown to have an approximately sixfold higher affinity for Arg compared to AdiC-wt as determined by isothermal titration calorimetry [10]. We obtained similar results using the SPA (**Table 2**) in line with the previously published results [10]. In addition, we determined the affinity of AdiC-N22A for Agm, which was about fourfold weaker than for AdiC-wt. A stronger affinity for Arg compared to Agm is an unexpected and intriguing result, which indicates an inversion of the specificity of AdiC-N22A for these two substrates compared to AdiC-wt (**Table 2**).

The determined binding affinities of AdiC-wt, AdiC-N22A and AdiC-S26A for Arg, Agm, Arg-OMe and Arg-NH_2 by SPA were not comparable, thus indicating significantly different ligand-protein interactions between the different AdiC forms. As an exception the K_is of AdiC-wt and AdiC-S26A for Arg were similar (**Table 2**). The two Arg-bound crystal structures of AdiC-N22A [10] and AdiC-N101A [11] revealed hydrogen bonding between the α-carboxyl group of Arg and the hydroxyl group of S26. From such a configuration a substrate-recognition mechanism would naturally be deduced. However, based on our SPA results (**Table 2** and **Supplementary Fig. 1**) the binding affinities of AdiC-wt and AdiC-S26A for Arg are similar indicating no significant contribution of S26 in binding of the substrate Arg.

In summary, inversion of the Arg and Agm specificity of AdiC-N22A compared to AdiC-wt, the significantly different ligand binding affinities for AdiC-wt, AdiC-N22A and AdiC-S26A and the unimportance of S26 in AdiC-wt for Arg binding compared to AdiC-N22A and AdiC-N101A raise the critical question of to which extend the structures of these two mutants reflect the real and full Arg binding mechanism of wild-type AdiC. Therefore, the here presented high-resolution structures provide the most accurate and reliable views on the architecture and protein-substrate interactions of the naturally occurring wild-type AdiC protein currently available. Finally, both AdiC-wt structures provide due to their high-resolutions a solid basis for upcoming homology modeling studies of APC family members to understand their working mechanisms at the molecular level and, last but not least, for structure-based drug design as exemplified by the recent work with human LAT1 [12].

METHODS

Methods and any associated references are available in the online version of the paper.

Accession codes. Coordinates and structure factors have been deposited in the Protein Data Bank under accession codes XXXX (^{Agm}AdiC-wt) and XXXX (^{apo}AdiC-wt).

ACKNOWLEDGEMENTS

We thank Dr. D. Harder for the help with the SPA experiments. X-ray diffraction data was collected at the Swiss Light Source (SLS) of the Paul Scherrer Institute (Villigen, Switzerland). We thank the staff of the X06SA beamline for the excellent support, especially Drs. T. Tomizaki and M. Wang. Financial support from the University of Bern, the Swiss National Science Foundation (grant 31003A_144168), the Bern University Research Foundation, and the National Centre of Competence in Research (NCCR) TransCure to DF is gratefully acknowledged.

ONLINE METHODS

Cloning of AdiC. The gene of AdiC was cloned from genomic DNA of *E. coli* XL1-Blue by polymerase chain reaction (PCR) using the forward primer 5' AAAA AAGCTT ATG TCT TCG GAT GCT GAT GCTC 3' and the reverse primer 5' AAAA CTCGAG ATC TTT GCT TAT TGG TGC ATC 3'. The PCR products were digested with the restriction enzymes *Hin*dIII and *Xho*I, and ligated into the pZUDF21 vector [14]. The DNA constructs were verified by sequencing. The pZUDF21-AdiC construct results in a recombinant AdiC protein with a human rhinovirus 3C (HRV3C) protease cleavage site followed by a deca-His tag at the C-terminus. The calculated molecular mass of the recombinant and cleaved monomeric AdiC is ~49.5 kDa.

Protein preparation. For overexpression, pZUDF21-AdiC was transformed into BL21(DE3) pLysS *E. coli* cells. The cells were allowed to grow in Luria Bertani (LB) medium supplemented with 0.1 mg/mL ampicillin at 37 ºC by shaking in an orbital shaker. Protein expression was induced at OD_{600} of 0.5-0.6 with 0.3 mM isopropyl-β-D-thiogalactopyranoside and incubated at 37 ºC for 3 h. Cells were then harvested by centrifugation (10,000 x *g* for 10 min at 4 ºC), resuspended in Lysis buffer (20 mM Tris-HCl pH 8.0, 500 mM NaCl) and stored at -20 ºC until further use. For membrane preparation, frozen cells were thawed and lysed through a Microfluidizer M-110P (Microfluidics, Newton, MA) at 16,000 psi (four passages). Cell debris were removed by centrifugation (12,000 x *g* for 20 min at 4 ºC) and from the supernatant, membranes were collected by ultracentrifugation (150,000 x *g* for 1 h at 4 ºC). The pellet was homogenized in 20 mM Tris-HCl pH 8.0, 500 mM NaCl, 5 mM EDTA and an additional ultracentrifugation was performed. The pellet was then homogenized in a small volume of Lysis buffer, e.g., 12 mL final volume for membranes from 8 L cell culture, and aliquoted into fractions corresponding to membranes from 1 L of cell culture. Membrane aliquots were frozen in liquid nitrogen and stored at -80 ºC until further use.

Purification of AdiC. For purification, one aliquot of membrane suspension was solubilized for 2 h at 4 ºC on a rotational shaker in 20 mM Tris-HCl pH 8.0, 300 mM NaCl, 10% (v/v) glycerol, 4% (w/v) *n*-nonyl-β-D-glucopyranoside (NG) (V_{tot} = 7 mL). After ultracentrifugation (100,000 x *g* for 1 h at 4 ºC), the supernatant was diluted twofold in 20 mM Tris-HCl pH 8.0, 300 mM NaCl, 10% glycerol, 0.4% NG (w/v) (Buffer A) containing 5 mM L-histidine and incubated with 0.5 mL (bed volume) pre-equilibrated Ni-NTA Superflow resin (Qiagen, Valencia, CA) for 2 h at 4º C on a rotational shaker (metal affinity chromatography). The resin was then transferred into a column and washed three times with 5 mL of Buffer A containing 5 mM L-histidine and 3 mL of Buffer A by gravity flow. The His-tag on AdiC was removed by on-column cleavage on a rotational shaker for 18 h at 4 ºC by addition of 200 µg of HRV3C protease (BioVision, Milpitas, CA, USA). Finally, the cleaved AdiC was eluted by centrifugation (3000 x *g* for 15 s at 4 ºC) and remaining HRV3C was removed by an additional incubation of the eluate with 100 µL (bed volume) pre-equilibrated Ni-NTA Superflow resin followed by a subsequent filtration to remove the resin. All detergents used in this study were obtained from Glycon Biochemicals GmbH (Luckenwalde, Germany).

Crystallization of AdiC. For crystallization, the purified protein was concentrated to about 17 mg/mL using a 50 kDa Amicon cutoff filter (Sigma-Aldrich) and ultracentrifuged (200,000 x *g* for 30 min at 4 ºC) before use. Initial search for crystallization hits was performed using a Mosquito nanoliter crystallization robot (TTP Labtech, Melbourn, UK) and the MemGold sparse matrix screening kit (Molecular Dimensions, Newmarket, UK). After several screening rounds, 100-200 µm crystals appeared after 5-7 days in sitting-drop vapor diffusion plates at a 1:1 drop ratio. The crystallization solution of the crystals contained 62.5 mM Tris-HCl pH 8.0, 35% (v/v) PEG400, and 1% (w/v) NG. For co-crystallization of AdiC with agmatine, 2 mM agmatine was added to the protein solution prior to crystallization using the same condition as described before. Crystals were collected, flash-frozen and stored in liquid nitrogen until X-ray analysis.

Structure determination. All native data sets of AdiC, i.e., with and without agmatine molecule, were collected at the X06SA (PXI) beamline of the Swiss Light Source (SLS; Paul Scherrer Institute, Villigen, Switzerland) and processed with XDS [15]. Phasing by molecular replacement using the coordinates of 3OB6 [11] and refinement were performed using the PHENIX suite [16]. Model building was performed using Coot [17] and figures were generated with PyMOL (https://www.pymol.org/). Data collection and refinement statistics are listed in Table 1.

K_i determination and binding assay. Inhibition constants were determined by applying the scintillation proximity assay (SPA) [18]. Briefly, AdiC was solubilized and purified as described above using *n*-dodecyl-*β*-D-maltopyranoside (DDM): 1.5% (w/v) for solubilization and 0.04% (w/v) for purification. The AdiC protein was eluted from the Ni-NTA column with 20 mM Tris-HCl pH 8.0, 300 mM NaCl, 10% glycerol, 0.04% (w/v) DDM, 400 mM imidazole. Imidazole was immediately removed using Zeba Spin Desalting Columns (Thermo Scientific). The competitive inhibition of L-[^{3}H]arginine binding to AdiC by increasing concentrations, e.g., 0, 0.000128, 0.00064, 0.0032, 0.016, 0.8, 4, 20 mM and 100 mM, of Arg, Agm, Arg-OMe and Arg-NH_2 in 50 mM Tris-HCl pH 8.0, 150 mM NaCl, 0.1% (w/v) DDM, 1 mM Tris(2-carboxyethyl)phosphine, 10% glycerol was determined. For the reaction, 2 µg of protein, 1 µCi L-[^{3}H]arginine (specific activity: 40 Ci/mmol, Perkin Elmer) and 500 µg PVT-copper beads (Perkin Elmer) in a final volume of 100 µl were incubated per 96-well plate (white OptiPlates, Perkin Elmer) well. After incubation for 18 h at 4°C in the dark, samples were counted for 1.5 min with a TopCount scintillation counter at 18°C. Nonspecific signals were determined by adding imidazole to each well to a final concentration of 100 mM imidazole followed by overnight incubation prior to measurement. Nonspecific signals were subtracted from data points. K_i values were calculated by nonlinear curve fit using the "one site – Fit K_i" Equation in Prism5 (GraphPad Software, La Jolla, CA).

[^{3}H]Arg binding experiments with AdiC-wt and AdiC-N22A-S26A (**Supplementary Fig. 3**) by SPA were performed similarly to the K_i determination assay described above, but in absence of competitor.

Determination of AdiC thermostability. Thermostability analysis of AdiC was performed as described previously [19]. AdiC was purified using the detergent n-dodecyl-β-D-maltopyranoside (DDM; purification as described previously for NG, but using 1.5% (w/v) DDM for solubilization and 0.04% (w/v) DDM for purification and cleavage). After removal of His-tag on AdiC, the protein buffer was exchanged to SEC-buffer (20 mM Tris-HCl pH 8.0, 150 mM NaCl, 0.04 % (w/v) DDM) using Zeba Spin Desalting Columns (Thermo Scientific) and diluted to a concentration of 0.5 mg/mL using the same buffer. To test the effect of ligands on the thermostability of AdiC, purified samples in aliquots of 35 µg (70 µl total volume and 5 µM AdiC concentration) were first incubated with the ligands (2 mM; corresponding to 200-fold molar excess) on ice for 10 min. Next, samples were incubated at different temperatures for 10 minutes using a Labcycler gradient PCR machine (SensoQuest GmbH, Göttingen, Germany). After a short centrifugation to remove eventual aggregates (18,000 x *g* for 30 s at room temperature), the supernatant was loaded on a Superdex 200 5/150 GL column (GE Healthcare) installed on an ÄKTA Purifier system (GE Healthcare). Prior to injection, the column was equilibrated with 1.5 column volumes of SEC-buffer. The untreated sample, kept on ice, was analyzed by SEC and used as a reference for normalization. The peak absorbance values at 280 nm were used for the melting temperature (T_m) determination. Finally, the T_m values were calculated by applying the Boltzmann sigmoidal equation in Prism5 (GraphPad Software, La Jolla, CA).

FIGURE LEGENDS

Figure 1 Physiology and selected conformational states of AdiC. (**a**) Schematic illustration of the arginine-dependent acid-resistance system of *E. coli*. Arg is decarboxylated in the cytoplasm by the acid-activated arginine-decarboxylase AdiA thereby consuming one proton (encircled in green). This ‘virtual proton’ ends up as C-H bond at the 1-position of the product 1-amino-4-guanidino-n-butane (Agm; ‘virtual proton’ indicated by a green circle) and is removed from the cell through the

AdiC-mediated Arg/Agm exchange across the inner membrane. (**b**) Conformational states of AdiC involved in Agm release on the periplasmic side. Arrows indicate the flow of the sequential conformational states. The AdiC monomer is colored in blue and the Agm molecule in red.

Figure 2 Structures of Agm-bound and substrate-free AdiC. (**a**, **b** and **c**) Superpositions of ^{Agm}AdiC-wt (blue ribbon) and ^{apo}AdiC-wt (yellow ribbon) dimers, individual monomers are indicated. The Agm molecule (magenta sticks) bound to ^{Agm}AdiC-wt is shown and is located about at the center of the transport path. Three different views are displayed: view from the membrane plane (**a**), and from the cytoplasmic (**b**) and periplasmic sides (**c**). (**d**) Omit electron density map at 3.0 σ (green) of the Agm molecule (magenta sticks) bound to ^{Agm}AdiC-wt.

Figure 3 Comparison of the substrate-binding sites in the Agm-bound and substrate-free AdiC structures. (**a** and **b**) Recognition of the substrate Agm by specific amino acids in AdiC and one protein associated water molecule. Important amino acids are labeled in the one letter code and when interacting with their main chain carbonyl oxygen atoms additionally labeled with (O). The three guanidinium group nitrogen atoms of Agm are labeled N1, N2 and N3. The top view from the periplasmic side (a) and side view (tilted by 90°) from the membrane plane (b) onto the Agm binding site are displayed. (**c** and **d**) Same views and labeling as in (**a** and **b**) for the substrate-free AdiC structure. The ^{Agm}AdiC-wt (**a** and **b**) and ^{apo}AdiC-wt (**c** and **d**) structures and specific amino acids in the substrate-binding pockets are represented as ribbons in blue and yellow, and as sticks in gold and salmon, respectively. Crystallographic water molecules are displayed as red balls, and potential H-bonds and interatomic distances are indicated as dotted lines and in Å, respectively.

Figure 4 Comparison of the substrate-binding sites of the Arg-bound AdiC-N22A and the Agm-bound AdiC-wt structures. (**a**) Recognition of the substrate Arg by specific amino acids of AdiC-N22A. Amino acids interacting with the substrate are labeled in the one letter code and if the main chain carbonyl oxygen atom or amide nitrogen are involved additionally labeled with (O) or (N). In the upper part of the figure a top view from the periplasmic side is shown whereas in the lower part a 90° tilted view is displayed. (**b**) For the ^{Agm}AdiC-wt structure same views and labeling as in (**a**) are shown. The Arg-bound AdiC-N22A (**a**) and AgmAdiC-wt (**b**) structures, and specific amino acids in the substrate-binding pockets are represented as ribbons in magenta and blue, and as sticks in light-blue and gold, respectively. The substrates are displayed as grey (Arg) and black (Agm) sticks and a specific crystallographic water molecule found in the ^{Agm}AdiC-wt substrate-binding pocket is represented as red ball. Potential H-bonds and interatomic distances are indicated as dotted lines and in Å, respectively.

Supplementary Figure 1 Ligand binding affinities of AdiC variants. K_i: inhibition constant (binding affinity). The determined K_i values are from at least two independent experiments, each in triplicate. 95% confidence interval values are indicated in brackets.

Supplementary Figure 2 Thermostabilities of AdiC variants. T_m: melting temperature. The determined T_m values are from at least two independent experiments, each in triplicate. 95% confidence interval values are indicated in brackets.

Supplementary Figure 3 Comparison of the van der Waals interactions between protein and aliphatic portion of the substrates in the Agm-bound AdiC-wt and Arg-bound AdiC-N22A structures. (**a**) Amino acid residues of ^{Agm}AdiC-wt involved in van der Waals interactions with the substrate Agm are displayed and labeled in the one letter code. In the upper part of the figure a top view from the periplasmic side is shown whereas in the lower part a 90° tilted view is displayed. (**b**) For the AdiC-N22A structure same views and labeling as in (**a**) are shown. The ^{Agm}AdiC-wt (**a**) and Arg-bound AdiC-N22A (**b**) structures, and specific amino acids are represented as ribbons in blue and magenta, and as sticks in gold and light-blue, respectively. The substrates are displayed as black (Agm) and grey (Arg) sticks, and potential H-bonds and interatomic distances are indicated as dotted lines and in Å, respectively.

TABLES

Table 1 Data collection and refinement statistics for AdiC

	^{Agm}**AdiC-wt**	^{apo}**AdiC-wt**
Data collection		
Wavelength (Å)	1.0	1.0
Space group	P 2_1 2_1 2	P 2_1 2_1 2
Unit-cell parameters,		
a, b, c (Å); α, β, γ (°)	72.9, 104.8, 175.6; 90	73.2, 104.8, 175.4; 90
Resolution (Å)	49.44-2.59 (2.73-2.59)	49.51-2.21 (2.33-2.21)
No. of observed reflections	280,724 (38,770)	401,210 (52,895)
No. of unique reflections	41,837 (5,764)	68,197 (9,571)
R_{merge} (%)	10.9 (117)	7.1 (114)
Completeness (%)	98.7 (94.9)	99.4 (96.8)
Multiplicity	6.7 (6.7)	5.9 (5.5)
I / σI	12.0 (1.6)	14.9 (1.5)
$CC_{1/2}$ (%)[i)]	99.9 (71.3)	99.9 (58.9)
Refinement		
Resolution (Å)	49.45-2.59 (2.63-2.59)	49.52-2.21 (2.29-2.21)
R_{work} / R_{free} (%)	22.09 / 25.07 (34.31 / 33.50)	19.72 / 21.01 (34.41 / 34.88)
Number of atoms		
Protein	6484	6480
Ligand	18	-
Water	12	159
Mean B factor (Å^2)	68.8	60.1
Protein	68.7	60.2
Ligand	70.5	-
Water	57.3	55.8
R.m.s deviations		
Bond length (Å)	0.007	0.007
Bond angle (°)	0.922	0.996
Ramachandran plot (%)		
Favored region	99.1	99.7
Allowed region	0.9	0.3
Disallowed region	0	0

Values in parentheses reflect the highest-resolution shell.

i) Percentage of correlation between intensities from random half data sets as described previously [20].

Table 2 Ligand binding affinities and thermostabilities of AdiC variants

	AdiC-wt		AdiC-N22A		AdiC-S26A	
Compound	**K_i (µM)**	**T_m (°C)**	**K_i (µM)**	**T_m (°C)**	**K_i (µM)**	**T_m (°C)**
No ligand	-	61.2 (61-62)	-	51.8 (51-52)	-	57.7 (57-58)
Arg	148 (103-212)	65.3 (65-66)	23 (20-27)	60.0 (59-60)	154 (86-274)	60.3 (61-62)
Agm	56 (38-82)	66.6 (66-67)	216 (191-245)	55.8 (55-56)	90 (44-183)	62.1 (62-63)
Arg-OMe	293 (2097-4086)	61.9 (61-62)	77 (66-89)	56.6 (56-57)	1693 (920-2534)	57.3 (57-58)
Arg-NH_2	864 (467-1118)	61.0 (61-62)	1816 (1282-2572)	52.3 (52-53)	1527 (1205-2379)	59.1 (59-60)

K_i: inhibition constant (binding affinities); T_m: melting temperature

The determined K_i and T_m values are from at least two independent experiments, each in triplicate. 95% confidence interval values are indicated in brackets.

Figure 1

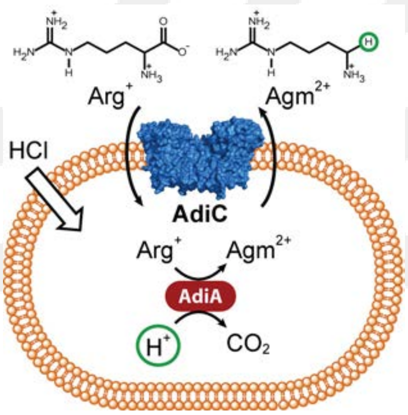

Figure 2

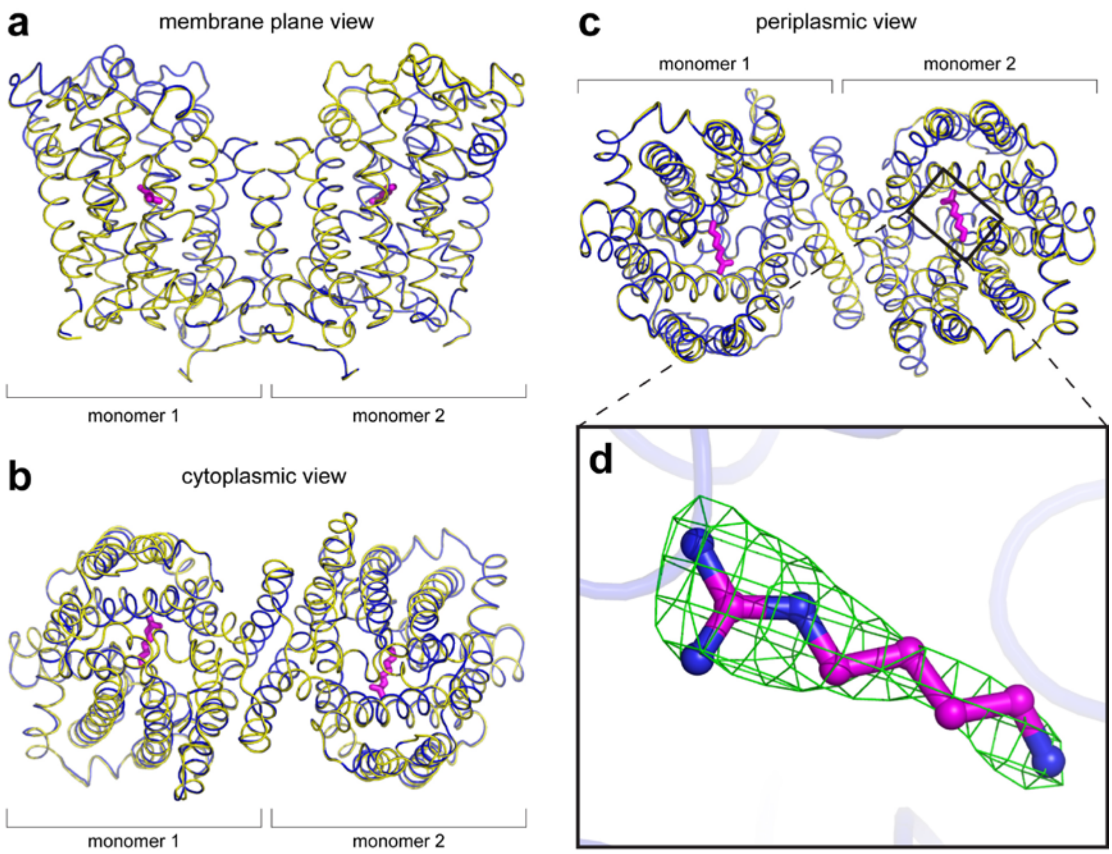
a
membrane plane view
monomer 1
monomer 2
b
cytoplasmic view
monomer 1
monomer 2
c
periplasmic view
monomer 1
monomer 2
d

Figure 3

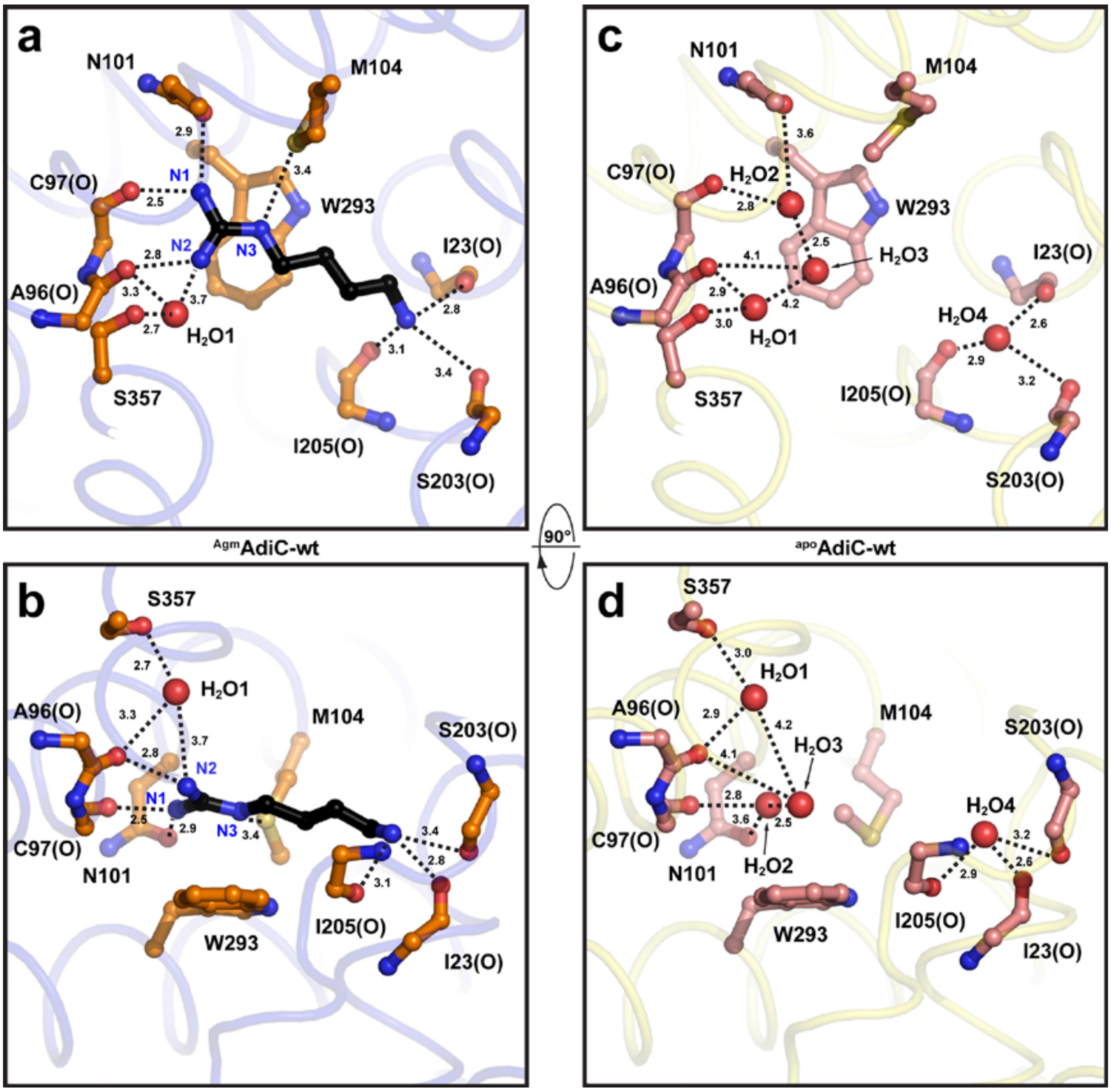

a
N101
M104
C97(O)
N1
W293
N2
N3
I23(O)
A96(O)
H2O1
S357
I205(O)
S203(O)
AgmAdiC-wt
90°
c
H2O2
H2O3
H2O4
apoAdiC-wt
b
d

Figure 4

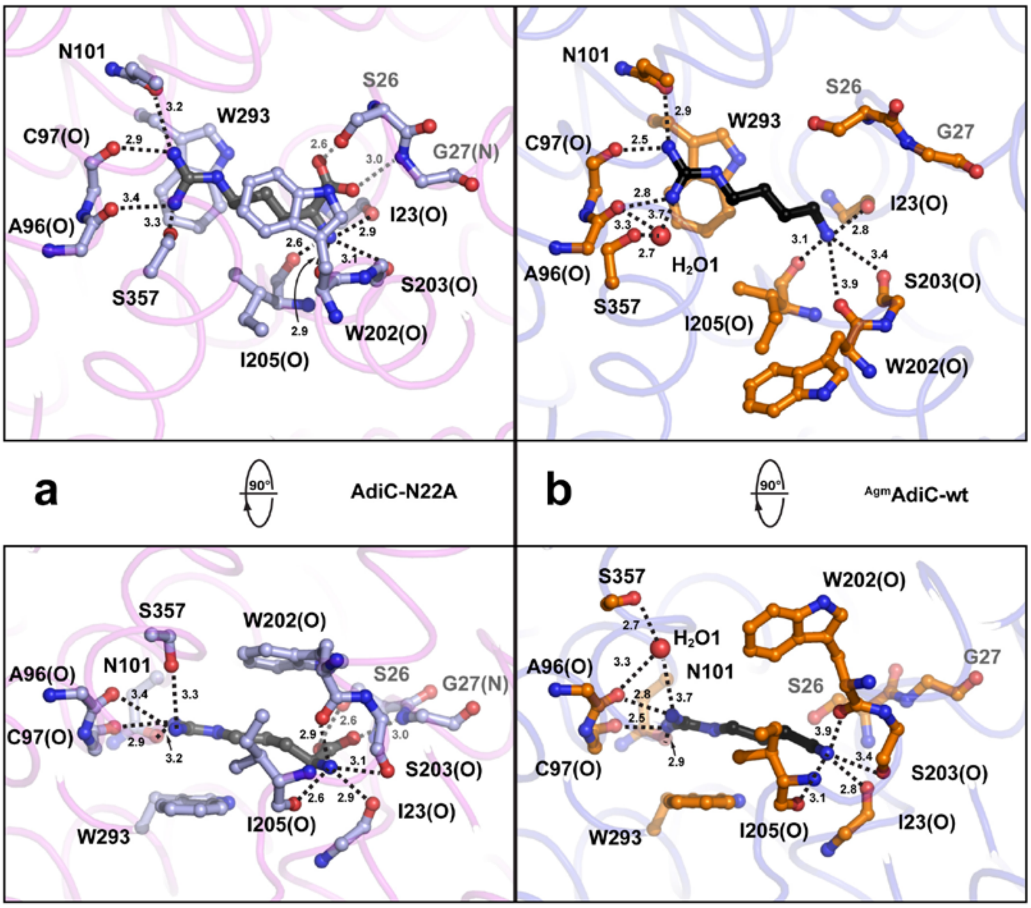

N101
W293
C97(O)
A96(O)
S357
S26
G27(N)
I23(O)
S203(O)
W202(O)
I205(O)
a
90°
AdiC-N22A
N101
W293
C97(O)
A96(O)
S357
H2O1
S26
G27
I23(O)
S203(O)
I205(O)
W202(O)
b
90°
AgmAdiC-wt

Supplementary Figure 1

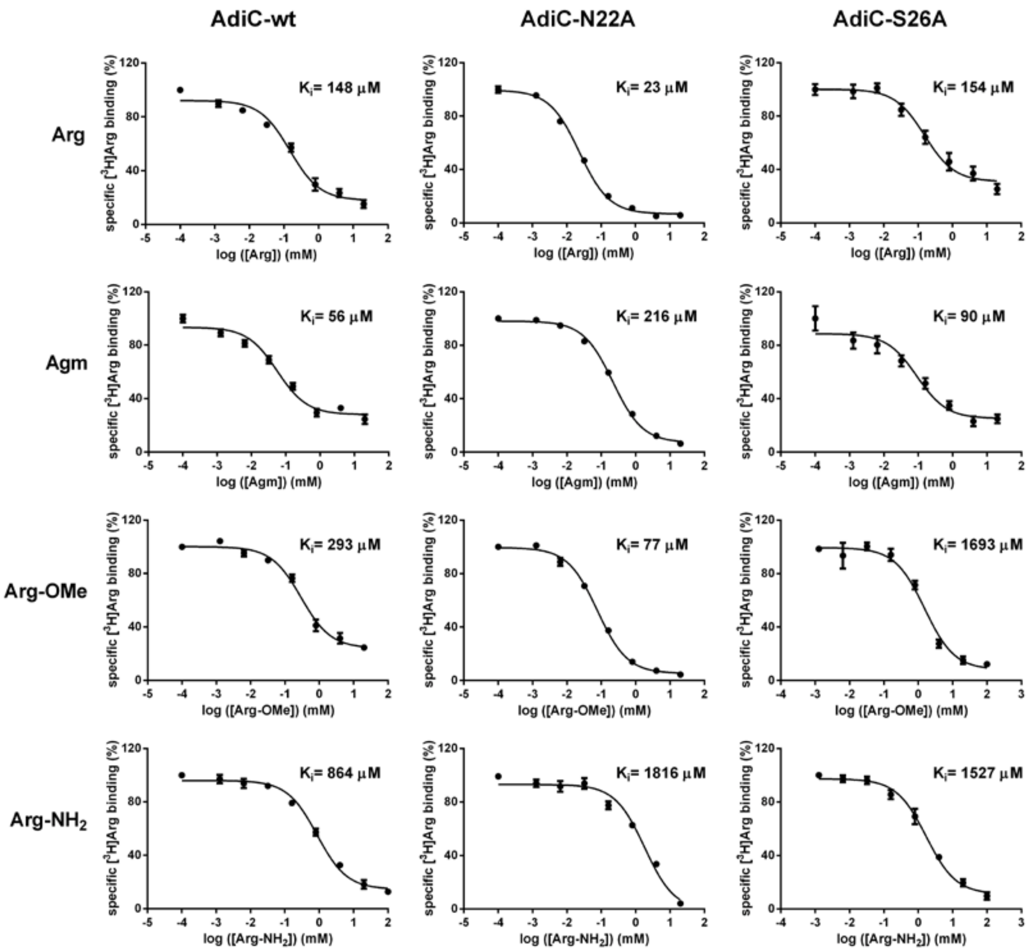

Supplementary Figure 2

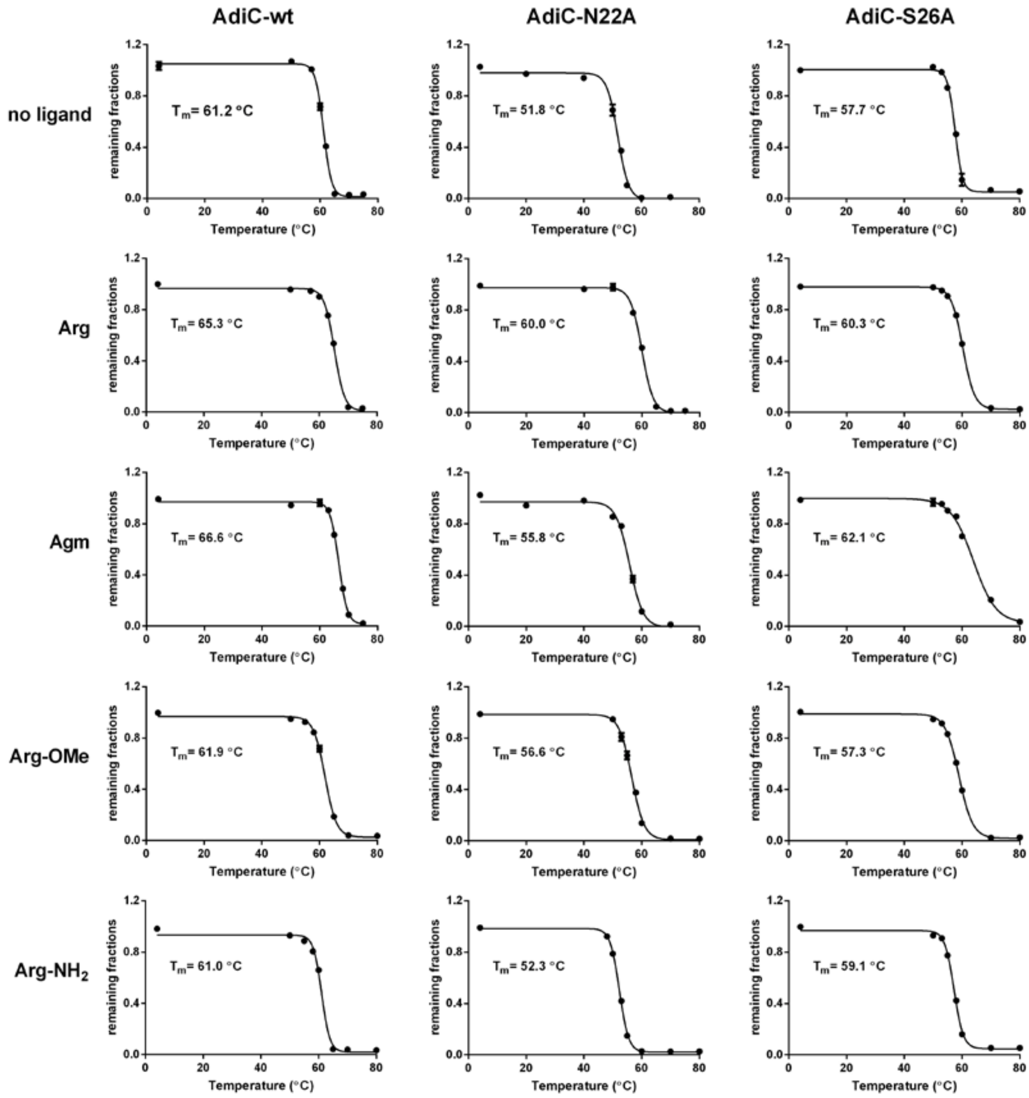

Supplementary Figure 3

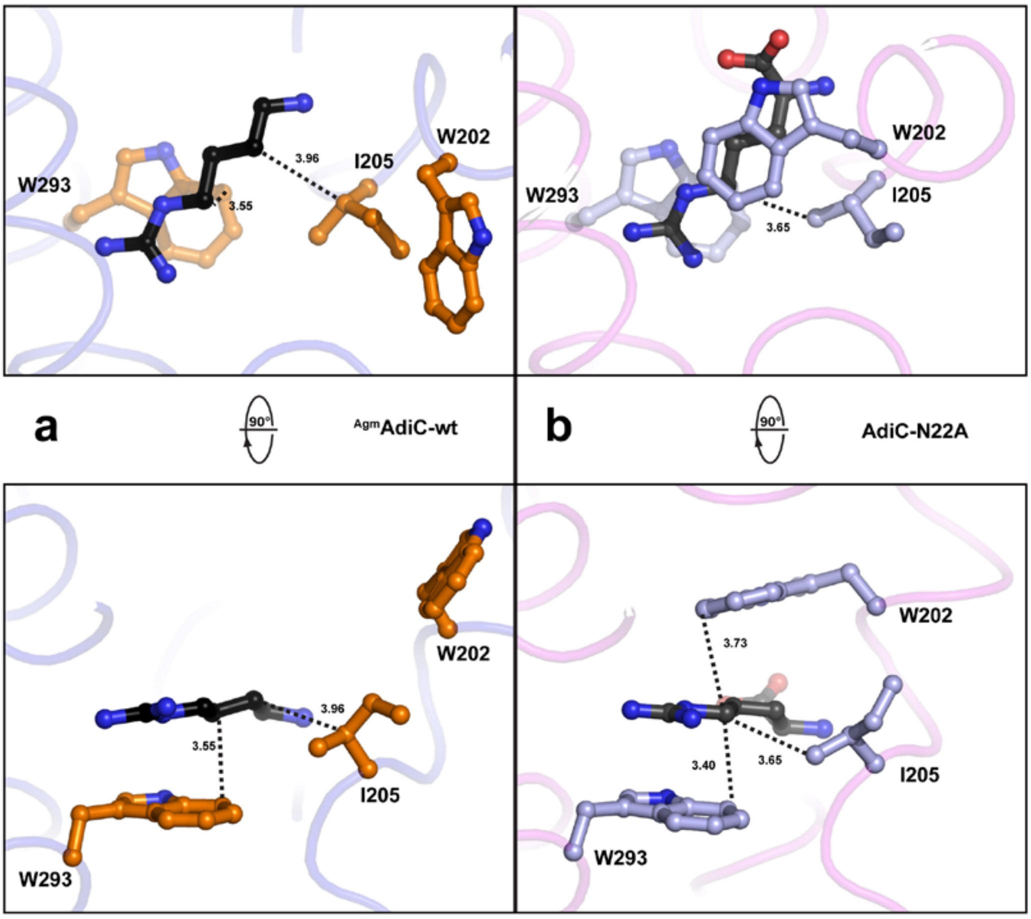

REFERENCES

1. Foster, J.W. *Escherichia coli* acid resistance: tales of an amateur acidophile. *Nat. Rev. Microbiol.* **2**, 898-907 (2004).
2. Casagrande, F. *et al.* Projection structure of a member of the amino acid/polyamine/organocation transporter superfamily. *J. Biol. Chem.* **283**, 33240-33248 (2008).
3. Fang, Y., Kolmakova-Partensky, L. & Miller, C. A bacterial arginine-agmatine exchange transporter involved in extreme acid resistance. *J. Biol. Chem.* **282**, 176-182 (2007).
4. Gong, S., Richard, H. & Foster, J.W. YjdE (AdiC) is the arginine:agmatine antiporter essential for arginine-dependent acid resistance in *Escherichia coli*. *J. Bacteriol.* **185**, 4402-4409 (2003).
5. Iyer, R., Williams, C. & Miller, C. Arginine-agmatine antiporter in extreme acid resistance in *Escherichia coli*. *J. Bacteriol.* **185**, 6556-6561 (2003).
6. Tsai, M.F. & Miller, C. Substrate selectivity in arginine-dependent acid resistance in enteric bacteria. *Proc. Natl. Acad. Sci. USA* **110**, 5893-5897 (2013).
7. Wang, S. *et al*. Molecular mechanism of pH-dependent substrate transport by an arginine-agmatine antiporter. *Proc. Natl. Acad. Sci. USA* **111**, 12734-12739 (2014).
8. Fang, Y. *et al.* Structure of a prokaryotic virtual proton pump at 3.2 Å resolution. *Nature* **460**, 1040-1043 (2009).
9. Gao, X. *et al.* Structure and mechanism of an amino acid antiporter. *Science* **324**, 1565-1568 (2009).
10. Gao, X. *et al.* Mechanism of substrate recognition and transport by an amino acid antiporter. *Nature* **463**, 828-832 (2010).
11. Kowalczyk, L. *et al.* Molecular basis of substrate-induced permeation by an amino acid antiporter. *Proc. Natl. Acad. Sci. USA* **108**, 3935-3940 (2011).
12. Geier, E.G. *et al.* Structure-based ligand discovery for the Large-neutral Amino Acid Transporter 1, LAT-1. *Proc. Natl. Acad. Sci. USA* **110**, 5480-5485 (2013).
13. Fotiadis, D., Kanai, Y. & Palacin, M. The SLC3 and SLC7 families of amino acid transporters. *Mol. Aspects Med.* **34**, 139-158 (2013).

14. Ilgü, H. *et al.* Variation of the detergent-binding capacity and phospholipid content of membrane proteins when purified in different detergents. *Biophys. J.* **106**, 1660-1670 (2014).
15. Kabsch, W. XDS. *Acta Crystallogr. D Biol. Crystallogr.* **66**, 125-132 (2010).
16. Adams, P.D. *et al.* PHENIX: a comprehensive Python-based system for macromolecular structure solution. *Acta Crystallogr. D Biol. Crystallogr.* **66**, 213-221 (2010).
17. Emsley, P. *et al*. Features and development of Coot. *Acta Crystallogr. D Biol. Crystallogr.* **66**, 486-501 (2010).
18. Harder, D. & Fotiadis, D. Measuring substrate binding and affinity of purified membrane transport proteins using the scintillation proximity assay. *Nature Protoc.* **7**, 1569-1578 (2012).
19. Mancusso, R. *et al*. Simple screening method for improving membrane protein thermostability. *Methods* **55**, 324-329 (2011).
20. Karplus, P.A. & Diederichs, K. Linking crystallographic model and data quality. *Science* **336**, 1030-1033 (2012).

III

Detergent-Induced Stabilization and Improved 3D Map of the Human Heteromeric Amino Acid Transporter 4F2hc-LAT2

Marcel Meury[1☯], Meritxell Costa[1☯], Daniel Harder[1], Mirko Stauffer[1], Jean-Marc Jeckelmann[1], Béla Brühlmann[2], Albert Rosell[3,4], Hüseyin Ilgü[1], Karin Kovar[2], Manuel Palacín[3,4,5]*, Dimitrios Fotiadis[1]*

1 Institute of Biochemistry and Molecular Medicine, and Swiss National Centre of Competence in Research (NCCR) TransCure, University of Bern, Bern, Switzerland, 2 Institute of Biotechnology, School of Life Sciences and Facility Management Zürich University of Applied Sciences (ZHAW), Campus Grüntal, Wädenswil, Switzerland, 3 Institute for Research in Biomedicine (IRB Barcelona), Barcelona, Spain, 4 Centro de Investigación Biomédica en Red de Enfermedades Raras, Barcelona, Spain, 5 Department of Biochemistry and Molecular Biology, Faculty of Biology, University of Barcelona, Barcelona, Spain

Abstract

Human heteromeric amino acid transporters (HATs) are membrane protein complexes that facilitate the transport of specific amino acids across cell membranes. Loss of function or overexpression of these transporters is implicated in several human diseases such as renal aminoacidurias and cancer. HATs are composed of two subunits, a heavy and a light subunit, that are covalently connected by a disulphide bridge. Light subunits catalyse amino acid transport and consist of twelve transmembrane α-helix domains. Heavy subunits are type II membrane N-glycoproteins with a large extracellular domain and are involved in the trafficking of the complex to the plasma membrane. Structural information on HATs is scarce because of the difficulty in heterologous overexpression. Recently, we had a major breakthrough with the overexpression of a recombinant HAT, 4F2hc-LAT2, in the methylotrophic yeast *Pichia pastoris*. Microgram amounts of purified protein made possible the reconstruction of the first 3D map of a human HAT by negative-stain transmission electron microscopy. Here we report the important stabilization of purified human 4F2hc-LAT2 using a combination of two detergents, i.e., n-dodecyl-β-D-maltopyranoside and lauryl maltose neopentyl glycol, and cholesteryl hemisuccinate. The superior quality and stability of purified 4F2hc-LAT2 allowed the measurement of substrate binding by scintillation proximity assay. In addition, an improved 3D map of this HAT could be obtained. The detergent-induced stabilization of the purified human 4F2hc-LAT2 complex presented here paves the way towards its crystallization and structure determination at high-resolution, and thus the elucidation of the working mechanism of this important protein complex at the molecular level.

Citation: Meury M, Costa M, Harder D, Stauffer M, Jeckelmann J-M, et al. (2014) Detergent-Induced Stabilization and Improved 3D Map of the Human Heteromeric Amino Acid Transporter 4F2hc-LAT2. PLoS ONE 9(10): e109882. doi:10.1371/journal.pone.0109882

Editor: Dmitri Boudko, Rosalind Franklin University, United States of America

Received June 11, 2014; **Accepted** September 12, 2014; **Published** October 9, 2014

Data Availability: The authors confirm that all data underlying the findings are fully available without restriction. All relevant data are within the paper and its Supporting Information files.

Funding: This work was supported by the University of Bern, the Swiss National Science Foundation (Grant 31003A_144168), the Bern University Research Foundation, the Novartis Foundation, and the Marie Curie Actions International Fellowship Program (IFP) and the NCCR TransCure (to D. F.), and the Spanish Ministry of Science and Innovation (Grant SAF2012-40080-C02-01), the Fundación Ramón Areces and the Generalitat de Catalunya (SGR2009-1355) (to M. P.). The funders had no role in study design, data collection and analysis, decision to publish, or preparation of the manuscript.

Competing Interests: D. F. confirms that he is a PLOS ONE Editorial Board member. This does not alter the authors' adherence to PLOS ONE Editorial policies and criteria.

* Email: dimitrios.fotiadis@ibmm.unibe.ch (DF); manuel.palacin@irbbarcelona.org (MP)

☯ These authors contributed equally to this work.

Introduction

Human heteromeric amino acid transporters (HATs) are antiporters composed of two subunits, a heavy (SLC3 family) and a light subunit (SLC7 family) covalently linked by two conserved cysteine residues [1–3]. Light subunit members are also called L-type amino acid transporters (LATs) and belong to the large amino acids, polyamines and organocations (APC) transporter superfamily [4]. The light subunit constitutes the transport system for large and neutral amino acids, whereas the heavy subunit is required for the functional expression of the HAT in plasma membranes [5–7]. Exchange of amino acids by HATs across membranes is driven in a Na^+-independent manner with a 1:1 stoichiometry [8,9]. In humans, two heavy subunits have been identified, i.e., rBAT and 4F2hc [1]. The latter is involved in the formation of heterodimeric complexes with six different light subunits, i.e., LAT1, LAT2, y^+LAT1, y^+LAT2, asc1 and xCT [3]. Due to the widespread expression of these transport systems in organs and tissues, HATs are determining factors for a variety of human diseases, e.g., aminoacidurias (cystinuria and lysinuric protein intolerance) [7,10,11], tumor cell growth [12,13], Kaposi's sarcoma-associated herpesvirus infection [14,15] and cocaine relapse [16].

Despite the relevance of HATs in human physiology, detailed structural information has only been published for the extracellular domain of human 4F2hc [17]. The SLC3 family member 4F2hc is a type II membrane N-glycoprotein. 4F2hc is composed of a single transmembrane (TM) α-helix, an intracellular N-terminus and a large extracellular C-terminus [1]. X-ray crystallography revealed that the structure of the 4F2hc-ectodomain (ED) is similar to bacterial glucosidases with the typical triose phosphate isomerase (TIM) barrel $(\beta\alpha)_8$ fold and eight additional antiparallel β-strands [17]. In contrast to the bacterial homologs, human 4F2hc is missing the catalytic key residues for glucosidase activity [17]. On the structure of LATs, cysteine-scanning mutagenesis studies of xCT identified a twelve TM α-helix topology with intracellular N- and C-termini [18]. Recently, with the crystal structures of AdiC (L-arginine/agmatine antiporter) [19–22], ApcT (broad-specificity amino acid transporter) [23] and GadC (glutamate/GABA antiporter) [24], atomic models of prokaryotic APC transporters have become available. These models provide insights into the architecture and molecular transport mechanisms of APC superfamily members. LATs are likely to share a common architecture with their distantly related (≤20% amino acid sequence identity) prokaryotic APC homologs, but to date little information is available on the structure of HATs.

In a recent publication on the expression screening of human HATs in the methylotrophic yeast *Pichia pastoris* (*P. pastoris*), we identified 4F2hc-LAT2 as a promising candidate for functional and structural studies of HATs [25]. Furthermore, a first glimpse on the supramolecular organization of HATs could be obtained recently for 4F2hc-LAT2 by transmission electron microscopy (TEM), single particle analysis, cysteine scanning mutagenesis and disulphide mapping [26]. Using these experimental data, *in silico* docking analyses were performed with the 4F2hc-ED structure and a homology model of LAT2 to predict the contact sites at the heterodimer interface. Interactions were found between 4F2hc and the external loop regions of LAT2 indicating that the heavy subunit acts as a scaffold protein for the stability of the transporter complex [26]. Stabilization of LAT2 by the 4F2hc-ED was further corroborated by biochemical experiments. In these two studies [25,26], His-tagged 4F2hc and StrepII-tagged LAT2 were overexpressed in *P. pastoris* and the heterodimer purified from n-dodecyl-*β*-D-maltoside (DDM) solubilized membranes. However, purification in DDM resulted not only in 4F2hc-LAT2 heterodimers, but also in 4F2hc and LAT2 monomers (from disrupted heterodimers) and aggregates [25,26]. Size exclusion chromatography (SEC) profiles of DDM-purified 4F2hc-LAT2 indicated, in addition to the heterodimer peak, heterogeneous protein populations characterized by a prominent aggregates/oligomers peak [25]. Substrate binding to purified 4F2hc-LAT2 could not be determined due to the relatively low stability of the HAT in DDM [26]. Nevertheless, transport activity of the recombinant human 4F2hc-LAT2 complex was demonstrated by two different methods, i.e., uptake experiments using Pichia cells and proteoliposomes reconstituted from isolated, DDM-solubilized membranes.

Results and Discussion

We significantly improved the stability of detergent-solubilized 4F2hc-LAT2 for ligand-binding experiments and structural characterization by scintillation proximity assay (SPA) and TEM/single particle analysis, respectively. The stabilization of 4F2hc-LAT2 was successfully achieved by membrane solubilisation and protein purification using the two detergents DDM and lauryl maltose neopentyl glycol (LMNG), and cholesteryl hemisuccinate (CHS) simultaneously. CHS [27,28] and LMNG [29] were shown to be beneficial for stability and retaining the function of purified mammalian membrane proteins (see indicated references for details on possible stabilizing mechanisms of CHS and LMNG). Inspired by these reports, we modified our original purification protocol [25] and included LMNG and CHS in addition to DDM.

We purified 4F2hc-LAT2 by sequential cobalt and Strep-Tactin affinity chromatographies [25] in the presence of DDM, LMNG and CHS. The integrity, homogeneity and stability of purified 4F2hc-LAT2 heterodimers was analysed by SDS-PAGE, Western blot analysis and SEC (Fig. 1). SDS-PAGE showed a single protein band with a molecular mass of ~125 kDa (Fig. 1A; lane C) corresponding to the purified heterodimer. Importantly, no 4F2hc and LAT2 monomers, i.e., disrupted heterodimers, or aggregates/oligomers were detected by Western blotting using anti-4F2hc and anti-StrepTagII antibodies in stark contrast to purification with DDM (see Fig. 4A in Ref. [25] and Fig. S1 for comparison). The presence of LMNG and CHS in addition to DDM even prevented disruption of 4F2hc-LAT2 heterodimers six days after purification (Fig. S1). Only some unspecific formation of dimers and higher oligomers of heterodimers was observed after such periods of time (Fig. S1A, *lower*). In contrast, Western blot analysis of DDM-purified 4F2hc-LAT2 detected significant amounts of 4F2hc and LAT2 monomers from disrupted heterodimers and high amounts of aggregates after the same timespan (Fig. S1B, *lower*). SEC profiles of 4F2hc-LAT2 purified with DDM/LMNG/CHS indicated a single almost symmetric peak at a retention volume of 13.7 ml (Fig. 1B). By comparing retention volumes of purified 4F2hc-LAT2 and soluble molecular weight markers, the molecular mass of the complex was estimated to be ~406 kDa indicating a significant amount of bound DDM, LMNG and CHS. Similar to the purified protein (Fig. 1A), SDS-PAGE and Western blot analysis of the SEC peak fraction demonstrated full integrity of the 4F2hc-LAT2 heterodimer (Fig. 1C). In summary, purification of 4F2hc-LAT2 in DDM, LMNG and CHS significantly increased the stability of the complex paving the way for new functional and structural studies. First, we performed substrate binding to purified heterodimer using the SPA as previously reported for transport proteins [30,31]. Fig. 1D (bar 1) shows clear binding of the substrate [^{3}H]L-leucine to purified 4F2hc-LAT2 by SPA. As expected, the SPA signal was lost by the addition of 4 mM L-leucine (Fig. 1D, bar 2) indicating competitive binding of unlabelled substrate to the heterodimer. The SPA signal was also lost by the addition of 100 mM imidazole (Fig. 1D, bar 3), which displaced the 4F2hc-LAT2 from the SPA beads. Second, the integrity, homogeneity, stability and ability to bind substate of DDM/LMNG/CHS-purified 4F2hc-LAT2, as determined biochemically, prompted us to perform TEM and single particle analysis. Fig. 2A shows a representative overview electron micrograph of negatively-stained 4F2hc-LAT2 complexes. In contrast to 4F2hc-LAT2 purified only in DDM [26], small protein aggregates, and 4F2hc or LAT2 monomers from disrupted heterodimers were rarely found supporting the high integrity, homogeneity and stability of the complex when purified in DDM/LMNG/CHS. As for DDM-purified 4F2hc-LAT2 [26], particles had a distinct shape composed of two globular domains of different sizes (Fig. 2B). This characteristic feature is even more prominent in calculated class averages (Fig. S2A) compared to the raw images. In Rosell *et al*. we assigned the large and small domains of DDM-purified heterodimer particles to LAT2 and 4F2hc, respectively [26]. To further support this assignment experimentally, we performed labelling of the N-terminally located His-tag of 4F2hc using 5 nm Ni-NTA-Nanogold probes. The N-terminus of 4F2hc is located on the cytoplasmic side followed by a single TM α-helix and the large C-terminal ED, which is located on the extracellular side. On electron micrographs, the Nanogold probe was identified at the large domain of 4F2hc-LAT2 heterodimers and opposite to the small domain (Fig. 2C) supporting our previous assignment [26]. We calculated a 3D reconstruction of DDM/LMNG/CHS-purified 4F2hc-LAT2 from 27'921 negatively-stained complexes (Fig. S2B). The resolution of the obtained 3D map was estimated to 20 Å (Fig. S2C). This resolution should be considered with caution because the 3D reconstruction was obtained from negatively-stained samples. The distribution of the particle orientations after the last refinement cycle is shown in Fig. S2D and indicates a homogenous angular distribution of single particle projections.

In congruence with the class averages, the 3D model of 4F2hc-LAT2 exhibits a particular shape consisting of two differently sized densities (Fig. 3A; for additional views see Fig. S2B). The overall architecture of the 3D model calculated from DDM/LMNG/CHS-stabilized 4F2hc-LAT2 is similar to the 3D reconstruction we previously published [26]. Both models feature a smaller density on top of a larger one, with the former being clearly tilted (Fig. 3A, black dotted lines). As a consequence of the tilt, the 3D map possesses a cavity (Fig. 3A, arrowheads) and a seal (Fig. 3A, white dotted curve) in the interface region between the smaller and larger density. We fitted the X-ray structure of 4F2hc-ED [17] into the smaller density of our 3D model. This resulted in a similar orientation of the ED structure as seen in our previous 3D map calculated from 4F2hc-LAT2 purified in DDM (Fig. 3B and 3C) [26]. The orientation of the ED reveals the approximate localization of the N-terminal TM α-helix of the heavy-chain 4F2hc (Fig. 3B and 3C, indicated by asterisks). The previous 3D reconstruction of 4F2hc-LAT2 purified in DDM was calculated from 15,210 single particle projections. In contrast, the 4F2hc-LAT2 3D map presented here was calculated from 27'921 negatively-stained complexes, thus containing almost twice the number of projections. More, importantly, the high protein quality of isolated 4F2hc-LAT2 when purifying with the DDM, LMNG and CHS combination allowed us to collect a significantly higher number of projections of intact complexes. We compared the 3D

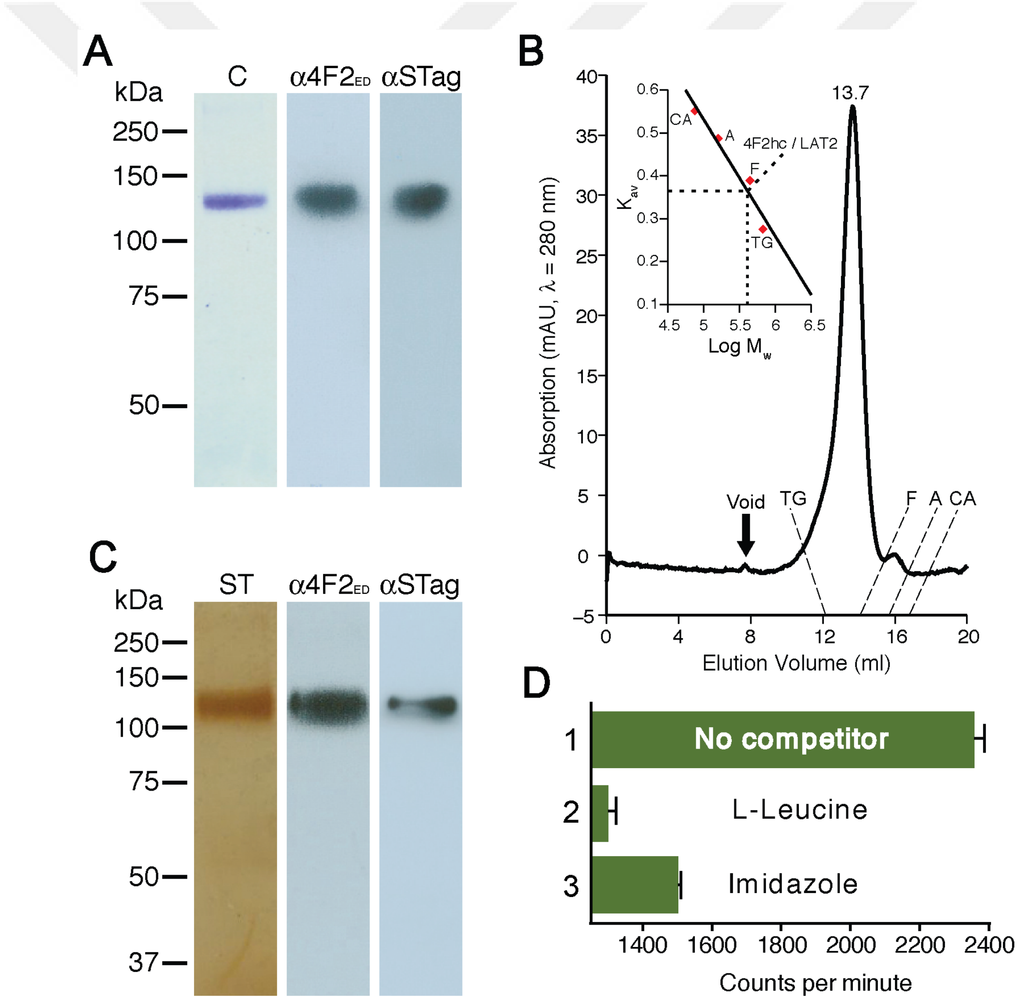

Figure 1. SDS-PAGE, Western blot analysis, SEC and SPA of 4F2hc-LAT2 purified in DDM, LMNG and CHS. (A) Coomassie Blue-stained 10% SDS/polyacrylamide gel (lane C) of 4F2hc-LAT2 after the two affinity chromatography steps. The complex runs as a prominent band at ~125 kDa. Western blot analysis using anti-4F2hc (lane α4F2$_{ED}$) and anti-StrepTagII (lane αSTag) antibodies indicated the presence of intact heterodimers only, i.e., no 4F2hc or LAT2 from disrupted complexes. (B) SEC of purified 4F2hc-LAT2 indicated a prominent almost symmetrical elution peak at 13.7 ml. (C) Silver-stained 10% SDS/polyacrylamide gel of purified 4F2hc-LAT2 after gel filtration (lane ST; from peak fraction). Again, one single band is visible corresponding to the heterodimer. Integrity of the complex was further supported by Western blotting using anti-4F2hc (lane α4F2$_{ED}$) and anti-StrepTagII (lane αSTag) antibodies. (D) Radioligand-binding assay by SPA using purified 4F2hc-LAT2 and [^{3}H]L-leucine. Bar 1: Binding of the radiolabelled substrate L-leucine to 4F2hc-LAT2, which is bound to scintillation beads, induces SPA signal. As expected, SPA signal was abolished by addition of 4 mM cold L-leucine (bar 2; competitive inhibition) or 100 mM imidazole (bar 3; detachment of the protein from the SPA beads). Bars represent mean ± SEM from triplicates. One representative of three similar independent experiments is shown.
doi:10.1371/journal.pone.0109882.g001

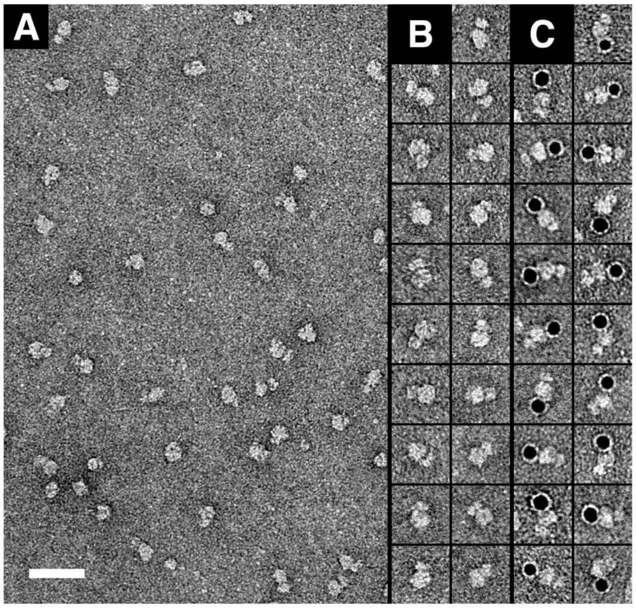

Figure 2. TEM and Nanogold labelling of purified human 4F2hc-LAT2 heterodimers. (A) Electron micrograph of purified negatively-stained 4F2hc-LAT2 heterodimers. Galleries of unlabelled (B) and 5 nm Ni-NTA-Nanogold labelled (C) 4F2hc-LAT2 heterodimers. Bilobed particles with two different sized domains are clearly visible. The 5 nm Ni-NTA Nanogold spheres are localized to the larger domains of the heterodimer. The scale bar in (A) represents 50 nm. The frame size of the boxes in (B) and (C) represent 28 nm.
doi:10.1371/journal.pone.0109882.g002

maps of 4F2hc-LAT2 calculated from protein purified in DDM [26] and DDM/LMNG/CHS (Fig. S3). While the densities of the EDs were similar, differences were found in the densities corresponding to LAT2. In the ellipsoid shaped LAT2 densities, the short axes differed by 14 Å (85 Å minus 71 Å; Fig. S3A) while the long axes were identical (i.e., 99 Å; Fig. S3B). Because of the same long axes, we attribute the obtained shorter axis and density in the 3D map previously calculated from complexes purified in DDM [26] to anisotropy in the data set. The 3D reconstruction of 4F2hc-LAT2 presented here was calculated from a significantly larger data set, thus guaranteeing a superior uniform angular coverage (i.e., azimuthal angles) of projections (Fig. S2D) and map quality.

Purification of human membrane proteins for functional and structural studies remains a challenge nowadays. Even more challenging is the purification of covalently bound human membrane protein complexes such as heterodimers where the connecting disulphide bridge is prone to breakage. Here we significantly stabilized purified human 4F2hc-LAT2 using a combination of two detergents, i.e., DDM and LMNG, and CHS. This made possible the application of the SPA radioligand-binding assay and the reconstruction of a solid 3D map. The stabilization of the human 4F2hc-LAT2 complex paves the way towards its crystallization for structure determination by crystallographic methods, and the elucidation of the molecular working mechanism of this important protein complex.

Materials and Methods

Overexpression, purification and SEC of 4F2hc-LAT2

Pichia cells overexpressing human 4F2hc-LAT2 were grown in batch culture or bioreactor as described previously [25,32]. Protein purification was performed similar to Costa *et al.* [25] using DDM (Anatrace, USA), LMNG (Anatrace, USA) and CHS (Sigma-Aldrich), and considering a 1:5 (w/w) ratio between CHS and total detergent. Briefly, *P. pastoris* membranes containing overexpressed 4F2hc-LAT2 were solubilized for 1 h at 4°C under gentle agitation in 1.5% DDM, 0.1% LMNG and 0.32% CHS in Buffer P (20 mM Tris–HCl pH 8, 300 mM NaCl and 10% glycerol). During detergent solubilisation the protein concentration was 3 mg/ml. After ultracentrifugation (100,000g at 4°C for 1 h), 4F2hc-LAT2 was purified from the supernatant by two sequential affinity chromatography steps, i.e., cobalt (TALON, Clontech, BD Biosciences, Germany) and Strep-Tactin (Superflow, high capacity resin; IBA, Germany) affinity chromatographies. 4F2hc-LAT2 was bound to a TALON column equilibrated with Buffer P containing 5 mM imidazole, 0.2% DDM, 0.013% LMNG and 0.0426% CHS. For washing and elution, the same buffer was used containing 20 mM and 200 mM imidazole, respectively. The elution was then bound to Strep-Tactin resin and washed in Buffer P containing 0.1% DDM, 0.0065% LMNG and 0.0213% CHS. 4F2hc-LAT2 was finally eluted with the same buffer supplemented with 8 mM desthiobiotin (IBA, Germany).

SEC of purified 4F2hc-LAT2 was performed with a Superose 6 10/300 GL column (GE Healthcare) using 20 mM Tris-HCl pH 8, 150 mM NaCl, 10% glycerol, 0.1% DDM, 0.0065% LMNG, 0.0213% CHS as elution buffer. The SEC column was calibrated using the marker proteins: Conalbumin (CA, 75 kDa), Aldolase (A, 158 kDa), Ferritin (F, 440 kDa) and Thyroglobulin (TG, 669 kDa), and the molecular weight (Mw) of the complex was determined similar to Ilgü *et al.* [33].

SPA of 4F2hc-LAT2

SPA was conducted with purified 4F2hc-LAT2 as described previously [30] using the following experimental conditions: 4.2 µg of protein, 0.5 µCi [^{3}H]L-leucine (specific activity: 120 Ci/mmol, Perkin Elmer), 300 µg PVT-copper beads (Perkin Elmer) per 96-well plate (white OptiPlates, Perkin Elmer) well. For the competition (Fig. 1D, bar 2) and background control (Fig. 1D, bar 3) experiments, 4 mM L-leucine and 100 mM imidazole were also present in the mixtures, respectively. The total assay volume was always 100 µl.

Negative-stain TEM, 3D reconstruction and on-grid Nanogold labelling

Purified human 4F2hc-LAT2 at ~30 µg/ml protein concentration was adsorbed for ~10 s to parlodion carbon-coated copper grids which were rendered hydrophilic by glow discharge at low pressure in air. Grids were washed with three drops of double-distilled water and stained with two drops of 0.75% uranyl formate (BDH Chemicals, USA). Electron micrographs were recorded with a Philips CM12 transmission electron microscope operated at 80 kV and equipped with a Morada CCD camera (Soft Imaging System, Olympus). For image processing and 3D reconstruction, the software package EMAN2 [34] was used. Initially, 28,993 single particles of 4F2hc-LAT2 were picked with a box size of 128 pixels using the e2boxer program. Electron micrographs were corrected for the contrast transfer function of the microscope using the e2ctf program. Reference-free classification and averaging was done with the e2refine2d program, which yielded about 200 class averages. From these class averages the e2initialmodel algorithm built a starting 3D model. The preliminary model was refined against a final set of 27,921 projections by running the iterative refinement procedure e2refine. During the refinement process the angular spacing was decreased from 15° to 2.5°. The resolution of the final 3D reconstruction was estimated by calculating the

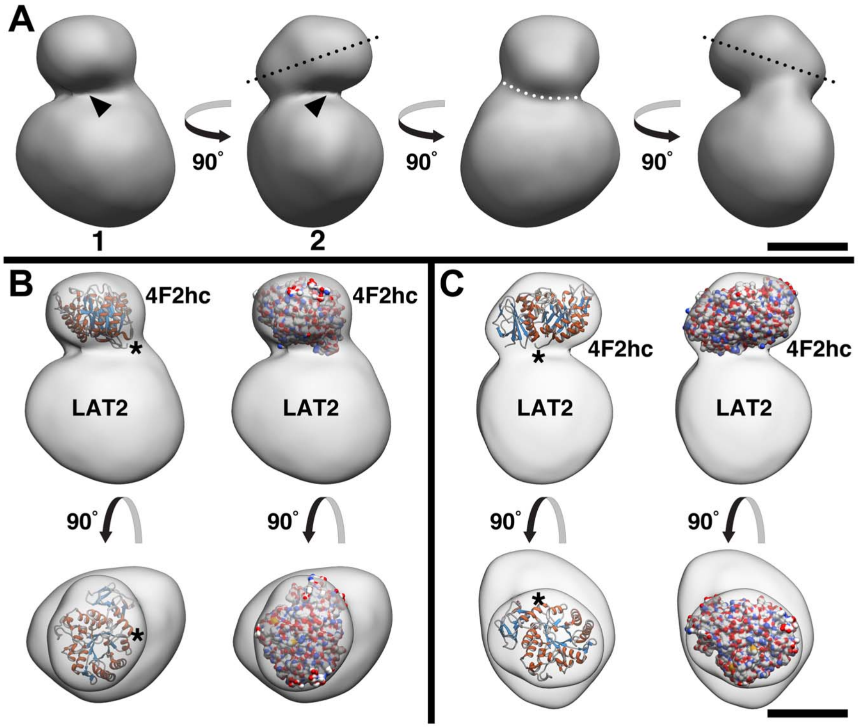

Figure 3. 3D reconstruction of human 4F2hc-LAT2 purified in DDM, LMNG and CHS. (A) Side views of the 3D map calculated from 27'921 projections of negatively-stained heterodimer particles (initially 28'993 picked). 4F2hc-LAT2 has a bilobed structure and consists of a smaller tilted density located on top of a larger density (tilt indicated by black dotted lines). As a consequence of the tilt, the 3D map features a distinct cavity (arrowheads) and on the opposite side a seal (marked by a white, dotted curve). Based on the Fourier shell correlation curve (0.5 criterion) the resolution is 20 Å (Fig. S2C). (B) and (C) Different views of the 4F2hc-LAT2 3D map with the fitted crystal structure of the 4F2hc-ED (PDB ID: 2DH2). Asterisks in (B) and (C) indicate the location of the N-terminus in the 4F2hc-ED crystal structure. The 4F2hc-ED structure is represented as cartoon (α-helices and β-strands in red and blue, respectively) and surface (CPK colours) models. The scale bar represents 50 Å.
doi:10.1371/journal.pone.0109882.g003

Fourier shell correlation (FSC) with the e2eotest program of EMAN2 and using the 0.5 criterion as a resolution indicator (conventional FSC calculation, not gold standard). The density threshold for volume rendering of the 4F2hc-LAT2 map was determined by fitting the surface representation of the 4F2hc ectodomain (4F2hc-ED; PDB: 2DH2) crystal structure into the small density of the 3D reconstruction and adjusting the threshold. Visualization of the 3D model and fitting of the 4F2hc-ED crystal structure was done in UCSF Chimera [35].

For Nanogold labelling, purified 4F2hc-LAT2 was adsorbed to electron microscopy grids as described above. Grids were washed with three drops of double-distilled water and blotted. Then immediately, 10 µl of 5 nm Ni-NTA Nanogold solution (Nanoprobes Inc., USA) diluted 1:5 in 60 mM Tris-HCl pH 8, 450 mM NaCl, 2.5 mM imidazole) were added. Grids were incubated for 30 min at room temperature in a humidity chamber (Petri dish with wet paper towel inside). After incubation, grids were blotted to remove the Nanogold solution, washed with one drop of double-distilled water and finally negatively-stained with 0.75% uranyl formate.

Supporting Information

Figure S1 Stability of purified human 4F2hc-LAT2. SDS-PAGE and Western blot analyses of 4F2hc-LAT2 purified in DDM, LMNG and CHS (A), and DDM only (B) after purification (day 1; *upper*) and 6 days later (*lower*). Purified protein was always kept on ice or 4°C. Western blot analysis was performed using anti-4F2hc (lanes α4F2$_{ED}$) and anti-StrepTagII (lanes αSTag) antibodies. 10% SDS/polyacrylamide gels were used. Gels in lanes C were stained with Coomassie Blue. In (A) no disruption of the complex was observed (*upper*). Only some higher aggregates were observed 6 days after purification (*lower*). In stark contrast, 4F2hc and LAT2 monomers from disrupted heterodimers as well as some higher aggregates were found in 4F2hc-LAT2 purified in DDM after purification (B) (*upper*). Incubation at 4°C for additional 6 days dramatically increased aggregation of the complex. In all lanes C, 5 µg protein were loaded with the exception of lane C in *lower*, panel (B). Here 20 µg were loaded in order to visualize bands not corresponding to higher aggregates (which were most abundant).
(TIF)

Figure S2 Single particle analysis and 3D reconstruction of human 4F2hc-LAT2. (A) Representative class averages of 4F2hc-LAT2 purified in DDM, LMNG and CHS. The reference-free class averages of the heterodimer were generated from 27'921 single projections. The frame size of the class averages is 39.6 nm. (B) Overview of the 3D reconstruction of 4F2hc-LAT2. The 3D model is rotated in increments of 45° around the x- (*lower*) or y-axis (*upper*). The scale bar represents 5 nm. (C) Resolution of the 4F2hc-LAT2 3D map. According to the 0.5 criterion the Fourier Shell Correlation (FSC) function indicates a resolution of 20 Å. (D) The Euler angle distribution of single particle projections demonstrates a homogeneous sampling.
(TIF)

Figure S3 Comparison of human 4F2hc-LAT2 3D reconstructions. Front (A) and side (B) views of 3D maps of 4F2hc-

LAT2 purified with DDM/LMNG/CHS (in grey) and with DDM only (in yellow). In (A) and (B), the X-ray crystal structure of 4F2hc-ED is shown as surface representation (PDB: 2DH2; CPK colours). In (A) the measured widths of LAT2 are different, i.e., 85 Å *versus* 71 Å, while in (B) identical, i.e., 99 Å.
(TIF)

Author Contributions

Conceived and designed the experiments: MM MC DF. Performed the experiments: MM MC MS JMJ BB HI. Analyzed the data: MM MC DH DF. Contributed reagents/materials/analysis tools: BB AR KK MP. Wrote the paper: MM MC DF.

References

1. Fotiadis D, Kanai Y, Palacin M (2013) The SLC3 and SLC7 families of amino acid transporters. Mol Aspects Med 34: 139–158.
2. Palacin M, Kanai Y (2004) The ancillary proteins of HATs: SLC3 family of amino acid transporters. Pflugers Arch 447: 490–494.
3. Verrey F, Closs EI, Wagner CA, Palacin M, Endou H, et al. (2004) CATs and HATs: the SLC7 family of amino acid transporters. Pflugers Arch 447: 532–542.
4. Verrey F, Jack DL, Paulsen IT, Saier MH, Jr., Pfeiffer R (1999) New glycoprotein-associated amino acid transporters. J Membr Biol 172: 181–192.
5. Reig N, Chillaron J, Bartoccioni P, Fernandez E, Bendahan A, et al. (2002) The light subunit of system b(o,+) is fully functional in the absence of the heavy subunit. EMBO J 21: 4906–4914.
6. Mastroberardino L, Spindler B, Pfeiffer R, Skelly PJ, Loffing J, et al. (1998) Amino-acid transport by heterodimers of 4F2hc/CD98 and members of a permease family. Nature 395: 288–291.
7. Torrents D, Estevez R, Pineda M, Fernandez E, Lloberas J, et al. (1998) Identification and characterization of a membrane protein (y+L amino acid transporter-1) that associates with 4F2hc to encode the amino acid transport activity y+L. A candidate gene for lysinuric protein intolerance. J Biol Chem 273: 32437–32445.
8. Chillaron J, Estevez R, Mora C, Wagner CA, Suessbrich H, et al. (1996) Obligatory amino acid exchange via systems bo,+-like and y+L-like. A tertiary active transport mechanism for renal reabsorption of cystine and dibasic amino acids. J Biol Chem 271: 17761–17770.
9. Busch AE, Herzer T, Waldegger S, Schmidt F, Palacin M, et al. (1994) Opposite directed currents induced by the transport of dibasic and neutral amino acids in Xenopus oocytes expressing the protein rBAT. J Biol Chem 269: 25581–25586.
10. Feliubadalo L, Font M, Purroy J, Rousaud F, Estivill X, et al. (1999) Non-type I cystinuria caused by mutations in SLC7A9, encoding a subunit ($b^{o,+}$AT) of rBAT. Nat Genet 23: 52–57.
11. Calonge MJ, Gasparini P, Chillaron J, Chillon M, Gallucci M, et al. (1994) Cystinuria caused by mutations in rBAT, a gene involved in the transport of cystine. Nat Genet 6: 420–425.
12. Nicklin P, Bergman P, Zhang B, Triantafellow E, Wang H, et al. (2009) Bidirectional transport of amino acids regulates mTOR and autophagy. Cell 136: 521–534.
13. Fuchs BC, Bode BP (2005) Amino acid transporters ASCT2 and LAT1 in cancer: partners in crime? Semin Cancer Biol 15: 254–266.
14. Veettil MV, Sadagopan S, Sharma-Walia N, Wang FZ, Raghu H, et al. (2008) Kaposi's sarcoma-associated herpesvirus forms a multimolecular complex of integrins (alphaVbeta5, alphaVbeta3, and alpha3beta1) and CD98-xCT during infection of human dermal microvascular endothelial cells, and CD98-xCT is essential for the postentry stage of infection. J Virol 82: 12126–12144.
15. Kaleeba JA, Berger EA (2006) Kaposi's sarcoma-associated herpesvirus fusion-entry receptor: cystine transporter xCT. Science 311: 1921–1924.
16. Baker DA, McFarland K, Lake RW, Shen H, Tang XC, et al. (2003) Neuroadaptations in cystine-glutamate exchange underlie cocaine relapse. Nat Neurosci 6: 743–749.
17. Fort J, de la Ballina LR, Burghardt HE, Ferrer-Costa C, Turnay J, et al. (2007) The structure of human 4F2hc ectodomain provides a model for homodimerization and electrostatic interaction with plasma membrane. J Biol Chem 282: 31444–31452.
18. Gasol E, Jimenez-Vidal M, Chillaron J, Zorzano A, Palacin M (2004) Membrane topology of system x_c^- light subunit reveals a re-entrant loop with substrate-restricted accessibility. J Biol Chem 279: 31228–31236.
19. Kowalczyk L, Ratera M, Paladino A, Bartoccioni P, Errasti-Murugarren E, et al. (2011) Molecular basis of substrate-induced permeation by an amino acid antiporter. Proc Natl Acad Sci USA 108: 3935–3940.
20. Gao X, Zhou L, Jiao X, Lu F, Yan C, et al. (2010) Mechanism of substrate recognition and transport by an amino acid antiporter. Nature 463: 828–832.
21. Fang Y, Jayaram H, Shane T, Kolmakova-Partensky L, Wu F, et al. (2009) Structure of a prokaryotic virtual proton pump at 3.2 Å resolution. Nature 460: 1040–1043.
22. Gao X, Lu F, Zhou L, Dang S, Sun L, et al. (2009) Structure and mechanism of an amino acid antiporter. Science 324: 1565–1568.
23. Shaffer PL, Goehring A, Shankaranarayanan A, Gouaux E (2009) Structure and mechanism of a Na+-independent amino acid transporter. Science 325: 1010–1014.
24. Ma D, Lu P, Yan C, Fan C, Yin P, et al. (2012) Structure and mechanism of a glutamate-GABA antiporter. Nature 483: 632–636.
25. Costa M, Rosell A, Alvarez-Marimon E, Zorzano A, Fotiadis D, et al. (2013) Expression of human heteromeric amino acid transporters in the yeast *Pichia pastoris*. Protein Expr Purif 87: 35–40.
26. Rosell A, Meury M, Alvarez-Marimon E, Costa M, Perez-Cano L, et al. (2014) Structural bases for the interaction and stabilization of the human amino acid transporter LAT2 with its ancillary protein 4F2hc. Proc Natl Acad Sci USA 111: 2966–2971.
27. Drew D, Newstead S, Sonoda Y, Kim H, von Heijne G, et al. (2008) GFP-based optimization scheme for the overexpression and purification of eukaryotic membrane proteins in *Saccharomyces cerevisiae*. Nat Protoc 3: 784–798.
28. O'Malley MA, Helgeson ME, Wagner NJ, Robinson AS (2011) The morphology and composition of cholesterol-rich micellar nanostructures determine transmembrane protein (GPCR) activity. Biophys J 100: L11–L13.
29. Chae PS, Rasmussen SG, Rana RR, Gotfryd K, Chandra R, et al. (2010) Maltose-neopentyl glycol (MNG) amphiphiles for solubilization, stabilization and crystallization of membrane proteins. Nat Methods 7: 1003–1008.
30. Harder D, Fotiadis D (2012) Measuring substrate binding and affinity of purified membrane transport proteins using the scintillation proximity assay. Nature Protoc 7: 1569–1578.
31. Quick M, Javitch JA (2007) Monitoring the function of membrane transport proteins in detergent-solubilized form. Proc Natl Acad Sci USA 104: 3603–3608.
32. Hyka P, Zullig T, Ruth C, Looser V, Meier C, et al. (2010) Combined use of fluorescent dyes and flow cytometry to quantify the physiological state of Pichia pastoris during the production of heterologous proteins in high-cell-density fed-batch cultures. Appl Environ Microbiol 76: 4486–4496.
33. Ilgü H, Jeckelmann JM, Gachet MS, Boggavarapu R, Ucurum Z, et al. (2014) Variation of the detergent-binding capacity and phospholipid content of membrane proteins when purified in different detergents. Biophys J 106: 1660–1670.
34. Tang G, Peng L, Baldwin PR, Mann DS, Jiang W, et al. (2007) EMAN2: an extensible image processing suite for electron microscopy. J Struct Biol 157: 38–46.
35. Pettersen EF, Goddard TD, Huang CC, Couch GS, Greenblatt DM, et al. (2004) UCSF Chimera—a visualization system for exploratory research and analysis. J Comput Chem 25: 1605–1612.